

# Chern Characteristics and Todd–Hirzebruch Identities for Transpolar Pairs of Toric Spaces

Per Berglund<sup>\*†</sup> and Tristan Hübsch<sup>‡</sup>

<sup>\*</sup>Department of Physics, University of New Hampshire, Durham, NH 03824, USA

<sup>†</sup>Theoretical Physics Department, CERN, CH-1211 Geneva, Switzerland

<sup>‡</sup>Department of Physics & Astronomy, Howard University, Washington, DC 20059, USA  
per.berglund@unh.edu and thubsch@howard.edu

## ABSTRACT

Standard toric geometry methods used to construct Calabi–Yau varieties may be extended to complete intersections in non-Fano varieties encoded by star triangulating non-convex polytopes. Similarly, mirror symmetry is conjectured to hold in terms of a transpolar duality generalizing the original construction of Batyrev and Borisov. The associated mirror pairs naturally include certain flip-folded, multi-layered polyhedral objects, inclusively named *VEX multitopes*, and a correspondingly generalized *transpolar* duality. These self-overlapping VEX multitopes, long since known in pre-symplectic geometry, are found to correspond to certain non-algebraic but smooth toric spaces with Chern classes that satisfy the standard Todd–Hirzebruch identities. The computation of diffeomorphism invariants, including characteristic submanifold intersection numbers, corroborates their recent inclusion in the connected web of Calabi–Yau spaces and associated string compactifications: They arise together with the standard (Fano/reflexive polytope) constructions, within deformation families of generalized complete intersections in products of projective spaces.

## Contents

<b>1</b>	<b>Introduction, Rationale and Summary</b>	<b>1</b>
1.1	The Mirror-Symmetric Framework	2
1.2	Main Results	5
<b>2</b>	<b>Todd–Hirzebruch Identities and Characteristic Classes</b>	<b>6</b>
2.1	Todd–Hirzebruch Identities	7
2.1.1	The 12-Theorem	7
2.1.2	Higher-Dimensional Todd–Hirzebruch Identities	9
2.2	Chern Classes and Invariants	10
2.2.1	Two Dimensions	10
2.2.2	Three Dimensions	12
2.2.3	Four Dimensions	14
2.2.4	Five Dimensions	18
<b>3</b>	<b>Intersection Numbers</b>	<b>20</b>
3.1	Two Dimensions	21
3.2	Three Dimensions	25
<b>4</b>	<b>Combinatorial and Cohomological Features of VEX Multitopes</b>	<b>27</b>
4.1	Dehn–Sommerville and Unimodality Relations	29
4.1.1	Two Dimensions	29
4.1.2	Three Dimensions	30
4.1.3	Four Dimensions	31
<b>5</b>	<b>Surgery</b>	<b>32</b>
5.1	Flip-Folded Extension Replacement	32
5.2	Complex vs. Pre-Complex Structure	35
5.3	Being Star-Triangulable	36
<b>6</b>	<b>Conclusions and Outlook</b>	<b>38</b>
<b>A</b>	<b>Additional Transpose-Mirror Examples</b>	<b>41</b>
A.1	A Network of Transpose-Mirrors	41
A.2	Origin-Enclosing Simplicial Reductions	43
A.3	Origin Non-Enclosing Simplicial Reductions	44

# 1 Introduction, Rationale and Summary

Calabi–Yau (complex, Kähler, Ricci-flat) spaces have been studied intensely in physics as factors of space-time through which superstrings propagate consistently [1]. String dynamics easily permits certain types of singularization [2], some of which connect topologically distinct models [3–9]; see also [10] and [11]. Within a decade, model construction and analysis refocused on *gauged linear sigma models* (GLSMs) [12, 13], where the supersymmetry-complexified<sup>1</sup> gauge group,  $T^n := U(1)^n \hookrightarrow (\mathbb{C}^*)^n$ , governs the underlying (complex algebraic) toric geometry [18–23]. This framework produced a database of almost half a billion *reflexive* polytopes [24], each encoding (weak/semi) Fano *complex algebraic* toric 4-folds, in which Calabi–Yau 3-folds are embedded as (finite quotients of) anticanonical hypersurfaces. This vast pool of constructions exhibits *mirror symmetry*, whereby the  $(\mathbb{C}^*)^n$ -equivariant cohomology rings of pairs of Calabi–Yau hypersurfaces,  $(Z, \tilde{Z})$ , satisfy  $H^{p,q}(Z) \approx H^{n-p,q}(\tilde{Z})$  [25–37].

However, Calabi–Yau hypersurfaces also exist in non-Fano varieties [38], as in their (weak/semi) Fano variants [39], all within the same deformation families of generalized complete intersections in products of projective spaces [40–42]. This framework and connected web of Calabi–Yau 3-folds and corresponding string vacua [43, 44] necessarily *extends futher* by mirror symmetry: Besides *reflexive* polytopes, *VEX multitopes* [38] also include non-convex, flip-folded and otherwise multi-layered multihedral but star-triangulable bodies,  $\Delta_X^*$ , which span<sup>2</sup> *multifans*,  $\Sigma_X \triangleleft \Delta_X^*$  [45–52]; see also [53–56]. The underlying  $T^n$ -equivariant geometry of the corresponding *toric spaces*,  $X_\Sigma$ , naturally matches the  $T^n = U(1)^n$ -gauge symmetry of GLSMs and the underlying string theory, and the purpose of this article is to explore the nature of such non-Fano toric spaces and their Calabi–Yau mirror hypersurfaces.

**Organization:** In the remainder of this introduction, we present the overarching mirror-symmetric framework with our key Claims 1.1 and 1.2, and Conjectures 1.1 and 1.2, and list the well established toric geometry results for which we explore the multifan generalizations: Section 2 verifies the multifan evaluation of Chern classes, invariants and the Todd–Hirzebruch identities, while corresponding intersection number results are discussed in Section 3. Section 4 explores several combinatorial and cohomological features of VEX multitopes, while their surgical implications are examined in Section 5. We summarize our conclusions in Section 6, and defer several technical details and examples to Appendix A.

In support of the Claims, Conjectures and Remarks herein, we cite the rigorous results in 2 dimensions [57, 58] and verify numerous mutually consistent computational results and identities with Chern classes and numbers, intersection numbers, Poincaré series and related data for two infinite sequences of pairs  $(X, \nabla X)$  in the mirror framework (1.1), in 2, 3 and 4 dimensions; many other purposefully constructed test-examples are here omitted for space. Similarly general computational results on the structure of the secondary fan were reported in [38]; the cumulative world-sheet instanton effects on the Kähler class discriminant loci being mirrored in the complex structure moduli space will be reported separately. Hopefully, these computational results provide ample and convincing motivation and invitation for a systematic study, with rigorous proofs, clarified qualifications, and corrections of our claims and conjectures.

---

<sup>1</sup>Reducing worldsheet supersymmetry generalizes the target-space (co)tangent bundle to much more general structures [14]; see also [15] and references therein. Also, the worldsheet-supersymmetric  $T^n = U(1)^n \hookrightarrow (\mathbb{C}^*)^n = U(1; \mathbb{C})^n = \mathbb{T}^n$  gauge-group complexification may admit some mild degeneration or boundary sources (target-space 'branes), which further relaxes the underlying assumptions. Finally, the superstring underlying worldsheet quantum field theory itself has a manifestly  $T$ -dual and mirror-symmetric formulation, whence our foundational reliance on it [16, 17].

<sup>2</sup>A VEX multotope *spans* a multifan,  $\Delta^* \triangleright \Sigma$ , with a *primitive* (lattice coprime) central cone over every face of  $\Delta^*$  [22]. A *k*-face  $\theta \in \partial \Delta^*$  is a closed, contiguous, multihedral, *k*-dimensional component in  $\partial \Delta^*$ , a *poset* of (codimension-1, proper) *facets*; standard definitions [19–23] can be adapted for non-convex, self-crossing, folded and otherwise multi-layered multitopes [45–47].

## 1.1 The Mirror-Symmetric Framework

Non-convex, flip-folded and otherwise multi-layered multitopes turn up routinely in the study of (pre)symplectic toric spaces [59–63], which should be expected in string theory, since mirror symmetry relates (pre)complex and (pre)symplectic structures<sup>3</sup> [17, 68–70]: The Batyrev–Borisov construction of mirror Calabi–Yau manifolds [27, 28, 31, 32] relies on swapping the roles played by the reflexive (convex) polytopes in a standard polar pair [19–23]. It generalizes to the *transpolar* involution of VEX multitopes,  $\Delta_X^* \xleftrightarrow{\nabla} \Delta_X =: \Delta_{\nabla X}^*$  [38, 39], including the rigorous results on 2-dimensional *generalized legal loops* [57, 58], and encoding the mirror map between entire deformation families of Calabi–Yau (anticanonical) hypersurfaces,  $X[c_1] \xleftrightarrow{\text{MM}} \nabla X[c_1]$ , vastly generalizing the transposition mirror construction [26, 29, 30, 33–37]:

**Claim 1.1** Each transpolar pair of VEX multitopes [38],  $(\Delta_X^*, \Delta_X)$  and cones over them,  $(\triangleleft \Delta_X^*, \triangleleft \Delta_X)$ , specifies multiple pairs of mirror Calabi–Yau spaces,  $(Z_f, \tilde{Z}_{Tf})$ :

$$\begin{array}{ccc}
 f \in \Gamma(\mathcal{K}_X^*) \leftrightarrow \mathcal{K}_X^* \leftrightarrow \triangleleft \Delta_X & \xleftrightarrow{\text{(trans)polar [38]}} & \triangleleft (\Delta_X^* =: \Delta_{\nabla X}) \leftrightarrow \mathcal{K}_{\nabla X}^* \leftrightarrow \Gamma(\mathcal{K}_{\nabla X}^*) \ni Tf \\
 \downarrow \text{def. section} & & \downarrow \text{def. section} \\
 X \leftrightarrow \Sigma_X \triangleleft \Delta_X^* & \xleftrightarrow[\Delta_X = (\Delta_X^*)^\nabla]{\text{(trans)polar [38]}} & (\Delta_X =: \Delta_{\nabla X}^*) \triangleright \Sigma_{\nabla X} \leftrightarrow \nabla X \\
 \uparrow f=0 & & \uparrow Tf=0 \\
 X[c_1] \ni (Z_f = f^{-1}(0)) & \xleftrightarrow{\text{transposition mirrors [26, 29, 33–36] \& [38, 39]}} & (Tf^{-1}(0) = \tilde{Z}_{Tf}) \in \nabla X[c_1]
 \end{array} \tag{1.1}$$

This mirror symmetry framework extends the *polar* involution amongst *reflex* polytopes to the *transpolar* involution amongst (non-convex) *VEX multitopes* (adapting from [38, 39] and conforming to [45–47]):

**Construction 1.1 (transpolar)** Given an  $L$ -lattice multitope,  $\Delta \subset L_{\mathbb{R}} := ((L \approx \mathbb{Z}^n) \otimes_{\mathbb{Z}} \mathbb{R})$ , with a 0-centered  $L$ -lattice star-triangulation:

1. Recursively subdivide  $\Delta$  into a facet-ordered poset of convex faces,  $\Delta = (\theta_\alpha, \triangleleft)$ .
2. Compute the polar image of each convex face:

$$\theta_\alpha^\nabla = \{v : \langle u, v \rangle = -1, u \in \theta_\alpha \in \Delta\} \subset (L^\vee \otimes_{\mathbb{Z}} \mathbb{R}). \tag{1.2}$$

3. Dually to the poset  $\Delta = (\theta_\alpha, \triangleleft)$ , assemble the transpolar poset  $\Delta^\nabla = (\theta_\alpha^\nabla, \triangleleft)$  satisfying the universal inclusion-reversing relations:

$$\partial \Delta \ni \vartheta = \theta_1 \cap \cdots \cap \theta_k \Leftrightarrow \theta_1^\nabla \cup \cdots \cup \theta_k^\nabla = \partial \vartheta^\nabla \in \partial \Delta^\nabla, \tag{1.3}$$

which **delimit** the polar of each face by the polars of its adjacent facets.

**Definition 1.1 (VEX multitopes and multifans)** An  $L$ -lattice **VEX multitope**,  $\Delta \subset L_{\mathbb{R}} := (L \otimes_{\mathbb{Z}} \mathbb{R})$ , is a continuously orientable, possibly multi-layered, multi-hedral  $n$ -dimensional body with every facet at unit integral distance [27, Def. 4.1.4] from  $0 \in L$ , and star-triangulated by a 0-centered **multifan** [47]:  $\Delta \triangleright \Sigma = (\sigma_\alpha, \triangleleft)$  is a facet-ordered poset of its 0-centered cones,  $\sigma_\alpha = \triangleleft(\theta_\alpha \in \partial \Delta)$ , where  $\varsigma \triangleleft \sigma$  denotes  $\varsigma \subset \partial \sigma$  and  $\text{codim}(\varsigma, \sigma) = 1$ .  $\partial \Delta = (\theta_\alpha, \triangleleft)$  has the same poset structure.

**Remark 1.1 (multiple mirror master)** Each invertible [33, 34] pair of transpose defining polynomials,  $(f, {}^T f)$ , is specified in terms of  $(\Delta_X^*, \Delta_X)$ -defined Cox coordinates, by a *sub-simplex reduction*,  $(\text{Red } \Delta_X, \text{Red } \Delta_X^*)$ , consisting of a pair of 0-enclosing top-dimensional simplices<sup>4</sup> with vertices in  $((\Delta_X \cap N), (\Delta_X^* \cap M))$ ; see

<sup>3</sup>Mutually compatible complex, symplectic and Kähler (target-space) structures are requisite in string theory, but a growing class of singularizations and degenerations turns out to be admissible or “repaired” by including suitable brane-like sources; hybrid phases of GLSM models [12] even include *stratified pseudo-manifolds* [64–67]. In *presymplectic*, i.e., *precomplex* and *pre-Kähler* spaces, the respective structures degenerate at positive codimension loci, and their inclusion then seems well warranted.

<sup>4</sup>For simplices with primitive vertices, enclosing the lattice origin seems necessary for the so-encoded polynomial to be transverse (to have its base-points in the Stanley–Reisner excluded set per spanning multitope) and to be usable for transpose mirror construction [26, 29, 33, 34] but we are not aware of a proof of this statement; see Appendices A.2 and A.3.

[39, § 3.4] and Appendix A for more details and examples. The combinatorial array of these *multiple mirrors* suggests the following **triple conjecture**. ▀

**Conjecture 1.1** For any transpolar pair of VEX multitoes,  $(\Delta_X^*, \Delta_X)$ , of Claim 1.1: (1) Origin-enclosing sub-simplex reductions of Remark 1.1 encode transpose mirror Calabi–Yau model pairs à la [26, 38, 39]. (2) Mirror symmetry extends throughout the pair of deformation families,  $(X[c_1], \nabla X[c_1])$ , generating all such multiple mirror models. (3) Calabi–Yau manifolds may be embedded in **suitable models** (see Remark 1.8) of toric spaces,  $X \leftarrow \Sigma_X \in \Delta_X^*$  and  $\nabla X \leftarrow \nabla \Sigma_X \in \Delta_X$  themselves [45–55, 62].

The following related remarks further explain the notation and flesh out the details of (1.1):

**Remark 1.2 (layers)** Every fan specifies the entire poset hierarchy of common facets,  $\tau \prec \sigma_1, \sigma_2$ , implying that  $\tau := \sigma_1 \cap \sigma_2$  but  $\text{relint}(\sigma_1) \cap \text{relint}(\sigma_2) = \emptyset$ . For this to hold when  $\sigma_2$  *folds over* (a part of)  $\sigma_1$  in a VEX multifan (as in Figure 1),  $\sigma_1$  and  $\sigma_2$  must lie in distinct layers, connected along the folding hyperplane  $H \supset \tau \prec \sigma_1, \sigma_2$ , satisfying in this sense the “Separation Lemma” condition [22, Lemma V.1.13, p. 147]. The (1.2)-transpolars of  $\theta_\alpha, \theta_\beta \in \partial\Delta$  are distinguished,  $(\theta_\alpha^\nabla \neq \theta_\beta^\nabla) \in \partial\Delta^\nabla$ , unless  $\theta_\alpha, \theta_\beta$  are subdividing parts of a single face in  $\partial\Delta$ . A subset of the poset  $\partial\Delta = (\theta_\alpha, \prec)$  often suffices in Construction 1.1. VEX multitoes include those that flip-fold *around*  $0 \in L$  with no relative interior; see (5.6) and (5.7) for examples. The continuous orientation of  $\partial\Delta$  orients  $\Sigma \in \Delta$ , provides a sign to the degree of each facet and central cone over it, and singles out a generalized Duistermaat–Heckman measure [46, 47]; see also [71]. ▀

**Definition 1.2** An  $L$ -lattice multifan is **regular** if each cone is generated by a basis for  $L$  [22, 23]. An  $L$ -lattice fan is **complete** if it covers all space by a simple surjection,  $\pi_\Sigma : \Sigma \rightarrow (L_\mathbb{R} \approx \mathbb{R}^n)$  [19–23], providing a “finite rational partial polyhedral (f.r.p.p) decomposition” of  $\mathbb{R}^n$  [18]. Extending completeness to multifans,  $\Sigma$ , is technically more involved [45–47], but insures each facet of a cone,  $\tau \prec \sigma$ , to again be the intersection  $\tau = \sigma \cap \sigma'$  for some  $\sigma' \in \Sigma$ , and provides a triangulation of  $\pi_\Sigma(S^{n-1})$ .

**Remark 1.3 (plain, convex case)** For any convex  $L$ -lattice polytope,  $\Delta$ , Construction 1.1 simplifies:

$$\Delta = \text{Conv}(\Delta) \quad \Rightarrow \quad \Delta^\nabla = \Delta^\circ := \{v : \langle u, v \rangle \geq -1, u \in \Delta\} \subset L_\mathbb{R}^\vee := L^\vee \otimes_{\mathbb{Z}} \mathbb{R}, \quad (1.4)$$

where  $\Delta^\circ$  is the *polar* of  $\Delta$ . Convex VEX polytopes are *reflexive*, the lattice center “ $0 \in L$ ” in Definition 1.1 the only inside lattice point,  $0 = L \cap (\Delta \setminus \partial\Delta)$ , and  $\Delta$  spans a *complete (plain, i.e., single-layer) central fan*,  $\Sigma \in \Delta$ , that encodes a *compact (weak/semi) Fano complex algebraic toric variety* [19–23, 27]. ▀

**Conjecture 1.2** For an  $L$ -lattice VEX multitope,  $\Delta$ : (1)  $\Delta^\nabla \subset L_\mathbb{R}^\vee$  is a VEX multitope, and (2)  $(\Delta^\nabla)^\nabla = \Delta$ : the transpolar duality 1.1 closes on VEX multitoes as an involution. (3) The star-triangulation of  $\Delta$  is  **$L$ -primitive**: lattice points of each star-triangulating simplex are only  $0 \in L$  and in  $\partial\Delta$ .

If  $\Delta$  has a **regular** triangulation: (4)  $\Delta^\nabla$  has a corresponding regular ( $L^\vee$ -)lattice triangulation, so both  $\Delta$  and  $\Delta^\nabla$  correspond to smooth toric spaces.

**Remark 1.4** All 2-dimensional VEX multigons are generalized legal loops (and their dual equals the transpolar of Construction 1.1), which have a unique regular subdivision by definition [57]. In more than two dimensions, the degree of a primitive star-simplex can be arbitrarily large [72, 73] and the transpolar (1.2) of its facet in  $\partial\Delta$  need not be integral, i.e., in  $L^\vee$ . The unit-distance defining requirement 1.1 would seem to preclude such facets in VEX multitoes, but we not aware of a rigorous proof. The statements of Conjecture 1.2 seem so inherent in the mirror-symmetric framework of Claim (1.1) that Definition 1.1 should be refined until all statements of Conjecture 1.2 hold. ▀

**Remark 1.5 (transpolar spaces)** Like reflexive polytopes, each VEX multitope,  $\Delta_X^*$ , corresponds to two toric spaces: (1)  $\Delta_X^*$  spans the central multifan,  $\Sigma_X \triangleleft \Delta_X^*$ : Its (simplicially subdivided, degree- $k_i$ ) top-dimensional cones (one over each facet of  $\Delta_X^*$ ) encode  $\mathbb{C}^n/\mathbb{Z}_{k_i}$ -like charts on  $X$ , glued as the cones intersect in  $\Sigma_X$ , a facet-ordered poset [46, 47]. (2) Its transpolar,  $\Delta_X = (\Delta_X^*)^\nabla$  spans the (normal) multifan,  $(\nabla_X =: \Sigma_{\nabla_X}) \triangleleft (\Delta_X = \Delta_{\nabla_X}^*)$ , which analogously corresponds to a toric space,  $\nabla X$ , the transpolar of  $X$ . ─

**Remark 1.6 (orientation)** Each reflexive polytope is a continuously (and uniformly) orientable multihedral convex body and encodes (both ways) a toric (complex algebraic) variety with  $\text{Td}(X) = \chi^h(X) = 1$ , equal to the winding number of its fan,  $w(\Sigma_X) = 1$ . Each VEX multitope,  $\Delta_X^*$ , is also continuously orientable, but the relative orientation of adjacent faces changes sign by flip-folding to (partially) overlay [38]; for multitopes,  $w(\Sigma_X \triangleleft \Delta_X^*)$  may differ from 1. This  $\Delta_X^*$ -orientation chooses a Duistermaat–Heckman measure over the multifan  $\Sigma_X$  [47] (see also [71]), and corresponds to an omniorientation on  $X$  [48, 54, 74]. ─

**Remark 1.7 (obstructions)** While (plain) fans encode (complex algebraic) toric varieties [19–23] (see also [75, 76]), a general (multi-layered) multifan,  $\Sigma$ , does not uniquely encode a torus manifold [45–47], nor its (complex, symplectic, Kähler, etc.) structures: Adjacent cone intersections,  $(\sigma_1 \cap \sigma_2 = \tau) \in \Sigma$ , encode transition functions that glue local coordinate charts,  $U_{\sigma_1} \uplus_{U_\tau} U_{\sigma_2}$ . Toric spaces with a regular (unit-degree<sup>5</sup>) subdivided multifan are smooth, and often known to be (weakly) almost (pre)complex and/or (pre)symplectic, with a  $\mathbb{T}^n$ -equivariant generalization of characteristic classes [45–47]. In general however, chart-wise defined structures need not extend properly over the entire atlas  $\bigcup_{\sigma \in \Sigma} U_\sigma$ , thus enclosing respective obstructions in the so-constructed compact and topologically nontrivial toric spaces. ─

**Remark 1.8 (optimal models)** Remarkably many numerical consequences of Claim 1.1, Conjecture 1.1 and the above remarks extend, and uniformly, through combinatorial networks including reflexive polytopes and non-convex VEX multitopes, and merely by persistent inclusion of multitope orientation [38]. This suggests that Claim 1.1 and Conjecture 1.1 hold for some (co)homologically optimal pair of embedding/ambient toric spaces,  $(X, \nabla X)$  corresponding to  $(\Delta_X^*, \Delta_X)$ , with but mildly obstructed requisite structures.<sup>6</sup> ─

**Remark 1.9 (desingularization)** While a mirror model of certain hypersurfaces  $f^{-1}(0) \in X[c_1]$  is a desingularization of a finite quotient of the transposed hypersurface<sup>7</sup>,  $\text{Bl}[\mathbb{T}f^{-1}(0)/G]$  [26], the transposition mirror of  $f^{-1}(0) \subset X$  in (1.1) is simply its transposed anticanonical hypersurface,  $\mathbb{T}f^{-1}(0) \subset \nabla X$  [38, 39]: The transpolar embedding space,  $\nabla X$ , already includes the exceptional loci of MPCP-blowups (for each lattice-point in  $\Delta_X = \Delta_{\nabla_X}^*$ ) and so automatically encodes both the finite group quotients and the required desingularizations — even when these do not stem from a global finite group action. ─

Originally focused on mirror pairs of Calabi–Yau hypersurfaces (bottom “floor” in (1.1)), the transpolar map between VEX multitopes ( $\Delta_X^* \xleftrightarrow{\nabla} \Delta_X$ ) also implies a (transpolar) duality between the corresponding (optimal choice of) ambient toric spaces ( $X \leftrightarrow \nabla X$ , middle “floor” in (1.1)), and their respective anticanonical bundles (sheaves, or other appropriate generalization,  $\mathcal{K}_X^* \xleftrightarrow{\nabla} \mathcal{K}_{\nabla_X}^*$ , top “floor” in (1.1)), the total spaces of which are themselves non-compact Calabi–Yau spaces. The Calabi–Yau hypersurfaces in (1.1) are typically expected to admit complex, symplectic and (complexified and enlarged) Kähler structures, with some degree of degeneration/singularization being admissible in stringy applications [2, 8–11, 64]. This engenders the leeway mentioned in Remarks 1.7–1.8, a precise determination of which continues to evolve.

<sup>5</sup>The degree of a  $k$ -face is the  $k!$ -multiple of the  $k$ -volume,  $d(\theta^{(k)}) := k! \cdot \text{Vol}_k(\theta^{(k)})$  [27]. Faces  $\theta$  with  $d(\theta) > 1$  and the cones they span encode singular charts in the toric variety; their desingularization is encoded by the subdivision of the cone.

<sup>6</sup>Calabi–Yau hypersurfaces that do intersect such obstruction loci and, e.g., end up with no global Kähler structure and  $h^{1,1} = 0$ , may still be connected by conifold transition (continuously in the Gromov–Hausdorff topology [77]) to the more familiar models, and may well also be mirrors to rigid ( $h^{2,1} = 0$ ) models, where in turn the symplectic structure is obstructed.

<sup>7</sup>The transposition construction generalizes the original [78] and overlaps with the toric construction [27]. Originally framed for Landau–Ginzburg orbifolds (LGO), the construction extends by each LGO being a phase of a GLSM [12]; see [38, 39].

## 1.2 Main Results

Verified by explicit computations for all  $m \in \mathbb{Z}$  cases of transpolar pairs of VEX multitopes  $(F_m^{(n)}, \nabla F_m^{(n)})$  for  $n=2, 3, 4$ ,  $(E_m^{(n)}, \nabla E_m^{(n)})$  for  $n=2, 3$ , and many other (mostly  $n=2$ ) testing examples, the main claims motivated by the multifan/multitope computations herein may then be summarized as follows:

**Claim 1.2** *Each transpolar pair of  $n$ -dimensional multitopes,  $(\Delta_X^*, \Delta_X)$ , admits a continuous, global and mutually compatible orientation so the multitope/multifan computations of:*

1. Todd–Hirzebruch theorems and all other Chern invariants,
  2. the Cox divisor intersection numbers and their relation to Chern invariants,
  3. the Poincaré polynomials,  $P_\Delta(t) = \Phi_\Delta(t)/(1-t)^{n+1}$  with  $\Phi_\Delta(t) = \sum_{k=0}^n h_k t^k$  (both for  $\Delta = \Delta_X^*$  and for  $\Delta = \Delta_X$ ), and (with exceptions noted below) even Betti numbers,
- are all mutually consistent, and are consistent with independently computed results where available.<sup>8</sup>
4. Optimal transpolar pairs of toric spaces,  $X \xleftrightarrow{\nabla} \nabla X$  (Remark 1.8), encoded by transpolar pairs of VEX multitopes (and spanned multifans) admit requisite (pre)complex, (pre)Kähler, etc. structures and bundles/sheaves or suitable generalizations, as suggested by the above; see Remark 2.1, below.

Furthermore, including the complete deformation families of transposition mirror pairs of Calabi–Yau hypersurfaces of Conjecture 1.1:

5. The transpolar relations,  $\Delta_X^* = \Delta_{\nabla X}$  and  $\Delta_X = \Delta_{\nabla X}^*$ , imply some novel relations among the Chern invariants. For example, for  $n = \dim \Delta = 4$ :

$$C_3 C_1|_X = \sum_{\nu_{ijk} \in \Delta_X^*(3)} d(\nu_{ijk}) d(\nu_{ijk}^\nabla) \stackrel{\nabla}{=} \sum_{\mu_{IJ} \in \Delta_X(2)} d(\mu_{IJ}^\nabla) d(\mu_{IJ}) = C_2 C_1^2|_{\nabla X}; \quad (1.5)$$

$$\chi(Z_f) = C_2^2|_X - C_2^2|_{\nabla X} = -\chi(\tilde{Z}_{T_f}), \quad (1.6)$$

$$= 2(d(\Delta_X) - d(\Delta_X^*)) - 12(\ell(\Delta_X) - \ell(\Delta_X^*)). \quad (1.7)$$

6. The **Dehn–Sommerville relations** ( $h_i = h_{n-i}$ ) hold and imply, e.g., for  $n = \dim \Delta = 4$ :

$$\ell(3\Delta) = 5\ell(2\Delta) - 9\ell(\Delta) + 5, \quad \ell(4\Delta) = 15\ell(2\Delta) - 35\ell(\Delta) + 21, \quad (1.8)$$

$$d(\Delta) = \ell(2\Delta) - 3\ell(\Delta) + 2, \quad (1.9)$$

and for the Calabi–Yau hypersurfaces:

$$\chi(Z_f) = 2(\ell(2\Delta_X) - \ell(2\Delta_X^*)) - 18(\ell(\Delta_X) - \ell(\Delta_X^*)). \quad (1.10)$$

7. **Unimodality inequalities** ( $h_{i-1} \leq h_i$  for  $i=1, \dots, \lfloor n/2 \rfloor$ ) hold and imply, e.g., for  $n = \dim \Delta = 4$ :

$$d(\Delta) \geq 3\ell(\Delta) - 13, \quad \ell(2\Delta) \geq 6\ell(\Delta) - 15, \quad \text{i.e.,} \quad d(\Delta) \geq \frac{1}{2}\ell(2\Delta) - \frac{11}{2}. \quad (1.11)$$

The standard correspondence with Betti numbers [21, § 4.5] relates #6 to Poincaré duality, and #7 to the Hard Lefschetz Theorem and  $\text{SL}(2)$ -action on  $H^{q,q}$ .

**Remark 1.10** All statements of Claim 1.2 hold within the convex (and so reflexive) polytope subset of VEX multitopes, where  $X$  and  $\nabla X$  are both (weak/semi) Fano complex algebraic toric varieties. In turn, multi-layered multifans and their spanning multitopes do not fully specify the underlying toric spaces (statements 3 and 7 of Claim 1.2), nor the  $T^n$ -equivariant (co)homology and Betti numbers [45–47]; see

<sup>8</sup>For example, Hirzebruch scrolls are also realized, à la [79, 80], both as projective bundles,  $F_m^{(n)} = \mathbb{P}(\oplus_{i=1}^n \mathcal{O}_{\mathbb{P}^1}(m_i))$  and also as specific bi-projective hypersurfaces in the explicit deformation family  $F_m^{(n)} \in \left[ \begin{smallmatrix} \mathbb{P}^n \\ \mathbb{P}^1 \end{smallmatrix} \middle| \begin{smallmatrix} 1 \\ m \end{smallmatrix} \right]$ , with  $m = \sum_i m_i$  [38, 39, 41].

Remark 1.8, Conjecture 4.1 and other computations below for examples. Nevertheless, all of Claim 1.2 has been verified to hold throughout the infinite sequence of transpolar pairs of VEX multitopes  $(\Delta_{F_m}^*, \Delta_{F_m}^{(n)})$ , and only unimodality (statement 7 of Claim 1.2) and the standard correspondence with Betti numbers fail for some  $n$ -dependent ranges of  $m$  in the infinite sequence  $(\Delta_{E_m}^*, \Delta_{E_m}^{(n)})$ .  $\blacksquare$

**Remark 1.11** The Chern characteristic used herein, and in particular in (1.6), (1.7) and (1.10),

$$\chi(Z_f \in X^{(n)}[c_1]) = \int_{X^{(n)}} c_1 \left( \sum_{k=2}^{n-1} (-1)^{n-1-k} c_k c_1^{n-1-k} \right), \quad (1.12)$$

is guaranteed to compute the topological Euler characteristic of the generic Calabi–Yau hypersurface in the deformation family  $X^{(n)}[c_1]$  only when  $X^{(n)}$  is almost complex. If  $X^{(n)}$  is only precomplex (for  $n=2$  conditions, see [56]), the precise (certainly  $T^n$ -equivariant) identification of the characteristic (1.12) remains to be determined, but is expected to include “corrections” corresponding to the Calabi–Yau hypersurface intersection with the obstructions of the complex structure; see Remark 1.7.  $\blacksquare$

Finally, Conjecture 5.1 below concludes that the mirror-symmetric framework (1.1) pairs non-Fano complex algebraic varieties with precomplex toric spaces, where flip-folded regions in a multitope spanning the multifan of a toric space obstruct the complex structure. By mirror symmetry, concave regions in a multitope spanning the multifan of a toric space are then expected to obstruct its symplectic structure.

## 2 Todd–Hirzebruch Identities and Characteristic Classes

Involving transpolar multitope pairs,  $(\Delta_X^*, \Delta_X)$ , the Todd–Hirzebruch combinatorial identities correspond to applications of the Hirzebruch–Riemann–Roch (HRR) theorem [81].<sup>9</sup> They involve Chern classes ( $\Delta_X^*$ -data) and the anticanonical bundle/sheaf,  $\mathcal{K}_X^*$  ( $\Delta_X$ -data); the total space of  $\mathcal{K}_X^*$  being a (non-compact!) Calabi–Yau space is key in string theory [12, 13]. For non-Fano  $X$ , the entire system of holomorphic anticanonical sections may even factorize, forcing Calabi–Yau hypersurfaces to *reduce*,  $Z = Z_1 \cup Z_2$ , i.e., Tyurin-degenerate [82], with  $\text{Sing}(Z) = Z_1 \cap Z_2$  itself a (codimension-2 in  $X$ ) Calabi–Yau subspace. Even such “Constructive Calabi–Yau manifolds” [83] admit the transposition mirror model construction [26, 38, 39], and so provide a broader testbed for the so-called *DHT conjecture* [84–90]. In turn, many of these singular and degenerate models in fact may be smoothed by certain *Laurent deformations* [38, 39], and we verify that the various Todd–Hirzebruch identities and relevant Chern data calculations continue to hold.

To this end, we list a few key standard results about toric (complex algebraic) varieties [19–23], where to each 1-cone  $\nu_i \in \Sigma_X$  and  $\Delta_X^*$ -vertex there corresponds a divisor class,  $D_i$ , and its defining (Cox) coordinate,  $x_i$  [91]; see also [23, Thm. 12.4.4]. For the more general *torus manifolds* (many of which are only weakly almost complex or precomplex), those are  $T^n := U(1)^n$ -characteristic (codim $_{\mathbb{R}} = 2$ ) submanifolds and corresponding elements of  $T^n$ -equivariant cohomology, respectively [45–50].

### Key standard results:

- R.1 The Chern class [19, Prop. 11.4] [23, Prop. 13.1.2 (a)] (& [45, Thm. 3.1] for *torus manifolds*) of the toric space  $X$  encoded by the fan  $\Sigma_X$  with generator 1-cones  $\nu_i$  is  $c(T_X) = \prod_i (1 + D_i)$ .
- R.2 Expanding the product  $c(T_X)$  yields  $c_1(X) = c_1(T_X) = D = \sum_i D_i = -K_X$ , the cohomology class of the anticanonical divisor. More generally,

$$c(T_X) = \left[ 1 + \underbrace{\sum_i D_i}_{c_1} + \underbrace{\sum_{i < j} D_i D_j}_{c_2} + \underbrace{\sum_{i < j < k} D_i D_j D_k + \dots}_{c_3} \right]_{S.R.}, \quad (2.1)$$

<sup>9</sup>A suitable generalization may be needed to include *stratified pseudo-manifold* and other “defects”; see, e.g., [11, 64–67].

the summands subject to the multifan-encoded Stanley–Reisner ideal of relations between the  $D_i$ .

R.3 Corollary 11.5 [19]:  $c_k(X) = \sum_{\sigma \in \Sigma(k)} [F_\sigma]$ . That is, the  $k^{\text{th}}$  Chern class is generated by the (cohomology classes of the) subvarieties  $F_\sigma$  corresponding to the  $k$ -cones  $\sigma \in \Sigma_X$ .

R.4 Corollary 11.6 [19]:  $C_n(X) = \int_X c_n = |\Sigma_X(\dim(X))| = d(\Delta_X^*) = \chi(X)$ . Also,  $d(\Delta_X^*) = \chi(X)$  for convex polytopes, but *for multi-layered multitopes, only if  $X$  is almost complex* [45].

R.5 Statement 11.12.2 [19, ¶5.8]:  $[D]^n = C_1^n(X) = d(\Delta_X)$ , where  $\Delta_X = (\Delta_X^*)^\vee$  is the Newton polytope, the (external [22], i.e., internal [23]) normal fan of which is  $\Sigma_X$ .

**Remark 2.1** Chern and other characteristic classes as well as the HRR theorem are typically employed for compact complex manifolds. Related computations however routinely involve the so-called Whitney product formula (splitting principle), which involves a (much less rigid)  $C^\infty$  decomposition [80], allowing the classic extension to smooth manifolds [92]. The HRR theorem and associated moment maps for  $\mathbb{T}^n$ -equivariant line bundles are known to correspond large classes of (presymplectic) toric spaces to non-convex and flip-folding multitopes [60]. It is then perhaps not surprising to find that many related results from *complex algebraic* toric geometry in fact extend rather straightforwardly to the radically larger class of torus manifolds corresponding to (by definition continuously oriented) VEX multitopes. ▀

## 2.1 Todd–Hirzebruch Identities

Todd–Hirzebruch identities stem from the special case of the HRR theorem:

$$\text{Td}(X) = \chi^h(X) = \chi(X, \mathcal{O}_X) = \int_X \text{td}(X) (\text{ch}(\mathcal{O}_X) = e^{c_1(\mathcal{O}_X)=0} = 1), \quad (2.2)$$

which is identifiable with  $w(\Delta_X^*) = w(\Sigma_X)$ , the winding number of the spanning multitope and multifan of the toric space  $X$  [45–47]. We will need the standard results [81, 93]:

$$\text{td}_2 = \frac{1}{12}(c_2 + c_1^2), \quad \text{td}_4 = \frac{1}{720}(-c_4 + c_3c_1 + 3c_2^2 + 4c_2c_1^2 - c_1^4), \quad (2.3a)$$

$$\text{td}_3 = \frac{1}{24}(c_2c_1), \quad \text{td}_5 = \frac{1}{1440}(-c_4c_1 + c_3c_1^2 + 3c_2^2c_1 - c_2c_1^3), \quad \text{etc.} \quad (2.3b)$$

### 2.1.1 The 12-Theorem

Integrated, the expression for  $\text{td}_2$  in (2.3) easily produces

$$C_2(X) + C_1^2(X) = 12 \text{Td}(X), \quad (2.4)$$

known as the *Noether formula* [80] for complex algebraic surfaces, where  $\text{Td}(X) = \chi(\mathcal{O}_X)$ , and which simplifies in the (weak/semi) Fano case:  $\text{Td}(X) = 1$ . Using the results R.4 and R.5 above, this yields

**Theorem 2.1** (“12-Theorem”) *For all polar pairs of reflexive ( $M$  and  $N$ ) lattice polygons,  $(\Delta, \Delta^\circ)$ ,*

$$|\partial\Delta \cap M| + |\partial\Delta^\circ \cap N| = 12. \quad (2.5)$$

The evident  $\Delta \leftrightarrow \Delta^\circ$  symmetry is also key in Batyrev’s construction of mirror manifolds [27, 32], the related [30, 35–37] toric rendition of the transposition mirror model construction [26, 29, 33, 34], as well as in the VEX generalization (1.1) [38, 39]. This makes the 12-Theorem (2.5) and its higher-dimensional generalizations discussed below directly related to mirror symmetry (1.1).

Besides toric geometry and combinatorial exhaustion [23, Thm. 10.5.10], Ref. [57] proves (2.5) both by elementary geometry and using modular forms, and then generalizes the polar operation (1.4) and the 12-Theorem relation (2.5) to an infinite class of *generalized legal loops* ( $\mathcal{L}$ ). By definition consisting

of (orientation-signed) regular lattice edges with lattice-primitive endpoints<sup>10</sup>, each  $\mathcal{L}$  spans a regularly subdivided, complete multifan,  $\Sigma_{\mathcal{L}}$ . By Remark 1.5,  $\Sigma_{\mathcal{L}}$  corresponds to a smooth, compact toric space,  $X_{\mathcal{L}}$ : Just as in fans [20–23], chart-gluing encoding is *local* to cones (facets) that are adjacent within the multifan [45–51, 54, 55, 62]. A multifan may flip-fold and wind multiply around the origin, its winding number<sup>11</sup> equal to the Todd genus of the corresponding toric space [45, 51], multiplying the right-hand side of (2.5) by the winding number of the multifan [58].

Applied to any non-convex  $\mathcal{L}$ , the standard *polar* operation (1.4) computes  $(\text{Conv}(\mathcal{L}))^\circ$ , and so cannot possibly be involutive. The *duality* operation  $\mathcal{L} \rightarrow \mathcal{L}^\vee$  of Ref. [57] instead is involutive, each dual pair  $(\mathcal{L}, \mathcal{L}^\vee)$  does satisfy (2.5), but has no direct higher-dimensional generalization.<sup>12</sup> In turn, the *transpolar* Construction 1.1 applies in all dimensions, and is in two dimensions easily shown to coincide (up to a relative 90°-rotation) with the duality of Ref. [57]. Thus, transpolar pairs of two-dimensional VEX multitope [38] are identical to dual pairs of generalized legal loops, which then implies [57, 58]:

**Corollary 2.1** *For every transpolar pair of VEX multigons,  $(\Delta, \Delta^\nabla)$ , the 12-Theorem relation (2.5) holds after replacing the right-hand side by  $12 w(\Delta)$ , where  $w(\Delta) = w(\Delta^\nabla)$  is the winding number (effective multi-layeredness) of the multifans spanned by  $\Delta$  and  $\Delta^\nabla$ .*

For illustration, consider the two infinite sequences of examples in Figure 1 and Section 5.3. Vertices of the spanning multigons  $(\Delta^*)$  are labeled  $\nu_i$ , which then labels the connecting edges,  $\nu_{ij}$ , as well as their

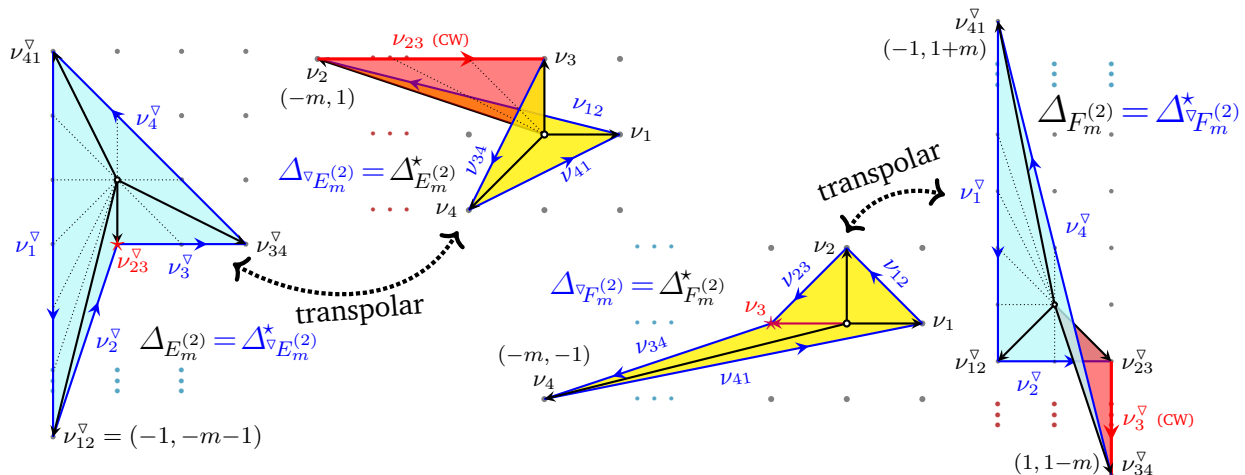


**Figure 1:** Two infinite sequences of transpolar (Construction 1.1) pairs of VEX multigons: with the orientation shown, the CW-oriented flip-folded facets  $\nu_{23} \subset \Delta_{E_m}^{*(2)}$  and  $\nu_{12}^\nabla \in \Delta_{F_m}^{(2)}$  are transpolar to a non-convex vertex

transpolar faces in the Newton multigons,  $\Delta := (\Delta^*)^\nabla$ :  $\nu_i^\nabla$  and  $\nu_{ij}^\nabla$ , respectively. The 12-Theorem formula may be recast:

$$d(\partial\Delta) + d(\partial\Delta^\nabla) = d(\Delta) + d(\Delta^\nabla) = 12 w(\Delta), \quad (2.6)$$

where the degree of the boundary of a multitope is the sum of the degrees of its facets, and  $w(\Delta) = 1$ . In all VEX (including reflexive) multitope, the degree of each facet equals the degree of the central pyramid (and also cone) over it, the sum of which is the degree of the total multitope (multifan), respectively. Negative orientation (in Figure 1 labeled “CW” and shaded red) renders the degree of a facet negative; counting

<sup>10</sup>The triangle from the lattice origin over each edge is *non-degenerate (primitive)*: it contains no lattice points other than those in the edge and the lattice origin [57] — in 2-dimensions, Definition 1.1 guarantees statement (2) of Conjecture 1.2.

<sup>11</sup>The (effective) winding number of a complete multifan is the (orientation-signed) multiplicity of its covering of the underlying real space, and is consistent with generalized Duistermaat–Heckman measure assignments [46, 47, 71].

<sup>12</sup>We thank B. Poonen for confirming this.

lattice points in a negatively oriented face is straightforward but decidedly less intuitive [38]; see also § 5.3. Not only does (2.6) hold for all multigons (generalized legal loops) with both CCW- and CW-oriented edges [57], but this orientation-depending count straightforwardly generalizes to higher dimensions [38], is interpretable as a signed multiplicity, and is consistent with a choice of a generalized Duistermaat–Heckman measure; see for example [47, 60]. Such a measure also governs the computation of tropical periods on the Calabi–Yau hypersurfaces in so-defined toric spaces [71].

The illustrations in Figure 1 thus exemplify the necessity of orientation-dependent sign of facet degrees for the 12-Theorem to hold: Indeed, reading directly from the diagrams (for all  $m \in \mathbb{Z}$ ):

$$[d(\Delta_{E_m^{(2)}}^* = 1+(-m)+1+1)] + [d(\Delta_{E_m^{(2)}} = (3+m)+1+2+3)] = 12. \quad (2.7a)$$

$$[d(\Delta_{F_m^{(2)}}^* = 1+1+1+1)] + [d(\Delta_{F_m^{(2)}}^* = (2+m)+2+2+(2-m))] = 12. \quad (2.7b)$$

With  $-3 \leq m \leq 0$  for  $E_m^{(2)}$  and  $|m| \leq 2$  for  $F_m^{(2)}$ , all facets are positively oriented and these (now convex) polytope pairs reproduce 11 of the 16 reflexive polytopes;  $\Delta_{E_{-3}^{(2)}}^* = \Delta_{E_{-3}^{(2)}}$ ,  $F_{-m}^{(2)} \approx F_m^{(2)}$  and  $E_{-1}^{(2)} \approx F_{\pm 1}^{(2)}$ . Outside these values of  $m$ , one of the multigons in each transpolar pair has a flip-folded edge (transpolar to a concave vertex) which contributes negatively, and exactly maintains the overall sum (2.7).

Each multigon in Figure 1 spans a multifan with a regular subdivision<sup>13</sup> and so corresponds to a compact smooth toric space, in fact a torus manifold [47]. Since  $\Delta_{E_m^{(2)}}^*$  for  $m > 0$  and  $\Delta_{F_m^{(2)}}^*$  for  $m > 2$  are *plain* but non-convex polytopes, they encode non-Fano toric (complex algebraic) varieties,  $\nabla E_m^{(2)}$  and  $F_m^{(2)}$ , respectively. Since their transpolars,  $\Delta_{E_m^{(2)}}^*$  and  $\Delta_{F_m^{(2)}}^*$ , are *flip-folded* multitopes, they correspond to torus manifolds,  $E_m^{(2)}$  and  $\nabla F_m^{(2)}$ , which are not complex algebraic varieties; see below. Since the (effective) winding number of each so-spanned multifan equals 1, so is the Todd genus. Of these, the Hirzebruch surfaces  $F_m^{(2)}$  are well known to admit a global complex structure for all  $m \in \mathbb{Z}$ ,  $\Delta_{F_m^{(2)}}^*$  being a plain polytope: its non-convexity for  $|m| \geq 3$  implies  $c_1(F_m^{(2)}) \not\geq 0$ . Other among these toric spaces ( $\nabla F_m^{(2)}$  for  $|m| \geq 3$ ,  $E_m^{(2)}$  for  $m \geq 1$  and  $\nabla E_m^{(2)}$  for  $m \leq -4$ ) admit only a *precomplex* structure, with a real codimension-2 obstruction to a global complex structure; see Conjecture 5.1 and footnote 31 (p. 36), below, and also [56].

### 2.1.2 Higher-Dimensional Todd–Hirzebruch Identities

The 3-dimensional case of (2.3) provides

$$24 \operatorname{Td}(X) = \int_X c_1 c_2 = C_1 C_2(X). \quad (2.8)$$

Writing  $c(X) = 1 + c_1 + c_2 + c_3$ , the Chern class of the anticanonical hypersurface,

$$c(X[c_1]) = \left[ \frac{1 + c_1 + c_2 + c_3}{1 + c_1} \right]_{\deg \leq 2} = 1 + (0) + (c_2), \quad (2.9)$$

identifies  $c_2(X[c_1]) = c_2(X)$ . Since  $c_1(X)$  pulls back anticanonical hypersurface integrals to  $X$ , the Todd–Hirzebruch identity (2.8) implies

$$\dim(X) = 3 : \quad 24 \operatorname{Td}(X) = 24 = \int_X c_1 c_2 = \int_{X[c_1]} c_2 = \chi(X[c_1]). \quad (2.10)$$

This is consistent with anticanonical hypersurfaces  $X[c_1]$  being K3 surfaces as long as  $\operatorname{Td}(X) = 1$ . This is true for all semi-Fano toric (complex algebraic) 3-folds  $X$ , but also includes the much more plentiful torus manifolds corresponding to flip-folded multifans with winding number  $w(\Sigma_X) = 1$ ; see below. The

<sup>13</sup>In higher dimensions, this may well involve diverse choices, which enriches the emerging structures.

identity (2.8) involves a Chern invariant,  $C_1 C_2(X)$ , which is not readily identified among the key standard results R.1–R.5 listed above.

In four dimensions,

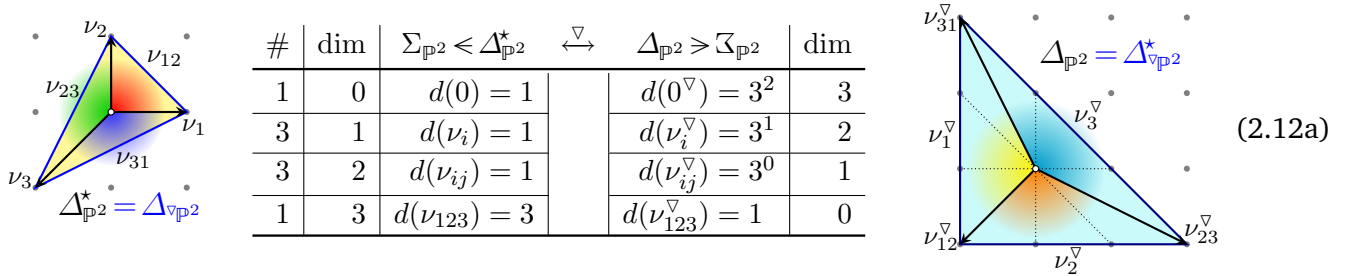
$$\dim(X) = 4: \quad 720 \operatorname{Td}(X) = \int_X (-c_4 + c_3 c_1 + 3c_2^2 + 4c_2 c_1^2 - c_1^4) \quad (2.11)$$

involves three additional Chern invariants, which are not readily identified within the key standard results R.1–R.5 above in terms of the corresponding multitope, i.e., the multifan it spans,  $\Delta_X^* \triangleright \Sigma_X$ . We now turn to find such concrete identifications and so verify the extension of the key standard results R.2–R.3 to VEX multitopes.

## 2.2 Chern Classes and Invariants

### 2.2.1 Two Dimensions

**The Template,  $\mathbb{P}^2$ :** For orientation and following the notation of Figure 1, consider the well-known case of  $\mathbb{P}^2$ , where the cones encoded in the polar pair of the “spanning” and Newton polytopes,  $(\Delta_{\mathbb{P}^2}^*, \Delta_{\mathbb{P}^2})$ , and the (plain, complete) fans they span may be tabulated as follows:



The 0-dimensional cone is the lattice origin itself, while  $\nu_{123} := \triangleleft \Delta_{\mathbb{P}^2}^*$  is the 3-dimensional cone over  $\Delta_{\mathbb{P}^2}^*$  encoding the anticanonical bundle,  $\mathcal{K}_{\mathbb{P}^2}^* = \mathcal{O}_{\mathbb{P}^2}(3)$ , so the tabulation (2.12a) provides:

$$C_1^2(\mathbb{P}^2) = \sum_{\nu_* \in \Sigma(0)} d(\nu_*) d(\nu_*^\nabla) = 1 \times (1) \cdot (3^2) = 9 = 3 \times (1) \cdot (3^1) = \sum_{\nu_* \in \Sigma(1)} d(\nu_*) d(\nu_*^\nabla); \quad (2.12b)$$

$$C_2(\mathbb{P}^2) = \sum_{\nu_* \in \Sigma(2)} d(\nu_*) d(\nu_*^\nabla) = 3 \times (1) \cdot (3^0) = 3 = 1 \times (3) \cdot (1) = \sum_{\nu_{123} = \triangleleft \Sigma} d(\nu_{123}) d(\nu_{123}^\nabla), \quad (2.12c)$$

which clearly satisfy the 12-Theorem (2.5).

The right-hand side fan  $(\Sigma_{\mathbb{P}^2} = \Sigma_{\nabla \mathbb{P}^2}) \triangleleft \Delta_{\mathbb{P}^2}$  in (2.12a) encodes  $\nabla \mathbb{P}^2$ , the transpolar of  $\mathbb{P}^2$ . Its top-dimensional cones all have degree  $d(\nu_i^\nabla) = 3$  and encode  $\mathbb{C}^2/\mathbb{Z}_3$ -like charts; their subdivision into three regular (sub)cones each identify  $\nabla \mathbb{P}^2$  as the (six-fold) MPCP-desingularization blowup of  $\mathbb{P}^2/\mathbb{Z}_3$  [27]. Swapping the roles of the polygons in (2.12b) and (2.12c) identifies:

$$C_2(\nabla \mathbb{P}^2) = \chi(\nabla \mathbb{P}^2) = 9 \quad \text{and} \quad C_1^2(\nabla \mathbb{P}^2) = 3. \quad (2.13)$$

The first of these is easy to verify:  $\chi(\operatorname{Bl}[\mathbb{P}^2/\mathbb{Z}_3]) = \frac{1}{|\mathbb{Z}_3|} (\chi(\mathbb{P}^2) - \chi(\{3\text{pts.}\})) + \sum_i \chi(E_i) = 9$ , since the exceptional set in each chart is  $E_i \approx (\mathbb{P}^1 \#_1 \mathbb{P}^1)$ , a 1-point connected union (plum-product) of two  $\mathbb{P}^1$ 's.

**Hirzebruch Scrolls:** Consider the right-hand side examples in Figure 1, the  $m$ -sequence of Hirzebruch surfaces,  $F_m^{(2)}$ , with  $m \in \mathbb{Z}$ . Here,  $d(\nu_3^\nabla) < 0$  for  $m \geq 3$  and  $d(\nu_1^\nabla) < 0$  for  $m \leq -3$ , so the corresponding facet of  $\Delta_{F_m^{(2)}}$  and the cone over it become CW-oriented, opposite of the other (CCW) facets.

dim	$\Sigma_{F_m^{(2)}} \triangleleft \Delta_{F_m^{(2)}}^*$	$\xleftrightarrow{\nabla}$	$\Delta_{F_m^{(2)}} \triangleright \mathfrak{Z}_{F_m^{(2)}}$	dim	$\sum d(\nu_*)d(\nu_*^\nabla)$
0	$d(0) = 1$		$d(0^\nabla) = 8$	3	$\rightarrow 8$
1	$d(\nu_1) = 1$ $d(\nu_2) = d(\nu_4) = 1$ $d(\nu_3) = 1$		$d(\nu_1^\nabla) = 2+m$ $d(\nu_2^\nabla) = d(\nu_4^\nabla) = 2$ $d(\nu_3^\nabla) = 2-m$	2	$\rightarrow 2+m$ $\rightarrow 2 \times 2$ $\rightarrow 2-m$ } $8 = C_1^2(F_m^{(2)})$
2	$d(\nu_{i,i+1}) = 1$		$d(\nu_{i,i+1}^\nabla) = 1$	1	$\rightarrow 4 \times 1$ $4 = C_2(F_m^{(2)})$
3	$d(\nu_{1234}) = 4$		$d(\nu_{1234}^\nabla) = 1$	0	$\rightarrow 4$

**Table 1:** The cones and their degrees, spanned by the transpolar pair  $(\Delta_{F_m^{(2)}}^*, \Delta_{F_m^{(2)}})$

Not only does the transpolar pair  $(\Delta_{F_m^{(2)}}^*, \Delta_{F_m^{(2)}})$  clearly satisfy the Todd–Hirzebruch “12-theorem” (2.6) for all  $m \in \mathbb{Z}$ , but the individual Chern numbers,

$$C_2(F_m^{(2)}) = \sum_{\nu_{ij} \in \Sigma(2)} d(\nu_{ij}) d(\nu_{ij}^\nabla) = 4 = d(\Delta_{F_m^{(2)}}^*), \quad (2.14a)$$

$$C_1^2(F_m^{(2)}) = \sum_{\nu_i \in \Sigma(1)} d(\nu_i) d(\nu_i^\nabla) = 8 = d(\Delta_{F_m^{(2)}}), \quad (2.14b)$$

also agree with key standard results R.4 and R.5, as well as the independent and standard computation done, e.g., for the bi-projective embedding,  $F_m^{(2)} = \{x_0y_0^m + x_1y_1^m = 0\}$  in  $\mathbb{P}^2 \times \mathbb{P}^1$  [79]. Moreover, Table 1 shows that the results (2.14) hold *if and only if* the degree of the facet  $\nu_1^\nabla \subset \Delta_{F_m^{(2)}}^*$  grows negative for  $m \geq 3$  [38]. The Euler number of Hirzebruch surfaces is indeed  $C_2(F_m^{(2)}) = \chi(F_m^{(2)}) = 4$ , for all  $m \in \mathbb{Z}$ .

Reversing the roles of the multitopes  $\Delta_{F_m^{(2)}}^* \xleftrightarrow{\nabla} (\Delta_{F_m^{(2)}} = \Delta_{F_m^{(2)}}^*)$  and the multifans they span, we learn about  $\nabla F_m^{(2)}$ , the *transpolar* of the Hirzebruch surfaces:  $C_1^2(\nabla F_m^{(2)}) = 4$  and  $C_2(\nabla F_m^{(2)}) = 8$ . The top-dimensional cones of  $\Sigma_{\nabla F_m^{(2)}} \triangleleft \Delta_{\nabla F_m^{(2)}}^*$  (right-most diagram in Figure 1), are all regularly subdivided, so that  $\nabla F_m^{(2)}$  are smooth. For  $|m| \leq 2$ ,  $\nabla F_m^{(2)}$  are (complex algebraic) toric varieties, but (only precomplex, possibly weakly complex) torus manifolds for  $|m| \geq 3$  since  $\Delta_{\nabla F_m^{(2)}}^*$  is flip-folded.

**The  $E_m^{(2)}$  Sequence:** The analogous computations also hold for  $E_m^{(2)}$  (left-hand half in Figure 1), for all<sup>14</sup>  $m \in \mathbb{Z}$ : While we do not have an independent verification of  $C_1^2(E_m^{(2)}) = d(\Delta_{E_m^{(2)}})$  and  $C_2(E_m^{(2)}) = d(\Delta_{E_m^{(2)}}^*)$ ,

dim	$\Sigma_{E_m^{(2)}} \triangleleft \Delta_{E_m^{(2)}}^*$	$\xleftrightarrow{\nabla}$	$\Delta_{E_m^{(2)}} \triangleright \mathfrak{Z}_{E_m^{(2)}}$	dim	$\sum d(\nu_*)d(\nu_*^\nabla)$
0	$d(0) = 1$		$d(0^\nabla) = 9+m$	3	$\rightarrow 9+m$
1	$d(\nu_1) = 1$ $d(\nu_2) = 1$ $d(\nu_3) = 1$ $d(\nu_4) = 1$		$d(\nu_1^\nabla) = 3+m$ $d(\nu_2^\nabla) = 1$ $d(\nu_3^\nabla) = 2$ $d(\nu_4^\nabla) = 3$	2	$\rightarrow 3+m$ $\rightarrow 1$ $\rightarrow 2$ $\rightarrow 3$ } $9+m = C_1^2(E_m^{(2)})$
2	$d(\nu_{i,i+1}) = 1, i \neq 2$ $d(\nu_{23}) = -m$		$d(\nu_{i,i+1}^\nabla) = 1$ $d(\nu_{23}^\nabla) = 1$	1	$\rightarrow 3 \times 1$ $\rightarrow -m$ } $3-m = C_2(E_m^{(2)})$
3	$d(\nu_{1234}) = 3-m$		$d(\nu_{1234}^\nabla) = 1$	0	$\rightarrow 3-m$

**Table 2:** The cones and their degrees, spanned by the transpolar pair  $(\Delta_{E_m^{(2)}}^*, \Delta_{E_m^{(2)}})$

we note that Table 2 does verify the consistency relations [38]:

$$\sum_{\nu_* \in \Sigma(0)} d(\nu_*) d(\nu_*^\nabla) = \sum_{\nu_* \in \Sigma(1)} d(\nu_*) d(\nu_*^\nabla) \quad \text{and} \quad \sum_{\nu_* \in \Sigma(2)} d(\nu_*) d(\nu_*^\nabla) = \sum_{\nu_* \in \Sigma(3)} d(\nu_*) d(\nu_*^\nabla), \quad (2.15)$$

<sup>14</sup>For simplicity of the discussion and computations, we omit the special cases  $m = 0, -3$ , when these quadrangular multitopes reduce to triangles, encoding the well known  $E_0^{(2)} = \mathbb{P}^2$  and  $E_{-3}^{(2)} = \mathbb{P}_{(1:2:3)}^2$ . In turn,  $E_1^{(2)}$  is discussed briefly in [47], while  $E_{-1}^{(2)} = F_1^{(2)}$  is a 1-point blowup of  $\mathbb{P}^2$  and  $E_{-2}^{(2)}$  its (secondary) blowup.

which also holds in Table 1. This is guaranteed since both multifans, spanned respectively by the transpolar pair of multitopes,  $\Sigma_X \triangleleft \Delta_X^*$  and  $(\mathfrak{I}_X = \Sigma_{\nabla X}) \triangleleft (\Delta_X = \Delta_{\nabla X}^*)$ , have a regular stellar subdivision, i.e., both corresponding toric spaces  $X$  and  $\nabla X$  are smooth, torus manifolds.

Just as for  $\Delta_{\mathbb{P}^2} = \Delta_{\nabla \mathbb{P}^2}^*$ , the indicated regular subdivisions in the multitopes in Figure 1 encode the MPCP-desingularizations in the toric spaces  $E_m^{(2)}$ ,  $\nabla E_m^{(2)}$  and  $\nabla F_m^{(2)}$ . However, since the degrees of the (unsubdivided) top-dimensional cones differ, the ‘‘MPCP contraction’’ of these toric spaces (where the exceptional sets encoded by the subdivisions collapse to a point each) are not global finite quotients.

With the multitope-orientation signed degree function, we find that the key standard results R.4 and R.5 above hold much more generally:

**Claim 2.1** *A transpolar pair of  $n$ -dimensional VEX multitopes,  $(\Delta_X^*, \Delta_X)$ , and the multifans they span,  $(\Sigma_X, \mathfrak{I}_X)$ , correspond to a transpolar pair of toric spaces,  $(X, \nabla X)$  by identifying  $\Delta_{\nabla X}^* := \Delta_X$ ,  $\Delta_{\nabla X} := \Delta_X^*$ , i.e.,  $\Sigma_{\nabla X} := \mathfrak{I}_X$  and  $\mathfrak{I}_{\nabla X} := \Sigma_X$ , such that:*

$$C_1^n(X) = d(\Delta_X = \Delta_{\nabla X}^*) = C_n(\nabla X) \quad \text{and} \quad C_n(X) = d(\Delta_X^* = \Delta_{\nabla X}) = C_1^n(\nabla X). \quad (2.16)$$

### 2.2.2 Three Dimensions

**Hirzebruch Scrolls:** Without further ado, the 3-dimensional analogue of Hirzebruch surfaces was analyzed in Ref. [38], and we simply tabulate the cones and degrees of its transpolar pair of multifans in Table 3; see also Figure 8 in Appendix A.1. The degree of each non-simplex (but *flat*<sup>15</sup>) cone has been computed

dim	$\Sigma_{F_m^{(3)}} \triangleleft \Delta_{F_m^{(3)}}^*$	$\xleftrightarrow{\nabla}$	$\Delta_{F_m^{(3)}} \triangleright \mathfrak{I}_{F_m^{(3)}}$	dim	$\sum d(\nu_*)d(\nu_{\nabla}^*)$
0	$d(0) = 1$		$d(0^{\nabla}) = 54$	4	$\rightarrow 54$
1	$d(\nu_1) = 1$ $d(\nu_2) = d(\nu_3) = 1$ $d(\nu_4) = d(\nu_5) = 1$		$d(\nu_1^{\nabla}) = 12 - 6m$ $d(\nu_2^{\nabla}) = d(\nu_3^{\nabla}) = 12 + 3m$ $d(\nu_4^{\nabla}) = d(\nu_5^{\nabla}) = 9$	3	$\rightarrow 12 - 6m$ $\rightarrow 2(12 + 3m)$ $\rightarrow 2 \times 9$ } $54 = C_1^3(F_m^{(3)})$
2	$d(\nu_{12}) = d(\nu_{13}) = 1$ $d(\nu_{ij})^* = 1$ $d(\nu_{23}) = 1$		$d(\nu_{12}^{\nabla}) = d(\nu_{13}^{\nabla}) = 2 - m$ $d(\nu_{ij}^{\nabla})^* = 3$ $d(\nu_{23}^{\nabla}) = 2 + 2m$	2	$\rightarrow 2(2 - m)$ $\rightarrow 6 \times 3$ $\rightarrow 2 + 2m$ } $24 = C_2 C_1(F_m^{(3)})$
3	$d(\nu_{ijk})^{\diamond} = 1$		$d(\nu_{ijk}^{\nabla})^{\diamond} = 1$	1	$\rightarrow 6 \times 1$ } $6 = C_3(F_m^{(3)})$
4	$d(\nu_{1\dots 5}) = 6$		$d(\nu_{1\dots 5}^{\nabla}) = 1$	0	$\rightarrow 6$

\* for  $(ij) = 14, 15, 24, 25, 34, 35$ ;  $\diamond$  for  $(ijk) = 412, 423, 431, 521, 532, 513$ ; ordering encodes orientation

**Table 3:** The cones and their degrees, spanned by the transpolar pair  $(\Delta_{F_m^{(3)}}^*, \Delta_{F_m^{(3)}})$  as specified in [38]

in several simplex subdivisions, verifying that they all produce the same result; see [38] for details. The tabulated degrees clearly satisfy the ‘‘24-Theorem’’ (2.8), and also reproduce the individual Chern characteristic results obtained for the bi-projective embedding,  $F_m^{(3)} \in [\mathbb{P}^3 | \mathbb{P}^1]_m$ . Moreover, these results evidently hold *precisely if* the degrees of the cones  $\nu_1^{\nabla}, \nu_{12}^{\nabla}, \nu_{13}^{\nabla} \subset \mathfrak{I}_{F_m^{(3)}}$  are negative for  $m \geq 3$  — exactly as argued in Ref. [38]. Since  $\nabla F_m^{(3)}$  is defined so  $\Delta_{\nabla F_m^{(3)}}^* = \Delta_{F_m^{(3)}}$  and *vice versa*,  $\Delta_{\nabla F_m^{(3)}} = \Delta_{F_m^{(3)}}^*$ , we learn that:

$$C_1^3(\nabla F_m^{(3)}) = d(\Delta_{\nabla F_m^{(3)}}) = 6 = d(\Delta_{F_m^{(3)}}^*) = C_3(F_m^{(3)}), \quad (2.17a)$$

$$C_3(\nabla F_m^{(3)}) = d(\Delta_{\nabla F_m^{(3)}}^*) = 54 = d(\Delta_{F_m^{(3)}}) = C_1^3(F_m^{(3)}). \quad (2.17b)$$

<sup>15</sup>A lattice  $k$ -dimensional cone is *flat* if its lattice-primitive generators (defining its base) lie in a  $(k-1)$ -plane.

Finally, swapping  $\Delta_{F_m^{(3)}}^* \leftrightarrow \Delta_{F_m^{(3)}}$ :

$$C_2 C_1(\nabla F_m^{(3)}) = 24 = C_2 C_1(F_m^{(3)}), \quad (2.17c)$$

corroborates that  $\nabla F_m^{(3)}[c_1]$  is also a family of K3 surfaces. The  $\dim = 2$  summation in the middle rows of Table 3 exactly reproduces Batyrev’s Euler characteristic formula [27, 94] for  $X = F_m^{(3)}$ :

$$\chi(\hat{Z}_f) = \sum_{k=1}^{\dim X - 2} (-1)^{k-1} \sum_{\substack{\dim(\theta)=k \\ \theta \subset \Delta_X}} d(\theta) d(\theta^*) = \sum_{\nu \subset \Sigma(2)} d(\nu) d(\nu^\nabla) \quad (2.18)$$

since  $\dim F_m^{(3)} = 3$  and  $\dim(\nu) = d(\theta) + 1$  for  $\nu = \triangleleft \theta$ .

**The  $E_m^{(3)}$  Sequence:** Consider the  $m > 0$  infinite sequence of transpolar pairs of 3-dimensional multitope analogues of the multigons in the left-hand half of Figure 1, the  $m = 2$  case shown in Figure 2. The

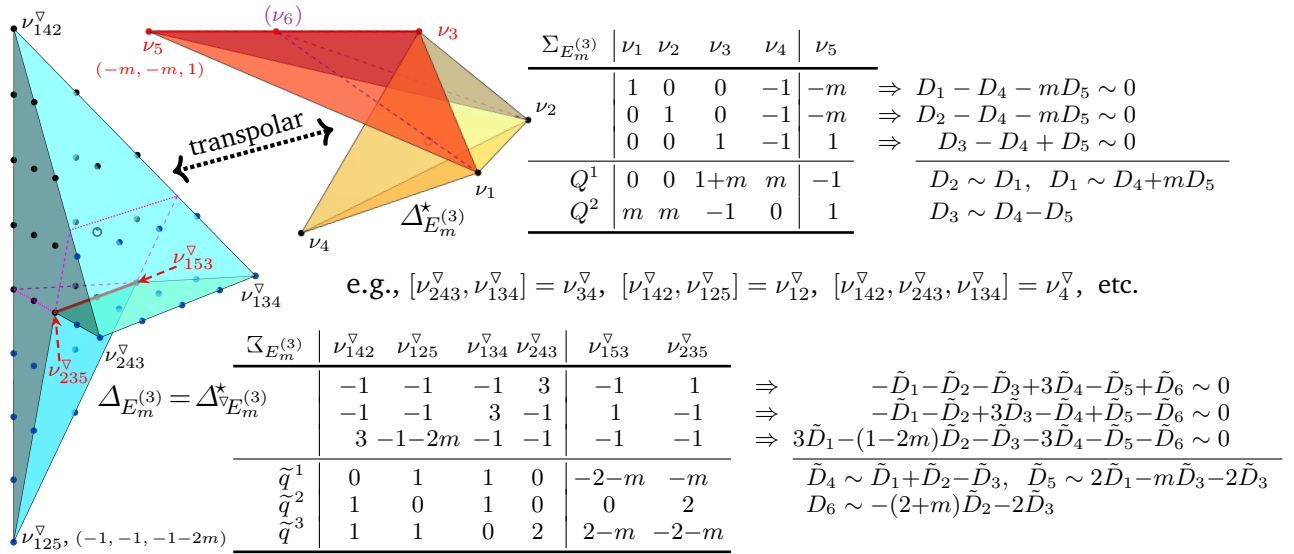


**Figure 2:** The non-convex VEX polytope  $\Delta_{E_m^{(3)}}$  (far left) and its transpolar multitope,  $\Delta_{E_m^{(3)}}^*$  (mid-left, top), their vertex systems, (proto) Mori vectors and the so-implied equivalences among the Cox divisors

(continuous) orientation of the top-dimensional cones is encoded by the order of the multi-index: e.g.,  $\nu_{142}$  and  $\nu_{134}$  are oriented positively<sup>16</sup> (away from the origin). Transporting this orientation continuously along the surface of  $\Delta_{E_m^{(3)}}^*$  orients  $\nu_{153}$  and  $\nu_{235}$  (shaded red) negatively (towards the origin) — and then  $\nu_{125}$  again positively. Counting with this signed multiplicity, every direction is covered effectively once, so  $w(\Sigma_{E_m^{(3)}}) = 1$  [45–47]. Its transpolar,  $\Delta_{E_m^{(3)}}$ , is a plain polytope, uniformly orientable away from the origin, but non-convex at the  $[\nu_{235}^{\nabla}, \nu_{153}^{\nabla}] = \nu_{35}^{\nabla}$  edge and the two adjacent facets.

The cones and their degrees, listed in Table 4, not only satisfy the “24-Theorem” (2.8) but also compute the two remaining Chern numbers:

$$C_1^3(E_m^{(3)}) = d(\Delta_{E_m^{(3)}}) = 64 + 8m = d(\Delta_{E_m^{(3)}}^*) = C_3(\nabla E_m^{(3)}), \quad (2.19)$$

$$C_3(E_m^{(3)}) = d(\Delta_{E_m^{(3)}}^*) = 4 - 2m = d(\Delta_{E_m^{(3)}}) = C_1^3(\nabla E_m^{(3)}), \quad (2.20)$$

<sup>16</sup>Stacking the vertex-vectors in the given order associates to each simplicial cone a square matrix, the determinant of which is the signed degree of the cone:  $d(\nu_{142}) = \det \begin{bmatrix} 1 & -1 & 0 \\ 0 & -1 & 1 \\ 0 & -1 & 0 \end{bmatrix} = 1$ ,  $d(\nu_{125}) = \det \begin{bmatrix} 1 & 0 & -m \\ 0 & 1 & -m \\ 0 & 0 & 1 \end{bmatrix} = 1$ , but  $d(\nu_{153}) = \det \begin{bmatrix} 1 & -m & 0 \\ 0 & -m & 0 \\ 0 & 1 & 1 \end{bmatrix} = -m$ , etc. Cones over non-simplex faces in a multitope are subdivided simplicially and the sub-cone degrees added; this sum does not depend on the choice of the subdivision [38]. In three dimensions, this sign agrees with the (quicker) right-hand rule.

dim	$\Sigma_{E_m^{(3)}} \triangleleft \Delta_{E_m^{(3)}}^*$	$\xleftrightarrow{\nabla}$	$\Delta_{E_m^{(3)}} \triangleright \mathfrak{Z}_{E_m^{(3)}}$	dim	$\sum d(\nu_*)d(\nu_*^\nabla)$
0	$d(0) = 1$		$d(0^\nabla) = 64+8m$	4	$\rightarrow 64+8m$
1	$d(\nu_1) = d(\nu_2) = 1$ $d(\nu_3) = 1$ $d(\nu_4) = 1$ $d(\nu_5) = 1$		$d(\nu_1^\nabla) = d(\nu_2^\nabla) = 16+4m$ $d(\nu_3^\nabla) = 12$ $d(\nu_4^\nabla) = 16$ $d(\nu_5^\nabla) = 4$	3	$\rightarrow 2(16+4m)$ $\rightarrow 12$ $\rightarrow 16$ $\rightarrow 4$
2	$d(\nu_{12}) = 1$ $d(\nu_{ij})^* = 1$ $d(\nu_{k4})^\diamond = 1$ $d(\nu_{35}) = -m$		$d(\nu_{12}^\nabla) = 4+2m$ $d(\nu_{ij}^\nabla)^* = 2$ $d(\nu_{k4}^\nabla)^\diamond = 4$ $d(\nu_{35}^\nabla) = 2$	2	$\rightarrow 4+2m$ $\rightarrow 4 \times 2$ $\rightarrow 3 \times 4$ $\rightarrow -2m$
3	$d(\nu_{ijk})^\natural = 1$ $d(\nu_{153}) = d(\nu_{235}) = -m$		$d(\nu_{ijk}^\nabla)^\natural = 1$ $d(\nu_{234}^\nabla) = d(\nu_{253}^\nabla) = 1$	1	$\rightarrow 4 \times 1$ $\rightarrow 2(-m)$
4	$d(\nu_{1\dots 5}) = 4-2m$		$d(\nu_{1\dots 5}^\nabla) = 1$	0	$\rightarrow 4-2m$

\* for  $(ij) = 13, 15, 23, 25$ ;  $\diamond$  for  $k = 1, 2, 3$ ;  $\natural$  for  $(ijk) = 142, 125, 134, 243$ ; ordering encodes orientation

**Table 4:** The cones spanned by the transpolar pair  $(\Delta_{E_m^{(3)}}^*, \Delta_{E_m^{(3)}})$  and their degrees

satisfying the key standard results R.4 and R.5 above, — and precisely because of the orientation-dependent signed degree values. Again,  $C_2C_1(E_m^{(3)}) = 24 = C_2C_1(\nabla E_m^{(3)})$  holds by simply swapping  $\Delta_{E_m^{(3)}}^* \leftrightarrow \Delta_{E_m^{(3)}}$ , and is consistent with  $(E_m^{(3)}[c_1], \nabla E_m^{(3)}[c_1])$  being deformation families of K3 surface mirrors.

**Remark 2.2** All tables of cone-degrees, in (2.12a), Tables 1, 2, 3 and 4 verify

$$\sum_{\nu \in \Sigma(0)} d(\nu)d(\nu^\nabla) = \sum_{\nu \in \Sigma(1)} d(\nu)d(\nu^\nabla) \quad \text{and} \quad \sum_{\nu \in \Sigma(n)} d(\nu)d(\nu^\nabla) = \sum_{\triangleleft \Sigma} d(\Sigma)d(\Sigma^\nabla), \quad (2.21)$$

for  $n = \dim \Sigma_X$ . This follows from the defining fact that each VEX multitope,  $\Delta$ , admits a star-triangulation that spans its multifan. The degree of the whole multitope,  $d(\Delta)$ , then equals the sum of the degrees of the lattice-primitive star-pyramids over its facets.  $\blacksquare$

### 2.2.3 Four Dimensions

**Hirzebruch Scrolls:** The CY 3-folds  $X_m^{(3)} \subset F_m^{(4)}$  have been analyzed in [38], where Batyrev’s formula (2.18) was found to confirm the direct Chern class computation. The relevant data is summarized here in Table 5, completed with  $d(\nu_*^\nabla)$ , which we compute using a simplicial subdivision as needed. We compare the row-computations in Table 5 with the explicit computation a Calabi–Yau hypersurface in any 4-fold:

$$c(X^4[c_1]) = \left\lfloor \frac{1+c_1+c_2+c_3+c_4}{1+c_1} \right\rfloor_{\leq \deg 3} = 1 + c_2 + (c_3 - c_2c_1); \quad (2.22a)$$

$$\chi(X^4[c_1]) = \int_{X^4} c_1 \cdot c(V^4[c_1]) = [C_3C_1 - C_2C_1^2]_X, \quad (2.22b)$$

as well as the specific case of  $X^4 = F_m^{(4)}$ . To this end, We note that for all  $F_m^{(n)} \in [\mathbb{P}^n \parallel \mathbb{P}^1 \parallel \mathbb{P}^1]$ , the identity  $\frac{(1+J_1)^2}{(1+J_1+mJ_2)} = 1 + J_1 - mJ_2$  is implied by  $J_2^2 = 0$ . Therefore,

$$\frac{(1+J_1)^{n+1}(1+J_2)^2}{(1+J_1+mJ_2)} = (1+J_1)^{n-1}(1+J_2)^2(1+J_1-mJ_2), \quad (2.23)$$

identifying the Mori (charge) vectors in the toric realization of  $F_m^{(n)}$  [38, Eq. (33)]. For  $F_m^{(4)}$  in particular, we identify:

$$c_1 = 4J_1 + (2-m)J_2, \quad c_2 = 6J_1^2 + (8-3m)J_1J_2, \quad (2.24a)$$

dim	$\Sigma_{F_m^{(4)}} \ll \Delta_{F_m^{(4)}}^* \xleftrightarrow{\nabla} \Delta_{F_m^{(4)}} \gg \mathfrak{Z}_{F_m^{(4)}}$	dim	$\sum d(\nu_*)d(\nu_*^\nabla)$
0	$d(0) = 1$	$d(\triangleleft 0^\nabla) = 512$	5 $\rightarrow$ 512
1	$d(\nu_1) = 1$ $d(\nu_i) = 1$ $d(\nu_\ell) = 1$	$d(\nu_1^\nabla) = 48(2-m)$ $d(\nu_i^\nabla) = 16(6+m)$ $d(\nu_\ell^\nabla) = 64$	4 $\rightarrow$ $\left. \begin{array}{l} (1)[48(2-m)] \\ \rightarrow 3(1)[16(6+m)] \\ \rightarrow 2 \times (1)(64) \end{array} \right\} 512 = C_1^4(F_m^{(4)})$
2	$d(\nu_{1i}) = 1$ $d(\nu_{a\ell}) = 1$ $d(\nu_{ij}) = 1$	$d(\nu_{1i}^\nabla) = 8(3-m)$ $d(\nu_{a\ell}^\nabla) = 16$ $d(\nu_{ij}^\nabla) = 8(3+m)$	3 $\rightarrow$ $\left. \begin{array}{l} 3(1)[8(2-m)] \\ \rightarrow 4 \times 2(1)(16) \\ 3(1)[8(2+m)] \end{array} \right\} 224 = C_2 C_1^2(F_m^{(4)})$
3	$d(\nu_{1ij}) = 1$ $d(\nu_{abl}) = 1$ $d(\nu_{234}) = 1$	$d(\nu_{1ij}^\nabla) = 2-m$ $d(\nu_{abl}^\nabla) = 4$ $d(\nu_{234}^\nabla) = 2+3m$	2 $\rightarrow$ $\left. \begin{array}{l} 3(1)(2-m) \\ \rightarrow 6 \times 2(1)(4) \\ \rightarrow 1(1)(2+3m) \end{array} \right\} 56 = C_3 C_1(F_m^{(4)})$
4	$d(\nu_{abcl}) = 1$	$d(\nu_{abcl}^\nabla) = 1$	1 $\rightarrow$ $4 \times 2(1)(1)$ 8 = $C_4(F_m^{(4)})$
5	$d(\triangleleft \nu_{1\dots 6}) = 8$	$d(\nu_{1\dots 6}^\nabla) = 1$	0 $\rightarrow$ 8

Throughout:  $a, b, c \in \{1, 2, 3, 4\}$ ;  $i, j, k \in \{2, 3, 4\}$ ; and  $\ell \in \{5, 6\}$ ; ordering encodes orientation

**Table 5:** The cones and their degrees, spanned by the transpolar pair  $(\Delta_{F_m^{(4)}}^*, \Delta_{F_m^{(4)}})$

$$c_3 = 4J_1^3 + (12-3m)J_1^2J_2, \quad c_4 = J_1^4 + (8-m)J_1^3J_2, \quad (2.24b)$$

and compute:

$$C_4|_{F_m^{(4)}} = [(J_1+mJ_2)(J_1^4+(8-m)J_1^3J_2)]_{F_m^{(4)}} = 8; \quad (2.25a)$$

$$C_3C_1|_{F_m^{(4)}} = [(J_1+mJ_2)(16J_1^4+8(7-2m)J_1^3J_2)]_{F_m^{(4)}} = 56; \quad (2.25b)$$

$$C_2^2|_{F_m^{(4)}} = [(J_1+mJ_2)(36J_1^4+12(8-3m)J_1^3J_2)]_{F_m^{(4)}} = 96; \quad (2.25c)$$

$$C_2C_1^2|_{F_m^{(4)}} = [(J_1+mJ_2)(96J_1^4+32(7-3m)J_1^3J_2)]_{F_m^{(4)}} = 224; \quad (2.25d)$$

$$C_2^2|_{F_m^{(4)}} = [(J_1+mJ_2)(256J_1^4+256(2-m)J_1^3J_2)]_{F_m^{(4)}} = 512. \quad (2.25e)$$

These clearly confirm both the Todd–Hirzebruch identity

$$720 = -C_4 + C_3C_1 + 3C_2^2 + 4C_2C_1^2 - C_1^4, \quad (2.26)$$

as well as the individual computations in Table 5, which however conspicuously omit  $C_2^2|_{F_m^{(4)}}$ .

Surveying the entries in Table 5, we seek to represent  $c_2^2$  by a pair of 2-cones,  $\nu_{ij} \otimes \nu_{kl}$ , where no four indices  $i, j, k, l$  are in the Stanley–Reisner ideal, so that all combinations contribute. On  $F_m^{(4)}$ , the Stanley–Reisner ideal excludes four or more of the  $\{1, 2, 3, 4\}$ -valued indices and two or more of the  $\{5, 6\}$ -valued ones, so that the 2-cone product contributing to  $C_2^2$  must be of the form

$$\#[d(\nu_{ab})d(\nu_{c\ell}) + d(\nu_{a\ell})d(\nu_{bc})] = (6 \cdot 1)(8 \cdot 1) + (8 \cdot 1)(6 \cdot 1) = 96, \quad (2.27)$$

where  $a, b, c \in \{1, 2, 3, 4\}$  and  $\ell \in \{5, 6\}$ , as in Table 5. This completes the multifan/multitope computation of Chern characteristic invariants for  $F_m^{(4)}$ , and offers the immediate transpolar consequences:

$$C_4|_{F_m^{(4)}} = \sum_{\nu \in \Sigma(4)} d(\nu_{abcl}) d(\nu_{abcl}^\nabla) = C_1^4|_{\nabla F_m^{(4)}}; \quad (2.28a)$$

$$C_3C_1|_{F_m^{(4)}} = \sum_{\nu \in \Sigma(3)} d(\nu_{ijk}) d(\nu_{ijk}^\nabla) = C_2C_1^2|_{\nabla F_m^{(4)}}; \quad (2.28b)$$

$$C_2^2|_{F_m^{(4)}} = \sum_{\nu \in \Sigma(2)} (d(\nu_{ab})d(\nu_{c\ell}) + d(\nu_{a\ell})d(\nu_{bc})) d(\nu_{abcl}^\nabla), \quad a, b, c \in \{1, 2, 3, 4\}, \ell \in \{5, 6\}; \quad (2.28c)$$

$$C_2C_1^2|_{F_m^{(4)}} = \sum_{\nu \in \Sigma(2)} d(\nu_{ij}) d(\nu_{ij}^\nabla) = C_3C_1|_{\nabla F_m^{(4)}}; \quad (2.28d)$$

$$C_1^4|_{F_m^{(4)}} = \sum_{\nu \in \Sigma(1)} d(\nu_i) d(\nu_i^\nabla) = C_4|_{\nabla F_m^{(4)}}. \quad (2.28e)$$

The index selections are specified in more detail in Table 5. While we defer the analogous (and hopefully computer-aided) computations for other VEX multitopes of interest for another time, the transpolar swap,  $F_m^{(n)} \xleftrightarrow{\nabla} \nabla F_m^{(n)}$ , in Table 5 easily implies that

$$C_4|_{\nabla F_m^{(4)}} = 512, \quad C_3 C_1|_{\nabla F_m^{(4)}} = 224, \quad C_2^2|_{\nabla F_m^{(4)}} = 96, \quad C_2 C_1^2|_{\nabla F_m^{(4)}} = 56, \quad C_1^4|_{\nabla F_m^{(4)}} = 8. \quad (2.29)$$

**Detailed Chern Class Relations:** Since  $F_m^{(4)} \in \left[ \begin{smallmatrix} \mathbb{P}^3 \\ \mathbb{P}^1 \\ m \end{smallmatrix} \right]$ , we may use the explicit, coordinate-level identification with the toric rendition [39] to compare the Chern class computations:

$$\begin{aligned} \int_{X_m} c(X_m) &= \left[ (J_1 + mJ_2)(4J_1 + (2-m)J_2) \left( \frac{(1+J_1)^3(1+J_2)^2(1+J_1-mJ_2)}{(1+4J_1+(2-m)J_2)} \right) \right]_{J_1^4 J_2}, \\ &= \left[ \underbrace{(J_1 + mJ_2)}_{p(x,y)=0} \underbrace{(1+J_1-mJ_2)}_{x_1 \rightarrow \mathfrak{s}(x,y)} \underbrace{(1+J_1)^3}_{c(X_{2,3,4})} \underbrace{(1+J_2)^2}_{c(X_{5,6})} \sum_{j=0}^3 (-1)^j (4J_1 + (2-m)J_2)^{j+1} \right]_{J_1^4 J_2}, \\ &= \left[ \underbrace{[(J_1 + mJ_2) + (J_1^2)]}_{c(p^*\mathfrak{s})-1} \underbrace{(1+J_1)^3}_{c(X_{2,3,4})} \underbrace{(1+J_2)^2}_{c(X_{5,6})} \sum_{k=-1}^4 (-1)^{k-1} \underbrace{(4J_1 + (2-m)J_2)^k}_{c_1^k(\mathcal{N})} \right]_{J_1^4 J_2}, \\ &=: \sum_{k=-1}^4 (-1)^{k-1} \hat{c}_k \quad \Rightarrow \quad \hat{c}_k = (8, 8, 56, 224, 512, 512). \end{aligned} \quad (2.30)$$

This identifies, in order, the pullback of the embedding  $F_m^{(4)} \xleftarrow{p=0} \mathbb{P}^4 \times \mathbb{P}^1$ , followed the Chern classes: of the  $\text{deg}(-\frac{1}{m})$  directrix,<sup>17</sup>  $\mathfrak{s}(x, y)$ , that replaces  $x_1 \in \Gamma \mathcal{O}(\frac{1}{0})$  on  $F_m^{(4)} = (p^{-1}(0) \subset \mathbb{P}^4 \times \mathbb{P}^1)$ , of the  $x_{2,3,4}$ -coordinate (toric  $X' := X_{2,3,4}$ ) line bundles  $\mathcal{O}(\frac{1}{0})^{\oplus 3}$ , and of the  $y_{0,1}$ -coordinate (toric  $X'' := X_{5,6}$ ) line bundles  $\mathcal{O}(\frac{0}{1})^{\oplus 2}$ . We then combined the first two factors, and also extend the summation to  $k \rightarrow -1$ , defining  $\hat{c}_1^0(\mathcal{N}) := 1$  and assign  $\hat{c}_1^{-1}(\mathcal{N}) := (4J_1 + (2-m)J_2)^{-1}$  the formal linear combination  $(4J_1^{-1} + (2-m)J_2^{-1})$ .

Not only do the numerical (and  $m$ -independent) values of the so-defined contributions  $\hat{c}_1$  and  $\hat{c}_2$  equal the total sums [38, Eqs. (69) and (70)], respectively, but they match *term-by-term* the contributions [38] in Batyrev's formula for the Euler characteristic [27, Thm. 4.5.3] (denoting  $X' = X_{2,3,4}$  and  $X'' = X_{5,6}$ ):

$$\hat{c}_{-1} = c_2(p^*\mathfrak{s}) c_3(X') c_1(X'') c_1^{-1}(\mathcal{N}) = (J_1^2)(J_1^2)(2J_2)(4J_1^{-1} + (2-m)J_2^{-1}) = 1 \cdot 1 \cdot 2 \cdot 4 = 8. \quad (2.31)$$

$$\hat{c}_0 = [c_1(p^*\mathfrak{s}) c_3(X') c_1(X'') + c_2(p^*\mathfrak{s}) c_2(X') c_1(X'')] (c_1^0(\mathcal{N}) = 1) = [1 \cdot 1 \cdot 2 + 1 \cdot 3 \cdot 2] \cdot 1 = 8. \quad (2.32)$$

$$\begin{aligned} \hat{c}_1 &= [c_1(p^*\mathfrak{s}) c_3(X') c_0(X'') + c_1(p^*\mathfrak{s}) c_2(X') c_1(X'') + c_2(p^*\mathfrak{s}) c_1(X') c_1(X'') + c_2(p^*\mathfrak{s}) c_2(X') c_0(X'')] c_1(\mathcal{N}), \\ &= \underbrace{[1 \cdot 1 \cdot 1 \cdot (2-m) + m \cdot 1 \cdot 1 \cdot 4]}_{2+3m} + \underbrace{[1 \cdot 3 \cdot 2 \cdot 4]}_{2 \times 6 \cdot 4} + \underbrace{[1 \cdot 3 \cdot 2 \cdot 4]}_{3(2-m)} + \underbrace{[1 \cdot 3 \cdot 1 \cdot (2-m)]}_{3(2-m)} = 56. \end{aligned} \quad (2.33)$$

$$\begin{aligned} \hat{c}_2 &= [c_1(p^*\mathfrak{s}) c_2(X') c_0(X'') + c_1(p^*\mathfrak{s}) c_1(X') c_1(X'') + c_2(p^*\mathfrak{s}) c_0(X') c_1(X'') + c_2(p^*\mathfrak{s}) c_1(X') c_0(X'')] c_1^2(\mathcal{N}), \\ &= \underbrace{[1 \cdot 3 \cdot 1 \cdot 8(2-m) + m \cdot 3 \cdot 1 \cdot 16]}_{3 \cdot 8(2+m)} + \underbrace{[1 \cdot 3 \cdot 2 \cdot 16]}_{4 \cdot 2 \cdot 16} + \underbrace{[1 \cdot 1 \cdot 2 \cdot 16]}_{2 \cdot 16} + \underbrace{[1 \cdot 3 \cdot 1 \cdot 8(2-m)]}_{3 \cdot 8(2-m)} = 224. \end{aligned} \quad (2.34)$$

$$\begin{aligned} \hat{c}_3 &= [c_1(p^*\mathfrak{s}) c_1(X') c_0(X'') + c_1(p^*\mathfrak{s}) c_0(X') c_1(X'') + c_2(p^*\mathfrak{s}) c_0(X') c_0(X'')] c_1^3(\mathcal{N}), \\ &= \underbrace{[1 \cdot 3 \cdot 1 \cdot 48(2-m) + m \cdot 3 \cdot 1 \cdot 64]}_{3 \cdot 16(6+m)} + \underbrace{[1 \cdot 1 \cdot 2 \cdot 64]}_{2 \cdot 64} + \underbrace{[1 \cdot 1 \cdot 1 \cdot 48(2-m)]}_{48(2-m)} = 512. \end{aligned} \quad (2.35)$$

$$\hat{c}_4 = c_1(p^*\mathfrak{s}) c_0(X') c_0(X'') c_1^4(\mathcal{N}) = [1 \cdot 1 \cdot 1 \cdot 256(2-m) + m \cdot 1 \cdot 1 \cdot 256] = 512. \quad (2.36)$$

as well as *each and every* entry in Table 5 (compare under-braced terms), clearly identifying the contributions that turn negative for  $m > 2$ .

<sup>17</sup>This is the unique such holomorphic section on  $F_m^{(4)} \subset \mathbb{P}^4 \times \mathbb{P}^1$ ; it's irreducible zero-locus has self-intersection  $[\mathfrak{s}^{-1}(0)]^4 = -3m$ .

It is easy to verify that the same term-by-term identifications hold also in lower dimensions, and we expect this to be uniformly true in all dimensions,  $n$ , and for all  $m \in \mathbb{Z}$ . In fact, following [39], an even more general “family picture” emerges: identifying each  $F_m^{(n)} \in \left[ \begin{smallmatrix} \mathbb{P}^n \\ \mathbb{P}^1 \end{smallmatrix} \middle| \begin{smallmatrix} 1 \\ m \end{smallmatrix} \right]$  with an  $m$ -twisted  $\mathbb{P}^n$ -bundle over  $\mathbb{P}^1$ , explicit deformations within the family distribute the twisting,  $m \rightarrow \vec{m} = (m_1, m_2, \dots)$ , with  $\sum_{i=1}^n m_i = m$ , each  $\vec{m}$  corresponding to a distinct toric variety. By explicit deformation, all such Hirzebruch scrolls explicitly form a diffeomorphism class, as do their (Laurent-smoothed for  $m > 2$  [38, 39]) Calabi–Yau hypersurfaces. Since the total number of so-constructed diffeomorphism classes is limited by Wall’s Theorem [95] to  $[m \pmod n]$ , the number of distinctly different (weakly/pre-)complex Calabi–Yau manifolds (dubbed *discrete deformations* [41]) within each diffeomorphism class grows unbounded with increasing  $m$ .

**A Novel Euler Characteristic Formula:** For the anticanonical hypersurface,  $Z_f = \{f(x) = 0\} \subset X$ ,

$$\chi(Z_f) = \int_{Z_f} c_3(Z_f) = \int_X c_1(c_3 - c_1 c_2) = [C_3 C_1 - C_1^2 C_2]_X. \quad (2.37)$$

The key standard results R.4 and R.5,  $C_4|_X = d(\Delta_X^*)$  and  $C_1^4|_X = d(\Delta_X)$  yields for  $X$ :

$$\text{Td}(X) = \frac{1}{720} [-C_4 + C_3 C_1 + 3C_2^2 + 4C_2 C_1^2 - C_1^4]_X, \quad (2.38)$$

$$\text{i.e., } 720 \text{Td}(X) = -d(\Delta_X^*) + \chi(Z_f) + 3C_2^2|_X + 5C_2 C_1^2|_X - d(\Delta_X). \quad (2.39)$$

Swapping  $\Delta_{\nabla X}^* = \Delta_X$  and  $\Delta_{\nabla X} = \Delta_X^*$  produces the analogous result for the mirror  $\tilde{Z}_{\tau_f} \subset \nabla X$  (using that  $\chi(\tilde{Z}_{\tau_f}) = -\chi(Z_f)$ ):

$$720 \text{Td}(\nabla X) = -d(\Delta_X) - \chi(Z_f) + 3C_2^2|_{\nabla X} + 5C_2 C_1^2|_{\nabla X} - d(\Delta_X^*). \quad (2.40)$$

Since  $\text{Td}(X) = w(\Delta_X^*) = w(\Delta_X) = \text{Td}(\nabla X)$ , subtracting (2.40) from (2.39) yields:

$$0 = 2\chi(Z_f) + 3(C_2^2|_X - C_2^2|_{\nabla X}) + 5(C_2 C_1^2|_X - C_2 C_1^2|_{\nabla X}). \quad (2.41)$$

Comparing now the assignments (2.28b) and (2.28d), we observe the identity (previously derived in [96] using the so-called Libgober–Wood formula [97]):

$$C_3 C_1|_X = \sum_{\nu_{ijk} \in \Sigma_X(3)} d(\nu_{ijk}) d(\nu_{ijk}^{\nabla}) \stackrel{\nabla}{=} \sum_{\mu_{IJ} \in \Sigma_{\nabla X}(2)} d(\mu_{IJ}^{\nabla}) d(\mu_{IJ}) = C_2 C_1^2|_{\nabla X}, \quad (1.5')$$

where the middle equality is implied by the transpolar relation. This identifies 1–1 not only the total sum of the contributions, but the individual factors in each contribution:  $\nu_{ijk}^{\nabla} = \mu_{IJ} \subset \Sigma_{\nabla X} = \mathfrak{Z}_X$  and  $\mu_{IJ}^{\nabla} = \nu_{ijk} \subset \Sigma_X = \mathfrak{Z}_{\nabla X}$  are the cones over individual transpolar pairs of faces. Using this identity in (2.41) to substitute  $C_2 C_1^2|_{\nabla X} \rightarrow C_3 C_1|_X$  yields:

$$0 = 2\chi(Z_f) + 3(C_2^2|_X - C_2^2|_{\nabla X}) + 5\left([C_2 C_1^2 - C_3 C_1]_X = -\chi(Z_f)\right), \quad (2.42)$$

$$\text{and so } \chi(Z_f) = C_2^2|_X - C_2^2|_{\nabla X} = -\chi(\tilde{Z}_{\tau_f}). \quad (1.6')$$

We used that  $\nabla X$  is the MPCP-desingularization of a suitable toric space, specified by (re)interpreting  $\Delta_X$  (with all its lattice points specifying the MPCP-subdivisions) as the spanning multitope of  $\nabla X$ , wherein anticanonical hypersurfaces in the deformation family  $\tilde{Z}_{\tau_f} \subset \nabla X[c_1]$  are transposition mirrors of the anticanonical hypersurfaces  $Z_f \subset X[c_1]$ , as stated in Claim 1.1.

**Hirzebruch–Riemann–Roch for  $\mathcal{K}^*$ :** The HRR theorem for the anticanonical bundle,<sup>18</sup>

$$\chi(X, \mathcal{K}^*) = \int_X \text{td}(X) \text{ch}(\mathcal{K}^*) = \sum_{k=0}^n (-1)^k H^k(X, \mathcal{K}^*) = \ell(\Delta_X) \quad (2.43)$$

<sup>18</sup>Standard for (semi/weak) Fano  $X$  encoded by convex polytopes [19–23], the final equality extends to torus manifolds with simplicial multifans [45–47], which includes all VEX multifans, as they have a simplicial subdivision by Definition 1.1.

interprets the (negative-contributing) flip-folded extension(s) in  $\Delta_X$  as counting  $H^1(X, \mathcal{K}^*)$ , and implies

$$\begin{aligned}\chi(X, \mathcal{K}^*) &= \int_X \left( 1 + \frac{c_1}{2} + \frac{c_2 + c_1^2}{12} + \frac{c_1 c_2}{24} + \frac{-c_4 + c_3 c_1 + 3c_2^2 + 4c_2 c_1^2 - c_1^4}{720} \right) \left( 1 + c_1 + \frac{c_1^2}{2!} + \frac{c_1^3}{3!} + \frac{c_1^4}{4!} \right) \Bigg|^4 \\ &= \int_X \left( \frac{c_1^4}{4!} + \frac{c_1}{2} \frac{c_1^3}{3!} + \frac{c_2 + c_1^2}{12} \frac{c_1^2}{2!} + \frac{c_1 c_2}{24} c_1 + \frac{-c_4 + c_3 c_1 + 3c_2^2 + 4c_2 c_1^2 - c_1^4}{720} \right),\end{aligned}\quad (2.44)$$

$$\ell(\Delta_X) = \frac{1}{720} (119 C_1^4|_X + 64 C_1^2 C_2|_X + 3 C_2^2|_X + C_1 C_3|_X - C_4|_X). \quad (2.45)$$

The analogous result for the transpolar uses that  $\Delta_{\vee X} = \Delta_X^*$ :

$$\ell(\Delta_X^*) = \frac{1}{720} (119 C_1^4|_{\vee X} + 64 C_1^2 C_2|_{\vee X} + 3 C_2^2|_{\vee X} + C_1 C_3|_{\vee X} - C_4|_{\vee X}). \quad (2.46)$$

The relation (1.5) allows replacing  $C_1^2 C_2|_{\vee X} \rightarrow C_1 C_3|_X$  and  $C_1 C_3|_{\vee X} \rightarrow C_1^2 C_2|_X$ , and (2.16) allows replacing  $C_1^4|_{\vee X} \rightarrow C_4|_X = d(\Delta_X^*)$  and  $C_4|_{\vee X} \rightarrow C_1^4|_X = d(\Delta_X)$ :

$$\ell(\Delta_X^*) = \frac{1}{720} (119 C_4|_X + 64 C_1 C_3|_X + 3 C_2^2|_{\vee X} + C_1^2 C_2|_X - C_1^4|_X). \quad (2.47)$$

Subtracting from (2.45) yields:

$$\begin{aligned}\ell(\Delta_X) - \ell(\Delta_X^*) &= \frac{1}{720} (120 C_1^4|_X + 64 [C_1^2 C_2 - C_1 C_3]|_X + 3 (C_2^2|_X - C_2^2|_{\vee X}) + [C_1 C_3 - C_1^2 C_2]|_X - 120 C_4|_X), \\ &= \frac{1}{720} (120 d(\Delta_X) - 64 \chi(Z_f) + 3 \chi(Z_f) + \chi(Z_f) - 120 d(\Delta_X^*)),\end{aligned}\quad (2.48)$$

$$= \frac{1}{6} (d(\Delta_X) - d(\Delta_X^*)) - \frac{1}{12} \chi(Z_f), \quad (2.49)$$

so that finally:

$$\chi(Z_f) = 2(d(\Delta_X) - d(\Delta_X^*)) - 12(\ell(\Delta_X) - \ell(\Delta_X^*)). \quad (1.7')$$

This relation was derived (slightly differently) and has already been used [96] in a machine-learning exploration of the Kreuzer–Skarke database of (convex) reflexive polytopes and associate (complex algebraic) toric varieties [24]. The above derivations imply (1.6) and (1.7) to hold also for the (smooth) toric spaces corresponding to VEX polytopes and anticanonical hypersurfaces therein, as long as (a suitable,  $T^n$ -equivariant generalization of) the Chern characteristic classes exists.

By considering also the sums, (2.39)+(2.40) and (2.45)+(2.46), we obtain

$$C_2^2|_X = 3d(\Delta_X) + d(\Delta_X^*) - 16\ell(\Delta_X) - 4\ell(\Delta_X^*) + 260 \text{Td}(X), \quad (2.50a)$$

$$C_2^2|_{\vee X} = 3d(\Delta_X^*) + d(\Delta_X) - 16\ell(\Delta_X^*) - 4\ell(\Delta_X) + 260 \text{Td}(X), \quad (2.50b)$$

in addition to (1.6). Similar manipulations can extract analogous, multitope-counting expressions for other Chern characteristics; for example,

$$C_3 C_1|_X = 2(6\ell(\Delta_X^*) - d(\Delta_X^*) - 6 \text{Td}(X)), \quad (2.50c)$$

$$C_3 C_1|_{\vee X} = 2(6\ell(\Delta_X) - d(\Delta_X) - 6 \text{Td}(X)). \quad (2.50d)$$

## 2.2.4 Five Dimensions

For simplicity, we showcase here only the “template” case of  $\mathbb{P}^5$  and its sextic hypersurfaces, where

$$\begin{aligned}c(\mathbb{P}^5) &= (1 + J)^6| = 1 + 6J + 15J^2 + 20J^3 + 15J^4 + 6J^5, \\ \Rightarrow c_1 &= 6J, \quad c_2 = 15J^2, \quad c_3 = 20J^3, \quad c_4 = 15J^4, \quad c_5 = 6J^5.\end{aligned}\quad (2.51)$$

For the Todd–Hirzebruch “1440-theorem” (2.3), we easily verify:

$$1440 \stackrel{?}{=} -C_4 C_1 + C_3 C_1^2 + 3C_2^2 C_1 - C_2 C_1^3 = \int \{ -(15J^4)(6J) + (20J^3)(6J)^2 + 3(15J^2)^2(6J) - (15J^2)(6J)^3 \},$$

$$= -(15)(6) + (20)(36) + 3(225)(6) - (15)(216) = -90 + 720 + 4050 - 3240 \stackrel{\checkmark}{=} 1440. \quad (2.52)$$

In turn, the list of cones and degrees is now

#	dim	$\Sigma_{\mathbb{P}^5} \leq \Delta_{\mathbb{P}^5}^*$	$\leftrightarrow$	$\Delta_{\mathbb{P}^5} \geq \Sigma_{\mathbb{P}^5}$	dim	$\sum d(\nu_*)d(\nu_*^\nabla)$
1	0	$d(0) = 1$		$d(\triangleleft 0^\nabla) = 6^5$	6	$\rightarrow 7776$
6	1	$d(\nu_i) = 1$		$d(\nu_1^\nabla) = 6^4$	5	$\rightarrow 7776 = C_1^5$
15	2	$d(\nu_{ij}) = 1$		$d(\nu_{ij}^\nabla) = 6^3$	4	$\rightarrow 3240 = C_2 C_1^3$
20	3	$d(\nu_{ijk}) = 1$		$d(\nu_{ijk}^\nabla) = 6^2$	3	$\rightarrow 720 = C_3 C_1^2$
15	4	$d(\nu_{ijkl}) = 1$		$d(\nu_{ijkl}^\nabla) = 6^1$	2	$\rightarrow 90 = C_4 C_1$
6	5	$d(\nu_{ijklm}) = 1$		$d(\nu_{ijklm}^\nabla) = 6^0$	1	$\rightarrow 6 = C_5$
1	6	$d(\triangleleft \nu_{1\dots 6}) = 6$		$d(\triangleleft \nu_{1\dots 6}^\nabla) = 1$	0	$\rightarrow 6$

For purposes of verifying the 5D Todd–Hirzebruch theorem (2.52), the tabulation (2.53) includes:

$$C_4 C_1|_{\mathbb{P}^5} \mapsto \sum_{\nu_{ijkl} \in \Sigma(4)} d(\nu_{ijkl}) d(\nu_{ijkl}^\nabla) = 15 \times (1)(6^1) \stackrel{\checkmark}{=} 90; \quad (2.54a)$$

$$C_3 C_1^2|_{\mathbb{P}^5} \mapsto \sum_{\nu_{ijk} \in \Sigma(3)} d(\nu_{ijk}) d(\nu_{ijk}^\nabla) = 20 \times (1)(6^2) \stackrel{\checkmark}{=} 720; \quad (2.54b)$$

$$C_2 C_1^3|_{\mathbb{P}^5} \mapsto \sum_{\nu_{ij} \in \Sigma(2)} d(\nu_{ij}) d(\nu_{ij}^\nabla) = 15 \times (1)(6^3) \stackrel{\checkmark}{=} 3240. \quad (2.54c)$$

Each of these reproduces exactly the corresponding term in (2.52), but the tabulation (2.53) conspicuously lacks the contribution for the  $3 C_2^2 C_1 = 3 \cdot 1350 = 4050$  term. Following the 4-dimensional case (2.28c), we assign:

$$C_2^2 C_1|_{\mathbb{P}^5} \mapsto \sum_{\nu_{ij}, \nu_{kl} \in \Sigma(2)} \underbrace{d(\nu_{ij}) d(\nu_{kl})}_{\Sigma(2) \times \Sigma(2) \rightarrow \Sigma(4)} d(\nu_{ijkl}^\nabla) = (15 \cdot 1)(15 \cdot 1)(6^1) \stackrel{\checkmark}{=} 1350, \quad (2.55)$$

which is now unrestricted by the only Stanley–Reisner relation, stemming from  $\nu_{1\dots 6} \notin \Sigma_{\mathbb{P}^5}$ .

There are three other Chern characteristics that do not occur in (2.54)–(2.55), but which are easily evaluated:

$$C_1^5|_{\mathbb{P}^5} = \int (6J)^5 = 7776 = \sum_{\nu_i \in \Sigma(1)} d(\nu_i) d(\nu_i^\nabla) = 6 \times (1)(6^4) \stackrel{\checkmark}{=} 7776, \quad (2.56)$$

$$C_5 C_1^0|_{\mathbb{P}^5} = \int (6J^5) = 6 = \sum_{\nu_{ijklm} \in \Sigma(1)} d(\nu_{ijklm}) d(\nu_{ijklm}^\nabla) = 6 \times (1)(6^0) \stackrel{\checkmark}{=} 6, \quad (2.57)$$

$$C_3 C_2|_{\mathbb{P}^5} = \int (20J^3)(15J^2) = 300 = \sum_{\substack{\nu_{ijk} \in \Sigma(3) \\ \nu_{ij} \in \Sigma(2)}} \underbrace{d(\nu_{ijk}) d(\nu_{lm})}_{\Sigma(3) \times \Sigma(2) \rightarrow \Sigma(5)} d(\nu_{ijklm}^\nabla) = (20 \cdot 15) \times (1)(6^0) \stackrel{\checkmark}{=} 300, \quad (2.58)$$

where none of the sums are restricted by the single Stanley–Reisner relation for  $\mathbb{P}^5$ ; for other 5-dimensional varieties, the summations in (2.54)–(2.58) do become restricted; see below.

We can also (re)verify the analogue of (2.17c) and (2.22b) (see Remark 1.11):

$$\begin{aligned} c(X^{(5)}[c_1]) &= \left[ \frac{1+c_1+c_2+c_3+c_4+c_5}{1+c_1} \right]_{\leq \deg 4} = \left[ (1+c_1+c_2+c_3+c_4)(1-c_1+c_1^2-c_1^3+c_1^4) \right]_{\leq \deg 4}, \\ &= 1 + c_2 + (c_3 - c_2 c_1) + (c_4 - c_3 c_1 + c_2 c_1^2); \end{aligned} \quad (2.59a)$$

$$\chi(X^{(5)}[c_1]) = \int_{X^{(5)}} c_1 \cdot c(X^{(5)}[c_1]) = \int_{X^{(5)}} c_1 (c_4 - c_3 c_1 + c_2 c_1^2) = [C_4 C_1 - C_3 C_1^2 + C_2 C_1^3]_{X^{(5)}}, \quad (2.59b)$$

$$\chi(\mathbb{P}^5[6]) \mapsto \sum_{\nu_{ijk} \in \Sigma(4)} d(\nu_{ijkl})d(\nu_{ijkl}^\nabla) - \sum_{\nu_{ijk} \in \Sigma(3)} d(\nu_{ijk})d(\nu_{ijk}^\nabla) + \sum_{\nu_{ij} \in \Sigma(2)} d(\nu_{ij})d(\nu_{ij}^\nabla), \quad (2.59c)$$

$$= 15 \times (1)(6^1) - 20 \times (1)(6^2) + 15 \times (1)(6^3) = 90 - 720 + 3240 = +2610. \quad (2.59d)$$

The structure of the summation (2.59c) conforms to Batyrev’s formula [27], and the above computations and cone degrees tabulation (2.53) again confirm that the result (2.59c) extends straightforwardly:

$$\chi(\mathbb{P}^5[6]) = \sum_{k=0}^6 (-1)^{4-k} \sum_{\nu_* \in \Sigma(k)} d(\nu_*) d(\nu_*^\nabla) = (6)-(6)+(90)-(720)+(3240)-(7776)+(7776) = +2610, \quad (2.60)$$

as explained in Remark 2.2. Also, mirror symmetry requires that  $\chi(X^{(5)}[c_1]) = \chi(\nabla X^{(5)}[c_1])$ , which is easily verified from (2.59b) on noting that the cones and degrees tabulation (2.53) generalizes (2.17) and (2.28):

$$C_5|_X = C_1^5|_{\nabla X}, \quad C_4 C_1|_X = C_2 C_1^3|_{\nabla X}, \quad C_3 C_1^2|_X = C_3 C_1^2|_{\nabla X}. \quad (2.61)$$

Since  $\chi(X^{(5)}[c_1]) = \chi(\nabla X^{(5)}[c_1])$  and  $\text{Td}(X) = \text{Td}(\nabla X)$ , combining (2.3b) with its  $X \rightarrow \nabla X$  analogue produce the Calabi–Yau 4-fold analogues of (1.6):

$$\chi(Z_f) = 3(C_2^2 C_1|_X - 480 \text{Td}(X)) = \chi(\nabla X[c_1]), \quad \text{and} \quad C_2^2 C_1|_X = C_2^2 C_1|_{\nabla X}, \quad (2.62)$$

$$= 24\ell(\Delta_X) + 24\ell(\Delta_X^*) - d(\Delta_X) - d(\Delta_X^*) - 144 \text{Td}(X) - C_3 C_1^2|_X, \quad (2.63)$$

the two results obtained by eliminating different Chern characteristics. Equating the two produces:

$$C_2^2 C_1|_X = 8(\ell(\Delta_X) + \ell(\Delta_X^*) + 54 \text{Td}(X)) - \frac{1}{3}(C_3 C_1^2|_X - d(\Delta_X) - d(\Delta_X^*)) = C_2^2 C_1|_{\nabla X}, \quad (2.64)$$

which evaluates  $C_2^2 C_1|_X = C_2^2 C_1|_{\nabla X}$  solely in terms of multitope characteristics upon using (2.54b) to so express  $C_3 C_1^2|_X = C_3 C_1^2|_{\nabla X}$ . Together with the  $\Delta_X^* \leftrightarrow \Delta_X$  analogues of (2.54)–(2.58), such computations then provide the Chern characteristics of  $\nabla X \leftrightarrow \Sigma_{\nabla X} \leftarrow \Delta_X$  from those of  $X$ .

Finally, a straightforward  $X \leftrightarrow \nabla X$  ( $\Delta_X^* \triangleright \Sigma_X \leftrightarrow \nabla \Sigma_X = \Sigma_{\nabla X} \leftarrow \Delta_X^* = \Delta_X$ ) analogue of (2.55),

$$C_2^2 C_1|_{\mathbb{P}^5} \mapsto \sum_{\nu_{ij}^\nabla, \nu_{kl}^\nabla \in \nabla \Sigma(2)} \underbrace{d(\nu_{ij}^\nabla) d(\nu_{kl}^\nabla)}_{\nabla \Sigma(2) \times \nabla \Sigma(2) \rightarrow \nabla \Sigma(4)} d(\nu_{ijkl}), \neq \underbrace{(15 \cdot 6^3)(15 \cdot 6^3)(1)}_{\neq 1350 = C_2^2 C_1|_{\mathbb{P}^5}, \text{ cf. (2.55)}} = 10\,497\,600, \quad (2.65)$$

cannot equal the indicated unrestricted product, as that would contradict the latter of the results (2.62). The pairing  $\nabla \Sigma(2) \times \nabla \Sigma(2) \rightarrow \nabla \Sigma(4)$  in the summation (2.65) must therefore be drastically restricted — unlike the one in (2.55). This difference must stem from the fact that whereas the fan  $\Sigma_{\mathbb{P}^5}$  already has only regular ( $\text{deg} = 1$ ) top-dimensional cones, those in  $\Sigma_{\mathbb{P}^5 = \text{Bl}[\mathbb{P}^5/\mathbb{Z}_6^4]}$  are regular owing to multiple MPCP-subdivision of each of its six  $\text{deg} = 6^4$  top-dimensional cones. The drastic restriction on the indicated pairing and the summation in (2.65) foreshadow the relative sparsity in the array of divisor intersections (see next section) and must insure agreement with (2.62); for now, we forego determining the details of this restriction.

### 3 Intersection Numbers

Adapting from the standard literature (esp. [23, Thm. 10.4.4 and Lemma 12.5.2]) and the algorithm given explicitly in [98], we use:

**Procedure 3.1** (Intersection numbers, Mori cone) *In a simplicial subdivided multifan,<sup>19</sup>  $\Sigma_X = \{\uplus_\alpha \sigma_\alpha, \leftarrow\}$ , let  $\nu_i \in \Sigma_X$  denote the 1-cone generators.*

<sup>19</sup>All non-simplicial cones in  $\Sigma_X$  are subdivided into simplicial (sub-)cones,  $\sigma_\alpha$ ; a subdivision is **smooth** if  $|d(\sigma_\alpha)| = 1$  for all top-dimensional cones, and **coarse** otherwise; “ $\sigma \uplus \sigma'$ ” is the disjoint (indexed) union of  $\sigma$  and  $\sigma'$  that retains  $\tau = \sigma \cap \sigma'$  in the facet ( $\leftarrow$ )-generated poset structure of the multifan [47].

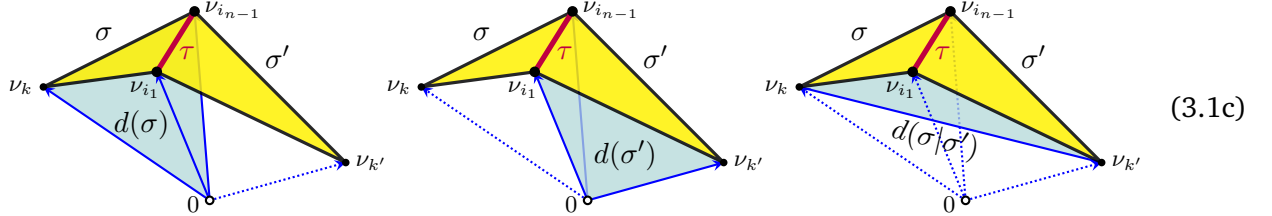
1. For each codimension-1 simplicial cone,  $\tau \in \Sigma_X(n-1)$ , its two adjacent top-dimensional simplicial cones,  $\sigma \cap \sigma' = \tau$ , and generators,  $\nu_i \in \sigma, \sigma'$ , find  $\ell_\tau^i \in \mathbb{Q}$  such that

$$\sum_{\nu_i \in \sigma, \sigma'} \ell_\tau^i \nu_i = 0, \quad \text{and} \quad \sum_{\nu_i \in \sigma, \sigma'} \ell_\tau^i = \frac{d(\sigma|\sigma')}{d(\sigma)d(\sigma')} = d(\tau^\nabla), \quad (3.1a)$$

where

$$d(\sigma) = \det[\nu_i \in \sigma], \quad d(\sigma') = \det[\nu_i \in \sigma'], \quad d(\sigma|\sigma') = \det[(\nu_i \in \sigma) - \nu_*]_{\substack{\nu_i \neq \nu_* \\ \nu_* \in (\sigma \uplus \sigma')}}. \quad (3.1b)$$

The degree,  $d(\sigma)$ , of a simplicial top-dimensional cone is the volume of its central (primitive) simplex, the determinant of the row-stacked matrix of generating vectors,  $\nu_i \in \sigma$ . The (relative) degree  $d(\sigma|\sigma')$  is the volume of the simplex hull of the adjoined bases of  $\sigma, \sigma'$ , and equals the degree of their intersection's transpolar:



This  $d(\sigma|\sigma')$  may be computed as the determinant of the row-stacked matrix of the generator vector differences  $(\nu_i - \nu_*)_{i \neq *}$  and is independent of the choice of  $\nu_* \in (\sigma \uplus \sigma')$ . The row-stacked matrices are ordered compatibly with a continuous orientation of the (yellow) facets,  $\sigma, \sigma'$ , in (3.1c).

2. Solutions to (3.1) provide the a priori nonzero (divisor class) intersection numbers:

$$\kappa_{i_1, \dots, i_{n-1}, k} := \underbrace{D_{i_1} \cdots D_{i_{n-1}}}_{\tau} \cdot D_k = \ell_\tau^k, \quad \nu_{i_1}, \dots, \nu_{i_{n-1}} \in \tau, \quad \nu_k \in (\sigma \cup \sigma' \setminus \tau), \quad (3.2)$$

and  $\ell_\tau^j = 0$  for  $\nu_j \notin (\sigma \cup \sigma' \setminus \tau)$ .

3. The so-obtained array of intersection numbers,  $\kappa_{i_1, \dots, i_n}$ , is totally symmetric.
4. The  $n$ -vectors computed in (3.1) in terms of which all others are non-negative linear combinations are the Mori vectors.

**Remark 3.1 (normalization)** The results (3.1) are local to  $\sigma, \sigma' \in \Sigma_X$ , i.e., independent of  $\Sigma_X \setminus (\sigma \uplus \sigma')$ . The whole array of intersection numbers,  $\kappa_{i_1, \dots, i_n}$ , in (3.2) is however global over  $\Sigma_X$ , and its total symmetry under index-permutations constrains the procedure. The relative degree  $d(\sigma|\sigma')$  in (3.1c) measures the dual of the “inner” dihedral angle between  $\sigma$  and  $\sigma'$  at  $\tau = \sigma \cap \sigma'$ , and vanishes when  $\sigma$  and  $\sigma'$  are coplanar. The second equation (3.1a) then fails to normalize the  $\ell_\tau^k$ , but the overabundant conditions of total symmetry in  $\kappa_{i_1, \dots, i_n}$  have sufficed to this end in all examples we checked.  $\blacksquare$



Owing to the key standard results R.1–R.2, the  $n$ -fold divisor class intersection numbers  $\kappa_{i_1, \dots, i_n} = D_{i_1} \cdots D_{i_n}$  are related to Chern characteristics. They also provide essential information (certain Yukawa couplings) for superstring applications, and we now verify their computability and consistency also for toric spaces corresponding to VEX multitopes.

### 3.1 Two Dimensions

**The Template,  $\mathbb{P}^2$ :** Let us exhibit and summarize a collection of standard results on a well-known example of  $\mathbb{P}^2$ , which also generalizes straightforwardly to higher-dimensional  $\mathbb{P}^n$  [21–23]:

$\Sigma_{\mathbb{P}^2} \in \Delta_{\mathbb{P}^2}^*$

$\Sigma_{\mathbb{P}^2}$	$\nu_1$	$\nu_2$	$\nu_3$
	1	0	-1
	0	1	-1
$Q$	1	1	1

$\mathbb{P}^2$	$D_1$	$D_2$	$D_3$	sum
$D_1$	1	1	1	3
$D_2$	1	1	1	3
$D_3$	1	1	1	3

$[D_i \cdot D_j]_{\mathbb{P}^2}$

$$\begin{aligned} \sum_i \nu_i D_i \sim 0 &\Rightarrow D_i \sim D_j; & C_2(\mathbb{P}^2) &= \sum_{i>j} D_i \cdot D_j = 3 \times (1) = 3; \\ \text{S.-R. : } D_1 \cdot D_2 \cdot D_3 &\sim 0. & C_1^2(\mathbb{P}^2) &= [\sum_i D_i] \cdot [\sum_j D_j] = \sum_{i,j} D_i \cdot D_j = 9 \times (1) = 9. \end{aligned} \quad (3.4)$$

The equivalences from the left-hand side tabulation simplify  $c(\mathbb{P}^3) \sim 1+3D+3D^2$ , so  $C_1^2 \sim [(3D)^2]_{\mathbb{P}^2} = 9$  and  $C_2(\mathbb{P}^2) \sim [3D^2]_{\mathbb{P}^2} = 3$ . The complete intersection number table maps to the spanning polygon,  $\Delta_{\mathbb{P}^2}^*$ , as shown in the right-hand side of (3.3): (encircled) self-intersections at the vertices, mutual intersections along the edges. The row-sums,  $\sum_i D_i \cdot D_j = [c_1] \cdot D_j = 3$  for  $j=1,2,3$ , exhibit the normalization (3.1a), the sum of labels of a vertex and its adjacent edges. For the right-most of the (3.1a) equalities, we read  $d(\nu_{ij}^\nabla) = 3$  directly from the left-hand side illustration (3.5) below. The evaluation of  $C_1^2$  in (3.4) of course confirms the key standard result R.5:  $C_1^n(X) = d(\Delta_X)$ , which equals  $\sum_{\nu_i^\nabla \in \mathfrak{Z}(2)} d(\nu_i^\nabla) = 3 \times (3) = 9$ , adding the edge indices in both directions since  $D_i \cdot D_j = D_j \cdot D_i$ ; see diagram in (3.5) below, or the tabulation (2.12a). Similarly, the intersection computation of  $C_2$  in (3.4) agrees with the key standard result R.4:  $C_2(\mathbb{P}^2) = \sum_{\nu_{ij} \in \Sigma(2)} d(\nu_{ij}) = 3 \times (1) = 3$ ; see illustration (3.3) and the tabulation (2.12a).

The analogous results for the transpolar polygon (with  $\nu_{ij}^\nabla \mapsto \tilde{D}_j$ ) are:

$\mathfrak{Z}_{\mathbb{P}^2}$	$\nu_{23}^\nabla$	$\nu_{31}^\nabla$	$\nu_{12}^\nabla$
	2	-1	-1
	-1	2	-1
$\tilde{Q}$	1	1	1

$\varepsilon^{ijk} \nu_{ij}^\nabla \hat{D}_k \sim 0 \Rightarrow \hat{D}_i \sim \hat{D}_j$   
S.-R.:  $\hat{D}_1 \cdot \hat{D}_2 \cdot \hat{D}_3 \sim 0$

$$(3.5)$$

$$\varepsilon^{ijk} \nu_{ij}^\nabla \hat{D}_k \sim 0 \Rightarrow \hat{D}_i \sim \hat{D}_j \quad \text{and} \quad \text{S.-R. : } \hat{D}_1 \cdot \hat{D}_2 \cdot \hat{D}_3 \sim 0. \quad (3.6)$$

The intersection numbers of the coarse (*un-subdivided*) fan,  $\mathfrak{Z}_{\mathbb{P}^2} = \Sigma_{\mathbb{P}^2/\mathbb{Z}_3}$  (middle diagram), pertain to the *singular orbifold*  $\mathbb{P}^2/\mathbb{Z}_3$ . The intersection computation of  $C_1^2$  again agrees with the key standard result R.5, but  $C_2(\mathbb{P}^2/\mathbb{Z}_3)$  *disagrees* with the key standard result R.4, [19, Cor. 11.6]:

$$C_1^2(\mathbb{P}^2/\mathbb{Z}_3) = \sum_{i,j} \hat{D}_i \cdot \hat{D}_j = 9 \times (1/3) = 3, \stackrel{(2.12b)}{=} C_2(\mathbb{P}^2); \quad (3.7a)$$

$$C_2(\mathbb{P}^2/\mathbb{Z}_3) = \sum_{i<j} \hat{D}_i \cdot \hat{D}_j = 3 \times (1/3) = 1, \stackrel{(2.12c)}{\neq} C_1^2(\mathbb{P}^2). \quad (3.7b)$$

Including the MPCP-desingularizing subdivisions, far right in (3.5), adds six MPCP-divisors ( $\approx \mathbb{P}^1$ ) with self-intersection  $-2$ , as their normal bundles are  $\mathcal{O}_{\mathbb{P}^1}(-2)$ . This and their intersections with the adjacent divisors add up to 0 since the MPCP-subdividing lattice points are *within* facets of  $\Delta_{\mathbb{P}^2}$ , are not vertices, and the “relative” degree (3.1) of the adjacent unit sub-facets vanishes; see Remark 3.1. The so-remaining normalizations in (3.5, right) are determined by the symmetry  $\tilde{D}_i \cdot \tilde{D}_j = \tilde{D}_j \cdot \tilde{D}_i$ . The intersection computations from (3.5, right) continue to agree with the key standard result R.5 for  $C_1^2(\nabla\mathbb{P}^2)$ :

$$C_1^2(\nabla\mathbb{P}^2) = \sum_{i,j=1}^9 [\tilde{D}_i \cdot \tilde{D}_j]_{\nabla\mathbb{P}^2} = 3 = \sum_{\nu_{ij} \in \Sigma_{\mathbb{P}^2}(2)} d(\nu_{ij}), \quad (3.8a)$$

but now also agree with the key standard result R.4 for  $C_2(\nabla\mathbb{P}^2)$ :

$$C_2(\nabla\mathbb{P}^2) = \sum_{i<j=1}^9 [\tilde{D}_i \cdot \tilde{D}_j]_{\nabla\mathbb{P}^2} = 9 = \sum_{\nu_i^\nabla \in \Sigma_{\nabla\mathbb{P}^2}(2)} d(\nu_i^\nabla), \quad (3.8b)$$

By encoding *smooth* toric spaces, it is thus indeed the regular subdivision of the considered fans that encode the correct diffeomorphism invariant relations.

We now turn to the non-convex and flip-folded examples from Figure 1 to verify that the same key standard results continue to hold for the analogous multitope/multifan computations. While this is guaranteed in two dimensions by the rigorous results in Ref. [57], we find that it continues to hold also in higher dimensional VEX multitopes/multifans.



2. The self-intersection of the divisors corresponding to the standard vertices in  $\Delta_{F_m^{(2)}}^* = \Delta_{F_m^{(2)}}$  are negative,  $\tilde{D}_1^2 = -1 = \tilde{D}_2^2$ , whereas those of the “extension” divisors are positive,  $\tilde{D}_3^2 = +1 = \tilde{D}_4^2$ .
3. Mutual intersections:  $\tilde{D}_i \cdot \tilde{D}_j = \begin{cases} +1, & \text{if } i, j \text{ are adjacent} \\ 0, & \text{otherwise} \end{cases}$ , as expected [21–23], — except  $\tilde{D}_{11} \cdot \tilde{D}_3 = -1$  and  $\tilde{D}_{11} \cdot \tilde{D}_4 = -1$ , because of the reversed, CW-orientation of the  $[\nu_{23}^\nabla, \nu_{34}^\nabla]$  facet, i.e., the extension.  $\blacksquare$

**Remark 3.3** The *standard* Newton polytope,  $\Delta_{F_m^{(2)}}^{(\text{std})} = (\Delta_{F_m^{(2)}}^*)^\circ = (\text{Conv}(\Delta_{F_m^{(2)}}^*))^\circ$  [19–23], is the (plain) left-hand half of the multitope in Figure 3, completed on the right-hand side with the vertex,  $(\frac{2}{m}, -1)$ . For  $m \geq 3$ , this polytope has no lattice point in the right-hand half-plane, its integral support spans an incomplete fan and so encodes a non-compact toric space. It contains  $6 + |m|$  lattice points, which cannot satisfy the 12-Theorem (2.5); correspondingly,  $d(\Delta_{F_m^{(2)}}^{(\text{std})}) = 4 + |m|$  cannot satisfy (2.6).  $\blacksquare$

**The  $E_m^{(2)}$  Sequence:** The  $E_m^{(2)}$  sequence (left-hand half of Figure 1) exhibits similar features<sup>20</sup>:

$\Sigma_{E_m^{(2)}}$	$\nu_1$	$\nu_2$	$\nu_3$	$\nu_4$
	1	$-m$	0	$-1$
	0	1	1	$-1$
$Q^1$	$m$	1	$-1$	0
$Q^2$	0	$-1$	$m+1$	$m$

The multifan  $\Sigma_{E_m^{(2)}}$  encodes the divisor relations:  $\widehat{D}_1 - m\widehat{D}_2 - \widehat{D}_4 \sim 0$  and  $\widehat{D}_2 + \widehat{D}_3 - \widehat{D}_4 \sim 0$ , which simplify computations, but we continue with the unreduced intersection numbers in (3.11), mid-right:

$$C_1^2(E_m^{(2, \#)}) = \sum_{i,j} \widehat{D}_i \cdot \widehat{D}_j = 9 + m \quad \text{but} \quad C_2(E_m^{(2, \#)}) = \sum_{i < j} \widehat{D}_i \cdot \widehat{D}_j = 3 - \frac{1}{m}, \quad (3.12)$$

which cannot possibly satisfy Noether’s relation (2.4). Again, unit-subdividing the (CW-oriented) cone,  $\nu_{23}$ , renders all intersection numbers integral (see (3.11) right), and satisfying Noether’s formula (2.4) for all  $m$ . Also, the self-intersection of the exceptional MPCP-divisors cancels the sum of its intersections with the two adjacent divisors just as in Figure 3, in the  $\pm(+1-2+1)$ -pattern, the overall sign chosen by the CCW/CW edge-orientation. Indeed,

$$C_2(E_m^{(2, \#)}) = 3 - \frac{1}{m} \quad \rightarrow \quad C_2(E_m^{(2)}) = 3 - m \quad (\text{MPCP desingularized}), \quad (3.13)$$

computed by adding up only the adjacent intersection numbers, once. The Mori vectors are  $\tilde{Q}^1_j := m\widehat{D}_2 \cdot \widehat{D}_j$  and  $\tilde{Q}^2_j := m\widehat{D}_3 \cdot \widehat{D}_j$ , of which the remaining vectors,  $\widehat{D}_1 \cdot \tilde{D}$  and  $\widehat{D}_4 \cdot \tilde{D}$ , are both positive linear combinations.

The analogous results for the transpolar multitope and multifan [38, 39] are:

$\Sigma_{E_m^{(2)}}$	$\nu_{41}^\nabla$	$\nu_{12}^\nabla$	$\nu_{23}^\nabla$	$\nu_{34}^\nabla$
	$-1$	$-1$	0	2
	2	$-1-m$	$-1$	$-1$
$\tilde{Q}^1$	1	$-1$	$3+m$	0
$\tilde{Q}^2$	0	2	$-3-2m$	1

<sup>20</sup>Here we focus on  $m > 0$ ; the  $m \leq 0$  cases are straightforward to analyze in the same manner, and in fact encode convex polytopes and fans for  $m \in [0, 3]$ ; see the discussion after (2.7).

where  $\tilde{D}_i = \hat{D}_i$  for  $i, 1 \dots, 4$  are the Cox divisors, and the exceptional MPCP divisors all have self-intersection  $-2$ , as indicated at far right in (3.14). The Mori vectors are now  $\tilde{Q}^1_j := (m+3)\hat{D}_2 \cdot \hat{D}_j$  and  $\tilde{Q}^2_j := 2\hat{D}_3 \cdot \hat{D}_j$ , of which the remaining vectors,  $\hat{D}_1 \cdot \tilde{D}$  and  $\hat{D}_4 \cdot \tilde{D}$ , are both positive linear combinations.

As with  $E_m^{(2)}$ , reading from the intersection diagrams yields:

$$C_2(\nabla E_m^{(2,\sharp)}) = \sum_{i<j} \hat{D}_i \cdot \hat{D}_j = \frac{1}{m+3} + 1 + \frac{1}{2} + \frac{1}{3} = \frac{11}{6} + \frac{1}{m+3}; \quad (3.15a)$$

$$C_1^2(\nabla E_m^{(2,\sharp)}) = \sum_{i,j} \tilde{D}_i \cdot \tilde{D}_j = (\frac{2}{3} - \frac{1}{m+3}) + (-\frac{1}{m+3}) + (-m - \frac{3}{2}) + (\frac{1}{6}) + 2(\frac{1}{m+3} + 1 + \frac{1}{2} + \frac{1}{3}) = 3 - m; \quad (3.15b)$$

$$C_2(\nabla E_m^{(2)}) = \sum_{i<j} \tilde{D}_i \cdot \tilde{D}_j = (9+m)(1) = 9+m; \quad (3.15c)$$

$$C_1^2(\nabla E_m^{(2)}) = \sum_{i,j} \tilde{D}_i \cdot \tilde{D}_j = 3(-1) + (-2-m) + (5+m)(-2) + 2(9+m)(1) = 3-m. \quad (3.15d)$$

Again, the intersection numbers *fail* to satisfy the Noether formula (2.4) for the *singular*  $\nabla E_m^{(2,\sharp)}$  encoded by the un-subdivided fan (3.14), but they *do satisfy* it for the *smooth*  $\nabla E_m^{(2)}$  encoded by the MPCP-subdivision of  $\Delta_{\nabla E_m^{(2)}}$  and its fan. The evaluation  $C_1^2(\nabla E_m^{(2,\sharp)}) = C_1^2(\nabla E_m^{(2)}) = 3-m = C_2(E_m^{(2)})$  is unaffected.

### 3.2 Three Dimensions

**Hirzebruch Scrolls:** With five vertices, the unreduced array of (Cox) divisor intersection numbers,  $D_i \cdot D_j \cdot D_k$ , now form a  $5 \times 5 \times 5$  *cube*. Computations with it are as straightforward as with the intersection number tables for 2-folds, but decidedly less intuitive and harder to display. This simplifies on using the relations among the Cox divisors  $D_i \leftarrow \nu_i$  implied by the fan and spanning polytope (far left in Figure 8, Appendix A.1),  $\Sigma_{F_m^{(3)}} \leftarrow \Delta_{F_m^{(3)}}$ :

$\Sigma_{F_m^{(3)}}$	$\nu_0$	$\nu_1$	$\nu_2$	$\nu_3$	$\nu_4$	$\nu_5$	$\Rightarrow -D_1 + D_2 - mD_5 \sim 0$
	0	-1	1	0	0	-m	$\Rightarrow -D_1 + D_3 - mD_5 \sim 0$
	0	-1	0	1	0	-m	$\Rightarrow D_4 - D_5 \sim 0$
	0	0	0	0	1	-1	$\Rightarrow D_3 \sim D_2, D_5 \sim D_4$
$Q^1$	-3	1	1	1	0	0	$D_1 \sim D_2 - mD_4$
$Q^2$	$m-2$	-m	0	0	1	1	

These relations permit using  $\{D_2, D_4\}$  as basis. Procedure 3.1 straightforwardly produces (for  $\tau = \nu_{23}$  and  $\tau = \nu_{24}$ ) the intersection numbers (immediately using commutativity)

$$D_2^3 \sim m, \quad D_2^2 \cdot D_4 \sim 1, \quad D_2 \cdot D_4^2 \sim 0, \quad (3.17)$$

normalized by using  $d(\nu_{23}^\nabla) = 2+2m$  and  $d(\nu_{24}^\nabla) = 3$  from Table 3. Using  $\tau = \nu_{12}$  similarly produces

$$D_1^2 \cdot D_2 \sim -m, \quad D_1 \cdot D_2^2 \sim 0, \quad D_1 \cdot D_2 \cdot D_4 \sim 0, \quad (3.18)$$

where the normalization by  $d(\nu_{12}^\nabla) = 2-m$  crucially becomes negative for  $m > 2$ , consistently with (3.16)–(3.17). In this way, Procedure 3.1 provides multiple verifications of the negative degrees in Table 3. The absence of the cones  $\nu_{123}$  and  $\nu_{45}$  from the fan  $\Sigma_{F_m^{(3)}}$  implies the Stanley–Reisner equivalence relations:

$$D_1 D_2 D_3 \sim 0 \quad \text{and} \quad D_4 D_5 \sim 0, \quad \xrightarrow{(3.16)} \quad D_2^3 \sim m D_2^2 D_4 \quad \text{and} \quad D_4^2 \sim 0. \quad (3.19)$$

the latter of which then implies  $D_4^2 \cdot D_i \sim 0$ , and  $D_4^3 \sim 0$  in particular.

The Chern class is given by the expansion, subject to the Stanley–Reisner relations (3.19) [19]:

$$c(F_m^{(3)}) = \prod_{\rho=1}^5 (1 + D_i) \Big|_{D^4=0} = 1 + \sum_{i=1}^5 D_i + \sum_{i<j=1}^5 D_i D_j + \sum_{i<j<k=1}^5 D_i D_j D_k, \quad (3.20)$$

$$c_1 \sim 3D_2 + (2-m)D_4, \quad c_2 \sim 3D_2^2 + 2(3-m)D_2D_4, \quad c_3 \sim 6D_2^2D_4. \quad (3.21)$$

This allows computing the Chern numbers from the divisor intersection numbers:

$$C_1^3 \sim [3D_2 + (2-m)D_4]^3 \sim [3D_2]^3 + 3[3D_2]^2[(2-m)D_4] = 27(m+2-m) = 54. \quad (3.22)$$

$$\begin{aligned} C_1C_2 &\sim [3D_2 + (2-m)D_4][3D_2^2 + (6-2m)D_2D_4] \sim [9D_2^3 + [3(6-2m) + 3(2-m)]D_2^2D_4] \\ &= 9m + [(18-6m) + (6-3m)] = 24. \end{aligned} \quad (3.23)$$

$$C_3 \sim [6D_2^2D_4] = 6, \quad (3.24)$$

which are in full agreement with the facet-orientation dependent results in Table 3. All these results are independently verified in the bi-projective embedding  $F_m^{(3)} \in [\mathbb{P}^3 \parallel \mathbb{P}^1 \mid \begin{smallmatrix} 1 \\ m \end{smallmatrix}]$ , by standard methods [9]:

$$\left[ \begin{array}{c|ccc} \mathbb{P}^3 & 1 & 1 & 1 \\ \mathbb{P}^1 & m & 0 & 0 \end{array} \right] \sim m, \quad \left[ \begin{array}{c|ccc} \mathbb{P}^3 & 1 & 1 & 0 \\ \mathbb{P}^1 & m & 0 & 0 \end{array} \right] \sim 1, \quad \left[ \begin{array}{c|ccc} \mathbb{P}^3 & 1 & 1 & 0 \\ \mathbb{P}^1 & m & 0 & 1 \end{array} \right] \sim 0 \sim \left[ \begin{array}{c|ccc} \mathbb{P}^3 & 1 & 0 & 0 \\ \mathbb{P}^1 & m & 1 & 1 \end{array} \right], \quad (3.25)$$

verifying the intersection numbers (3.17) to pertain to all smooth models in this deformation family.

The analogous intersection number computations are as straightforward for the transpolar toric space  $\nabla F_m^{(3)}$ , encoded by the flip-folded multifan,  $\Sigma_{\nabla F_m^{(3)}} \leftarrow \Delta_{\nabla F_m^{(3)}}^* = \Delta_{F_m^{(3)}}^*$ , shown (for  $m=3$ ) at right in [38, Fig. 3]. Since the MPCP-subdivided multitope  $\Delta_{\nabla F_m^{(3)}}^*$  contains  $30 + 8\vartheta_3^m(m-2)$  lattice points<sup>21</sup>, we forego computing here the cubically growing  $(^{32+8\vartheta_3^m(m-2)})$  (albeit mostly vanishing) triple divisor intersection numbers.

**The  $E_m^{(3)}$  Sequence:** Following Procedure 3.1 through all 2-cones ( $\nu_{45} \notin \Sigma_{E_m^{(3)}}$ ) of the multifan spanned by  $\Delta_{E_m^{(3)}}^*$  (mid-left in Figure 2), we find the redundant listing

$\tau: D_i \cdot D_j$	$D_1$	$D_2$	$D_3$	$D_4$	$D_5$	sums = $d(\nu_{ij}^\nabla)$
$\nu_{12}: D_1 \cdot D_2$	$m+1$	$m+1$	0	1	1	$2(2+m) = d(\nu_{12}^\nabla)$
$\nu_{13}: D_1 \cdot D_3$	0	0	$\frac{m+1}{m}$	1	$-1/m$	2 = $d(\nu_{13}^\nabla)$
$\nu_{14}: D_1 \cdot D_4$	1	1	1	1	0	4 = $d(\nu_{14}^\nabla)$
$\nu_{15}: D_1 \cdot D_5$	1	1	$-1/m$	0	$1/m$	2 = $d(\nu_{15}^\nabla)$
$\nu_{23}: D_2 \cdot D_3$	0	0	$\frac{m+1}{m}$	1	$-1/m$	2 = $d(\nu_{23}^\nabla)$
$\nu_{24}: D_2 \cdot D_4$	1	1	1	1	0	4 = $d(\nu_{24}^\nabla)$
$\nu_{25}: D_2 \cdot D_5$	1	1	$-1/m$	0	$1/m$	2 = $d(\nu_{25}^\nabla)$
$\nu_{34}: D_3 \cdot D_4$	1	1	1	1	0	4 = $d(\nu_{34}^\nabla)$
$\nu_{35}: D_3 \cdot D_5$	1	1	$-1/m$	0	$1/m$	2 = $d(\nu_{35}^\nabla)$

where each fractional entry (for  $m > 1$ ) stems from  $d(\nu_{153}) = d(\nu_{235}) = -m$ , i.e., by  $d(\nu_{35}) = -m$ . Each row of entries in (3.26) is normalized by the right-most sum in (3.1a), reading the  $d(\nu_{ij}^\nabla)$  directly from the left-most (plain but non-convex) polytope in Figure 2; its only  $m$ -dependence stems from the downward growing ‘‘icicle,’’ at  $\nu_{125}^\nabla$ . This listing conforms to the total symmetry of the intersection numbers.

The divisor relations in Figure 2 permit using  $\{D_4, D_5\}$  as a basis, wherein  $c_1(E_m^{(3)}) = 4D_4 + 2mD_5$ ,  $c_2(E_m^{(3)}) = 6D_4^2 + (m^2 - 1)D_5^2$ , and  $c_3(E_m^{(3)}) = 4D_4^3 - 2mD_5^3$ , since  $D_4 \cdot D_5 \sim 0$  the Stanley–Reisner relation. Then (for  $m \neq 0$ ),<sup>22</sup>

$$D_4^3 \sim 1 \quad \text{and} \quad D_5^3 \sim 1/m^2, \quad (3.27)$$

<sup>21</sup>Here,  $\vartheta_i^j = \{0 \text{ if } j < i, 1 \text{ if } j \geq i\}$  is the step-function. Each lattice point corresponds to a divisor, and so to the array of intersection numbers, regardless of the orientation of the face that contains it.

<sup>22</sup>Using that  $D_2 \sim D_1$ , the intersection table (3.26) implies  $D_1^3 \sim 1+m$ . With the Stanley–Reisner relation  $D_1 \cdot D_2 \cdot D_3 \sim 0$  and translated via the divisor relations in Figure 2 into the  $\{D_4, D_5\}$  basis, these become  $D_4^3 + m^3 D_5^3 \sim 1+m$  and  $D_4^3 - m^2 D_5^3 \sim 0$ , respectively, which imply (3.27). When  $m = -1$ , we find that  $D_4^3 \sim D_5^3$ . We then also use  $D_1 \cdot D_3 \cdot D_5 \sim 1$  to find  $D_5^3 \sim 1$ .

so:

$$c_1^3 \sim 64D_4^3 + 8m^3D_5^3 \xrightarrow{(3.27)} 64(1) + 8m^3\left(\frac{1}{m^2}\right) = 64+8m; \quad (3.28a)$$

$$c_1c_2 \sim 24D_4^3 + 2(m^3-m)D_5^3 \xrightarrow{(3.27)} 24(1) + 2(m^3-m)\left(\frac{1}{m^2}\right) = 24+2m-\frac{2}{m}; \quad (3.28b)$$

$$c_3 \sim 4D_4^3 - 2mD_5^3 \xrightarrow{(3.27)} 4(1) - 2m\left(\frac{1}{m^2}\right) = 4-\frac{2}{m}. \quad (3.28c)$$

Much as with the 2-dimensional analogue,  $E_m^{(2,\#)}$ , only the first of these, (3.28a),  $C_1^3(E_m^{(3,\#)}) = C_1^3(E_m^{(2)}) = C_3(\nabla E_m^{(2)}) = 64+8m$ , agrees with the results in Table 4; the other two Chern numbers are fractional for  $m > 2$ , disagree with Table 4 and fail to satisfy the Todd–Hirzebruch theorem (2.8).

The regular subdivision of the cones  $\nu_{35}$ ,  $\nu_{153}$  and  $\nu_{235}$  introduces  $m-1$  MPCP Cox divisors  $D_{5+k} \leftarrow (-k, -k, 1)$  for  $k=1, 2, \dots, (m-1)$ . While this considerably increases the collection of intersection numbers, it effectively replaces  $^{23} \frac{2}{m} \rightarrow 2m$  in (3.28b)–(3.28c), somewhat akin to the effective replacement (3.13). This makes the divisor intersection computed Chern numbers (3.28) perfectly reproduce the cone-degree results in Table 4, and of course also satisfy the Todd–Hirzebruch identity (2.8).

The analogous computations are as straightforward for the transpolar toric space  $\nabla E_m^{(3)}$ , encoded by the plain multifan,  $\Sigma_{\nabla E_m^{(3)}} \leftarrow \Delta_{\nabla E_m^{(3)}}^* = \Delta_{E_m^{(3)}}$ , shown (for  $m=2$ ) in the left-most illustration in Figure 2. Since the MPCP-subdivided multitope  $\Delta_{\nabla E_m^{(3)}}^*$  contains  $34+4m$  lattice points, we forego here computing the  $\binom{36+4m}{3}$  (albeit mostly vanishing) triple divisor intersection numbers.

## 4 Combinatorial and Cohomological Features of VEX Multitopes

**Betti Numbers:** Plain fans encode complex algebraic toric varieties (“toric crystals” [19, § 0.6]), for which the Betti numbers are completely determined by the fan:

**Theorem 4.1** (Danilov [19, p. 140], Fulton [21, p. 92]) *For the complex  $n$ -dimensional toric variety,  $X$ , encoded by the fan,  $\Sigma_X$ ,  $\dim H^{p,q}(X) = 0$  for  $p \neq q$ , and the Betti numbers,  $b_q(X) = \sum_{r=0}^q \dim H^{r,q-r}(X)$ , are:*

$$b_{2k+1}(X) = 0 \quad \text{and} \quad b_{2k}(X) = \sum_{i=k}^n (-1)^{i-k} \binom{i}{k} e_{n-i}, \quad k=0, 1, \dots, n, \quad (4.1)$$

where  $e_k$  is the number of  $k$ -dimensional cones in a regular subdivision of  $\Sigma_X \leftarrow \Delta_X^*$ .

**Remark 4.1** By definition,  $e_0 := 1$ . Also,  $e_n = d(\Delta_X^*)$  for all smooth (unit-subdivisible) VEX multitopes. Rational fans of toric varieties for which  $b_{2k+1}(X) = 0$  are *quasi-convex*, with boundaries supported by *real homology manifolds* [99, Thm. 4.2–4].  $\blacksquare$

The related classic result [19, Lemma 1.5], expressing the Poincaré series of a complex  $n$ -dimensional algebraic variety encoded by the polytope  $\Delta$  as  $P_\Delta(t) = \Phi_\Delta(t)(1-t)^{-n-1}$ , has a suitable generalization:

**Lemma 4.1** (T. Hibi [100]) *Let  $\Delta$  be an  $(L \approx \mathbb{Z}^n)$ -lattice polyhedral complex (a finite connected union of convex lattice polytopes) of dimension  $n$  that contains the faces of all (component) polytopes as well as all their intersections, and which is star-shaped, i.e., homeomorphic to an  $n$ -ball. Then*

$$\Phi_\Delta(t) = (1-t)^{n+1} \sum_{k=0}^{\infty} \ell_L(k\Delta) t^k = \sum_{k=0}^{\infty} h_k t^k, \quad \begin{cases} h_1 = \ell_L(\Delta) - (n+1), & h_0 = 1, \\ h_n = \ell_L(\Delta \setminus \partial\Delta), & h_i = 0 \text{ for } i > n. \end{cases} \quad (4.2)$$

<sup>23</sup>The mechanics of this owes to the fact that when a cone is subdivided,  $\sigma \rightarrow \sigma_1 \uplus \sigma_2$ , its sub-cones,  $\sigma_1, \sigma_2$ , replace  $\sigma$  in the specification of the multifan, so that  $\sigma$  enters the Stanley–Reisner (“irrelevant”) ideal. Thus, when  $\nu_{35}$  in the top, mid-left ( $m=2$ ) in Figure 2 is subdivided by adding  $\nu_6$ , the Stanley–Reisner ideal acquires contributions from both  $\nu_{35}$  and  $\nu_{46}$ , and so also  $\nu_{35i}$  and  $\nu_{46i}$  for all  $i = 1, \dots, 6$ . The absence of the latter 3-cones from the (unit-subdivided) multifan enforces the vanishing of the corresponding intersection numbers:  $D_3 \cdot D_5 \cdot D_i \sim 0$  and  $D_4 \cdot D_6 \cdot D_i \sim 0$ .

Also,  $h_1 \leq h_k$  for  $k \in [2, n]$  and

$$\sum_{i=0}^k h_i \leq \sum_{i=0}^k h_{n-i} \text{ for } k \in [0, \lfloor n/2 \rfloor], \quad \text{but} \quad \sum_{i=0}^{k+1} h_i \geq \sum_{i=0}^k h_{n-i} \text{ for } k \in [0, \lfloor (n-1)/2 \rfloor]. \quad (4.3)$$

Finally, if the monoid  $\oplus_k \vec{x}^{\vec{v}_k} t^k$  for  $\vec{v}_k \in (k\Delta \cap L)$  with  $0 \leq k \in \mathbb{Z}$  is Gorenstein (see [100] for precise details), then  $h_k = h_{n-k}$  for  $0 \leq k \leq n$ .

**Remark 4.2** The identification  $h_k(\Delta) = b_{2k}(X_\Delta)$  [21, §4.5] and Poincaré duality then imply the Dehn–Sommerville relations,  $h_k = h_{n-k}$ . Also, the Hard Lefschetz Theorem and the Kähler form generated SL(2)-action on  $H^{q,q}$  implies the so-called “unimodality”:  $h_{i-1} \leq h_i$  for  $i = 1, \dots, \lfloor n/2 \rfloor$ .  $\blacksquare$

Multifan/multitope generalizations of  $e_k$  and  $h_k$  exist and define the  $T_y$ -genus<sup>24</sup>,

$$T_y[\Sigma] = \sum_{k=0}^n h_k(\Sigma)(-y)^k = \sum_{k=0}^n e_{n-k}(\Sigma)(-1-y)^k, \quad e_{n-k}(\Sigma) = \sum_{i=k}^n \binom{i}{k} h_i(\Sigma), \quad (4.4)$$

but encode torus manifolds *incompletely* [47]: Betti numbers satisfy (4.1) only if the cohomology of  $X$  is (independently known to be) generated in degree two [48]. Multiple torus manifolds may therefore have the same multifan, but differing Betti numbers; see [45], and [54] for a (qualified) resolution. Akin to *minimal models* of birational geometry, we then propose (cf. Remark 1.8):

**Conjecture 4.1** (optimal torus manifold) *From among the real  $2n$ -dimensional torus manifolds [45–51, 53–55, 62],  $X$ , corresponding to a multifan,  $\Sigma_X$ , there exists an **optimal torus manifold** such that its ( $T^n$ -equivariant) Betti numbers are minimally non-negative, and with minimal values*

$$b_{2k}(X) \geq h_k(\Sigma_X) = \sum_{i=k}^n (-1)^{i-k} \binom{i}{k} e_{n-i}(\Sigma_X), \quad k = 0, 1, \dots, n, \quad (4.5)$$

that satisfy: (1) the Poincaré duality,  $b_{2n-r} = b_r$ , and (2) the Hard Lefschetz theorem, and (3) are consistent with all ( $T^n$ -equivariant) characteristic classes of  $X$ , as encoded by  $\Sigma_X$ .

**Remark 4.3** While VEX multitopes are indeed star-shaped [38], they may be flip-folded and multi-layered. Lemma 4.1 was found to hold for many examples such as the entire  $(F_m^{(n)}, \nabla F_m^{(n)})$ -sequence, but non-negativity (4.3) fails in the  $(E_m^{(n)}, \nabla E_m^{(n)})$ -sequence for some  $m$ ; see (4.10) and (4.11) as well as (4.14) and (4.15). This would imply that flip-folded (“extension” [38]) portions of a multifan/multitope encode locations in the corresponding torus manifold where some of the requisite (complex, symplectic, Kähler, ...) global structures degenerate, singularize or *reverse*; see footnote 3, p. 2. In examples such as  $\Delta_{E_m^{(n)}}^*$ , the relative sizes of the “extension” and the “standard part” depend on  $m$ , and may reverse roles.  $\blacksquare$

The fact that  $T^n$ -equivariant cohomology is key in distinguishing various *quasitoric manifolds* [101] corroborates its applications in string theory applications [102], especially since  $T^n = U(1)^n$  is the gauge group of the underlying worldsheet theory. An important class of generalizations is obtained by extending the  $\mathbb{C}^* \ni \lambda = |\lambda| e^{i\vartheta}$ -action to separate  $|\lambda|$ - and  $e^{i\vartheta}$ -actions [54]. In turn, intersection homology mentioned in Remark 4.1 is known to be modified in “middle dimension” by the (co)homology theory consistent with both mirror symmetry and geometric (conifold) transitions [67], as needed in string theory [65–67, 103]. It is at present not clear which combination (if any) of such generalizations may provide the necessary framework for Claims 1.1 and 1.2 and Conjectures 1.1 and 4.1 to hold, especially regarding the balance between the “standard” and “extension” parts and the corresponding degenerations in the requisite structures; see Remark 4.3 and also applications in string theory [94, 104], but also, e.g., [105–107].

<sup>24</sup>This extends the classic  $\chi_y$ -characteristic [81], interpolating between the Euler characteristic,  $\chi = T_{-1}$  and signature,  $\tau = T_1$

#### 4.1 Dehn–Sommerville and Unimodality Relations

Regarding the  $\Phi_\Delta(t)$ -function (4.2), we now test the validity and consequences of the Dehn–Sommerville and unimodality relations, and so also Hibi’s Lemma 4.1 and Theorem 4.1; see Remark 4.2.

##### 4.1.1 Two Dimensions

The Dehn–Sommerville relations for a 2-dimensional  $\Delta$  imply that  $\Phi_\Delta(t) = 1 + h_1 t + t^2$ . Then,

$$\Phi_\Delta(1) = d(\Delta) \quad \Rightarrow \quad h_1 = d(\Delta) - 2; \quad (4.6a)$$

$$P_\Delta(t) = 1 + (1 + d(\Delta))t + (1 + 3d(\Delta))t^2, \quad (4.6b)$$

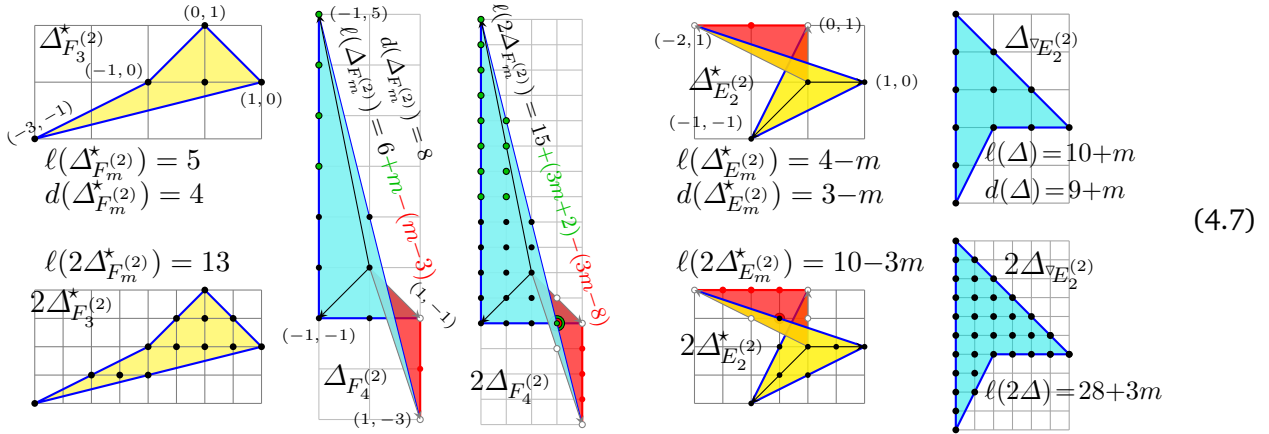
$$\ell(\Delta) = d(\Delta) + 1 \quad \text{and} \quad \ell(2\Delta) = 3d(\Delta) + 1. \quad (4.6c)$$

The first of the results (4.6c) holds for every VEX multitope  $\Delta_X^*$ : whether plain, flip-folded or otherwise multilayered — even when its winding number is 0, and there is no “interior”: All vertices of  $\Delta_X^*$  are primitive and so the first lattice point from the origin. All central triangles over facets contain lattice points only in the facets and the origin, so that each lattice point in  $\partial\Delta_X^*$  is primitive. Thereby,  $\Delta_X^*$  has a regular subdivision, the number of facet unit-segments equals the number of lattice points in  $\partial\Delta_X^*$ , so  $d(\Delta_X^*) = \ell(\partial\Delta_X^*)$ . Including by definition the origin in  $\ell(\Delta_X^*)$  results in  $\ell(\Delta_X^*) = d(\Delta_X^*) + 1$ . This also provides a sign-assignment to lattice points, i.e., 1-cones:

1.  $d(\nu_i) = +1$  if  $\nu_i = \nu_{ji} \cap \nu_{ik}$  and  $d(\nu_{ji}), d(\nu_{ik}) > 0$ , i.e., if the orientation remains +1 (CCW) through  $\nu_i$ .
2.  $d(\nu_i) = -1$  if  $\nu_i = \nu_{ji} \cap \nu_{ik}$  and  $d(\nu_{ji}), d(\nu_{ik}) < 0$ , i.e., if the orientation remains  $-1$  (CW) through  $\nu_i$ .
3.  $d(\nu_i) = 0$  if  $\nu_i = \nu_{ji} \cap \nu_{ik}$  and  $d(\nu_{ji}) \cdot d(\nu_{ik}) < 0$ , i.e., if the orientation changes through  $\nu_i$ .

This is exactly the counting that consistently determines the Euler and Hodge numbers of the Calabi–Yau hypersurfaces, Laurent-smoothed as needed [38].

**Explicit Verification:** It then remains to verify the second of the relations (4.6c):



As itemized above, lattice points occurring in the interior of negatively (CW) oriented cones (red-shaded in (4.7)) contribute negatively, while lattice points occurring in the interior of 1-cone intersections of positively (CCW) and negatively (CW) oriented 2-cones are counted with both signs, i.e., effectively do not count [38]. For both infinite sequences in Figure 1, this indeed confirms the relations (4.6):

$\Delta$	$d(\Delta)$	$\ell(\Delta) \stackrel{?}{=} d(\Delta) + 1$	$\ell(2\Delta) \stackrel{?}{=} 3d(\Delta) + 1$	$\Phi_\Delta(t)$
$\Delta_{F_m}^{*(2)}$	4	$5 \stackrel{\checkmark}{=} 4 + 1$	$13 \stackrel{\checkmark}{=} 3(4) + 1$	$1 + 2t + t^2$
$\Delta_{F_m}^{(2)}$	8	$9 \stackrel{\checkmark}{=} 8 + 1$	$25 \stackrel{\checkmark}{=} 3(8) + 1$	$1 + 6t + t^2$
$\Delta_{E_m}^{(2)}$	$9 + m$	$10 + m \stackrel{\checkmark}{=} 9 + m + 1$	$28 + 3m \stackrel{\checkmark}{=} 3(9 + m) + 1$	$1 + (7 + m)t + t^2$
$\Delta_{E_m}^{*(2)}$	$3 - m$	$4 - m \stackrel{\checkmark}{=} 3 - m + 1$	$10 - 3m \stackrel{\checkmark}{=} 3(3 - m) + 1$	$1 + (1 - m)t + t^2$

(4.8)

Furthermore, the first row in (4.8) confirms the independently known values  $\dim H^{*,*}(F_m^{(2)}) = (1, 2, 1)$ . The transpolar (Newton) multitope produces the results in the 2nd row, which correspondingly imply  $\dim H^{*,*}(\nabla F_m^{(2)}) = (1, 6, 1)$ , consistently with the 12-Theorem:  $\Phi_{F_m^{(2)}}(1) + \Phi_{\nabla F_m^{(2)}}(1) = 12$ . This is consistent with Lemma 4.1 holding for both the Hirzebruch surfaces,  $F_m^{(2)}$ , and their transpolar,  $\nabla F_m^{(2)}$ .

**The  $E_m^{(2)}$  Sequence:** The sum of  $\Phi$ -polynomials in the bottom half of (4.8) is also consistent with the 12-Theorem, the  $m$ -dependent contributions canceling between the two polynomials:  $\Phi_{E_m^{(2)}}(1) + \Phi_{\nabla E_m^{(2)}}(1) = 12$ . On the other hand,  $h_1(E_m^{(2)}) = (1-m)$  becomes negative for  $m > 1$ , fails the second of conditions (4.3), and clearly cannot equal any Hodge number. Similarly, for  $m < 0$ ,  $E_m^{(2)}$  is the  $|m|$ -fold iterated blowup of  $\mathbb{P}^2$ , its exceptional set consisting of a linear daisy-chain of  $\mathbb{P}^1$ s, for which  $\dim H^{1,1}(E_{-|m|}^{(2)}, \mathbb{Z}) = 1 + |m|$ . The transpolar toric space,  $\nabla E_{-|m|}^{(2)}$ , however has  $\Phi(t) = 1 + (7 - |m|)t + t^2$ , where  $h_1 = 7 - |m|$  cannot possibly equal a Hodge number when  $|m| > 7$ .

A *partial solution* is presented by the choice of the overall  $\Delta$ -orientation (using (4.6a)):

$d(\Delta_{E_m^{(2)}}^*) \Rightarrow h_1(\Delta_{E_m^{(2)}}^*)$	$d(\Delta_{\nabla E_m^{(2)}}^*) \Rightarrow h_1(\Delta_{\nabla E_m^{(2)}}^*)$	
<b>CCW :</b> $3-m \Rightarrow 1-m$	$9+m \Rightarrow 7+m$	(4.9)
<b>CW :</b> $m-3 \Rightarrow m-5$	$-9-m \Rightarrow -11-m$	

This shows that switching the overall orientation of the flip-folded multitope  $\Delta_{E_m^{(2)}}^*$  does permit a standard cohomological interpretation of  $h_1$ :

$$\text{CCW : } b_2(E_m^{(2)}) \stackrel{\checkmark}{=} h_1(E_m^{(2)}) = 1-m \geq 1, \quad \text{for } m \leq 0, \quad (4.10a)$$

$$\text{CW : } b_2(E_m^{(2)}) \stackrel{\checkmark}{=} h_1(E_m^{(2)}) = m-5 \geq 1, \quad \text{for } m \geq 6, \quad (4.10b)$$

excluding  $m = 1, \dots, 5$ . In turn,

$$\text{CCW : } b_2(\nabla E_m^{(2)}) \stackrel{\checkmark}{=} h_1(\nabla E_m^{(2)}) = 7+m \geq 1, \quad \text{for } m \geq -6, \quad (4.11a)$$

$$\text{CW : } b_2(\nabla E_m^{(2)}) \stackrel{\checkmark}{=} h_1(\nabla E_m^{(2)}) = -11-m \geq 1, \quad \text{for } m \leq -12, \quad (4.11b)$$

excludes a standard cohomological interpretation of  $h_1(\nabla E_m^{(2)})$  for  $m = -11, \dots, -7$ . Notably, *both*  $h_1(E_m^{(2)})$  and  $h_1(\nabla E_m^{(2)})$  can *simultaneously* have a standard cohomological interpretation only with overall CCW orientation and for  $m = -6, \dots, 0$ , when  $E_{-|m|}^{(2)} = \text{Bl}^{|m|}(\mathbb{P}^2)$ .

While reversing the overall multigon orientation may be consistent with a standard cohomological interpretation of  $\Phi_{\Delta}(t)$  for some multigons, this is not true for VEX multigons in general, nor for transpolar pairs of VEX multigons *simultaneously*; see also § 5.

#### 4.1.2 Three Dimensions

Dehn–Sommerville relations for a 3-dimensional  $\Delta$  imply  $\Phi_{\Delta}(t) = 1 + h_1 t + h_1 t^2 + t^3$ . Then,

$$\Phi_{\Delta}(1) = d(\Delta) \Rightarrow h_1 = \frac{1}{2}d(\Delta) - 1, \quad (4.12a)$$

$$P_{\Delta}(t) = \Phi_{\Delta}(t)/(1-t)^4 \Big|_{t^4=0} = 1 + (h_1+4)t + (5h_1+10)t^2 + (14h_1+21)t^3, \quad (4.12b)$$

$$\ell(\Delta) = \frac{1}{2}d(\Delta) + 3, \quad \ell(2\Delta) = \frac{5}{2}d(\Delta) + 5, \quad \text{and} \quad \ell(3\Delta) = 7d(\Delta) + 7. \quad (4.12c)$$

It remains to verify the relations (4.12c), which we do by direct counting:

$\Delta$	$d(\Delta)$	$\frac{\ell(\Delta)}{2}+3$	$\frac{\ell(2\Delta)}{2}+5$	$\frac{\ell(3\Delta)}{7}+7$	$\Phi_\Delta(t)$
$\Delta_{F_m^{(3)}}^*$	6	6 ✓	20 ✓	49 ✓	$1 + 2t + 2t^2 + t^3$
$\Delta_{F_m^{(3)}}$	54	30 ✓	140 ✓	385 ✓	$1 + 26t + 26t^2 + t^3$
$\Delta_{E_m^{(3)}}$	$64+8m$	$35+4m$ ✓	$165+20m$ ✓	$455+56m$ ✓	$1 + (31+4m)t + (31+4m)t^2 + t^3$
$\Delta_{E_m^{(3)}}^*$	$4-2m$	$5-m$ ✓	$15-5m$ ✓	$35-14m$ ✓	$1 + (1-m)t + (1-m)t^2 + t^3$

The lattice points in the scaled flip-folded multitopes,  $k\Delta_{F_m^{(3)}}$  and  $k\Delta_{E_m^{(3)}}^*$ , are counted according to the orientation of the cones containing them in their relative interior, directly extending the counting that was used in [38] to compute the Euler characteristic and the Hodge numbers of the Calabi–Yau hypersurface.

The so-computed  $\Phi_\Delta(t)$ -polynomial correctly identifies the known values  $h^{1,1}(F_m^{(3)})=2=h^{2,2}(F_m^{(3)})$ . The corresponding identifications  $h^{1,1}(\nabla F_m^{(3)})=26=h^{2,2}(\nabla F_m^{(3)})$  are consistent with the general expectation. (The signed total of 81 subdividing unit-degree edges<sup>25</sup> connecting the signed total of 29 lattice points of  $\partial\Delta_{F_m^{(3)}}$  encode a wealth of MPCP-desingularizations, which contribute to the  $(q, q)$ -cohomology.)

On the other hand,  $h_1(E_m^{(3)})=(1-m)$  in  $\Phi_{E_m^{(3)}}(1)$  becomes negative for  $m>1$  and so clearly cannot equal a Hodge number, just as in the 2-dimensional case (4.8). Again, for  $m<0$ ,  $E_m^{(2)}$  is an  $|m|$ -fold iterated blowup of  $\mathbb{P}^3$ . Now  $h_1$  for the transpolar toric space,  $\nabla E_m^{(3)}$ , becomes negative for  $m<-8$  and so cannot possibly equal a Hodge number. As in §4.1.1 for  $(E_m^{(2)}, \nabla E_m^{(2)})$ , we use (4.12a) and now find that

$$\text{CCW} : b_2(E_m^{(3)}) \stackrel{\check{=}}{=} h_1(E_m^{(3)}) = 1-m \geq 1, \quad \text{for } m \leq 0, \quad (4.14a)$$

$$\text{CW} : b_2(E_m^{(3)}) \stackrel{\check{=}}{=} h_1(E_m^{(3)}) = m-3 \geq 1, \quad \text{for } m \geq 4, \quad (4.14b)$$

excluding  $m=1, 2, 3$  — which is better than (4.10). In turn,

$$\text{CCW} : b_2(\nabla E_m^{(3)}) \stackrel{\check{=}}{=} h_1(\nabla E_m^{(3)}) = 31+4m \geq 1, \quad \text{for } m \geq -7, \quad (4.15a)$$

$$\text{CW} : b_2(\nabla E_m^{(3)}) \stackrel{\check{=}}{=} h_1(\nabla E_m^{(3)}) = -33-4m \geq 1, \quad \text{for } m \leq -9, \quad (4.15b)$$

excludes a standard cohomological interpretation of  $h_1(\nabla E_m^{(2)})$  only for  $m=-8$  — again better than (4.11). Notably, both  $h_1(E_m^{(2)})$  and  $h_1(\nabla E_m^{(2)})$  can simultaneously have a standard cohomological interpretation only with overall CCW orientation and for  $m=-6, \dots, 0$ , when  $E_{-|m|}^{(3)} = \text{Bl}^{|m|}(\mathbb{P}^3)$ .

This last result being the *same* as in the 2-dimensional case reinforces the closing conclusion of §4.1.1, that the standard cohomological interpretation of  $\Phi_\Delta(t)$  cannot hold for VEX multitopes in general.

### 4.1.3 Four Dimensions

By definition, VEX polytopes are star-shaped with respect to a preferred  $L$ -lattice point (the origin) [38], so Lemma 4.1 applies to all of them. It has also been conjectured [108] that unimodality,  $h_{k-1} \leq h_k$  for  $k \in [1, \lfloor n/2 \rfloor]$ , requires an additional (“integer decomposition”) property [109] — which the above computations show *fails* for at least some VEX multitopes, such as  $\Delta_{E_m^{(n)}}^*$ .

Focusing thus on the Dehn–Sommerville relations (Poincaré duality), for 4-dimensional  $\Delta$ ,

$$\Phi_\Delta(t) = \left(1 + \sum_{k=1}^4 \ell(k\Delta)t^k\right)(1-t)^5 \Big|_{t^5=0} = 1 + h_1t + h_2t^2 + h_1t^3 + t^4 \quad (4.16)$$

<sup>25</sup>Each VEX multotope is a star-shaped domain with a signed multiplicity, and the multifan spanned by  $\Delta_{F_m^{(3)}} = \Delta_{\nabla F_m^{(3)}}^*$  covers  $M \otimes_{\mathbb{Z}} \mathbb{R} \approx \mathbb{R}^3$  effectively once: the winding number  $w(\Delta_{\nabla F_m^{(3)}}^*)=1$  and so is the Todd genus,  $\text{Td}[\nabla F_m^{(3)}]=1$ . Therefore,  $\Delta_{F_m^{(3)}} = \Delta_{\nabla F_m^{(3)}}^*$  is homotopic (with signed multiplicity) to a 3-ball, and  $\partial\Delta_{F_m^{(3)}}^*$  to  $S^2$ , for which Euler’s well-known triangulation result determines the number of unit-degree edges as  $(\ell(\Delta_{F_m^{(3)}})-1)+d(\Delta_{F_m^{(3)}})-2=81$  — which is verified by direct counting.

which implies

$$\begin{aligned} \ell(3\Delta) - 5\ell(2\Delta) + 10\ell(\Delta) - 10 &\stackrel{\doteq}{=} \ell(\Delta) - 5 &\Rightarrow \ell(3\Delta) &= 5\ell(2\Delta) - 9\ell(\Delta) + 5, \\ \ell(4\Delta) - 5\ell(3\Delta) + 10\ell(2\Delta) - 10\ell(\Delta) + 5 &\stackrel{\doteq}{=} 1 &\Rightarrow \ell(4\Delta) &= 15\ell(2\Delta) - 35\ell(\Delta) + 21. \end{aligned} \quad (1.8')$$

Using also that

$$d(\Delta) = \Phi_{\Delta}(1) = 1 + \underbrace{(\ell(\Delta) - 5)}_{h_1} 1 + \underbrace{(\ell(2\Delta) - 5\ell(\Delta) + 10)}_{h_2} 1^2 + (\ell(\Delta) - 5)1^3 + 1^4, \quad (4.17)$$

implies that

$$d(\Delta) = \ell(2\Delta) - 3\ell(\Delta) + 2, \quad \text{i.e.,} \quad \ell(2\Delta) = 3\ell(\Delta) + d(\Delta) - 2, \quad (1.9')$$

which allows rewriting the formula (1.7) for the Euler number of the Calabi–Yau hypersurface as

$$\chi(Z_f) \stackrel{(1.9)}{=} 2 \left[ (\ell(2\Delta_X) - \ell(2\Delta_X^*)) - 9(\ell(\Delta_X) - \ell(\Delta_X^*)) \right]. \quad (1.10')$$

The weaker condition of unimodality would imply that

$$h_1 \leq h_2 \Rightarrow \ell(\Delta) \leq \frac{13}{3} + \frac{1}{3}d(\Delta), \quad \text{i.e.} \quad d(\Delta) \geq 3\ell(\Delta) - 13, \quad (4.18a)$$

$$1 \leq h_1 \leq h_2 \Rightarrow d(\Delta) \geq 5 \ \& \ 6 \leq \ell(\Delta) \leq \frac{13}{3} + \frac{1}{3}d(\Delta). \quad (4.18b)$$

Based on the above results for  $E_m^{(2)}$  and  $E_m^{(3)}$ , these are expected to fail for some multitoes, but perhaps hold for torus manifolds with the “additional (integer decomposition) property [109].” A systematic testing of the above relations and the inequalities (4.18) is clearly best left to computer-aided counting.

## 5 Surgery

A multifan,  $\Sigma_X$ , and its spanning VEX multitope,  $\Delta_X^*$ , both correspond to a toric space,  $X$ , *directly*<sup>26</sup>: Each  $k$ -dimensional cone  $\sigma \in \Sigma_X$ , corresponds to a  $k$ -dimensional subspace of  $X$ . Two such  $k$ -dimensional subspaces “glue” along the  $(k-r)$ -dimensional “interface” corresponding to the  $(k-r)$ -dimensional intersection  $\sigma \cap \sigma'$  as specified by the multifan  $\Sigma_X$  (= a facet-ordered poset [46, 47]). This may be used to reconstruct the corresponding spaces.

### 5.1 Flip-Folded Extension Replacement

Let us reconsider the example  $(F_3^{(2)}, \nabla F_3^{(2)})$  from (3.9) and Figure 3, shown here in the top half of Figure 4 upon the  $\text{GL}(2; \mathbb{Z})$  transformation  $\begin{bmatrix} x \\ y \end{bmatrix} \rightarrow \begin{bmatrix} -1 & -1 \\ 2 & 1 \end{bmatrix} \begin{bmatrix} x \\ y \end{bmatrix}$ . The doubling of  $\nu_* \in \Sigma_{\widehat{F}_3^{(2)}}$  (Figure 4, bottom mid-right) is transpolar to the double-covering of the 1st quadrant (outward fading shade in Figure 4, bottom mid-left) by parts of  $\langle \nu_{12}^{\nabla}, \nu_{23}^{\nabla} \rangle$  and  $\langle \nu_{45}^{\nabla}, \nu_{51}^{\nabla} \rangle$ , which are in different (Riemann sheet like) layers of  $\Sigma_{\nabla \widehat{F}_3^{(2)}}$ . In turn, the (CCW-oriented, large, right-triangular) “sail” in  $\Sigma_{\widehat{F}_3^{(2)}}$  (bottom mid-right) is transpolar to the dart-shaped portion  $\langle \nu_{23}^{\nabla}, \nu_{34}^{\nabla}, \nu_{45}^{\nabla} \rangle \subset \Sigma_{\nabla \widehat{F}_3^{(2)}}$  (bottom mid-left).

**Surgery Result:** The cone-degree data are also straightforward to read off directly from Figure 4 and are shown in Table 6. Here,  $C_1^2(\widehat{F}_3^{(2)}) + C_2(\widehat{F}_3^{(2)}) = 2 \cdot 12$ , indicating that  $\text{Td}(\widehat{F}_3^{(2)}) = \chi^h(\widehat{F}_3^{(2)}) = 2$  [47, 57], all in complete agreement with the intersection number computations indicated in Figure 4. The double-winding multitoes at the bottom of Figure 4 correspond to torus manifolds,  $\nabla \widehat{F}_3^{(2)}$  (left) and its transpolar,  $\widehat{F}_3^{(2)}$  (right), both with  $\text{Td} = 2$ , such as discussed in [45–48]. Figure 4 then relates by surgery the transpolar pair  $(F_3^{(2)}, \nabla F_3^{(2)})$  to a transpolar pair of such torus manifolds,  $(\widehat{F}_3^{(2)}, \nabla \widehat{F}_3^{(2)})$ .

<sup>26</sup>In contrast, the transpolar Newton multitope,  $\Delta_X$ , and its multifan,  $\mathfrak{S}_X$ , encode anticanonical sections,  $f \in \Gamma(\mathcal{K}_X^*)$ , over a toric space,  $X$ ; thereby,  $\Delta_X$  corresponds *dually* to  $X$ .

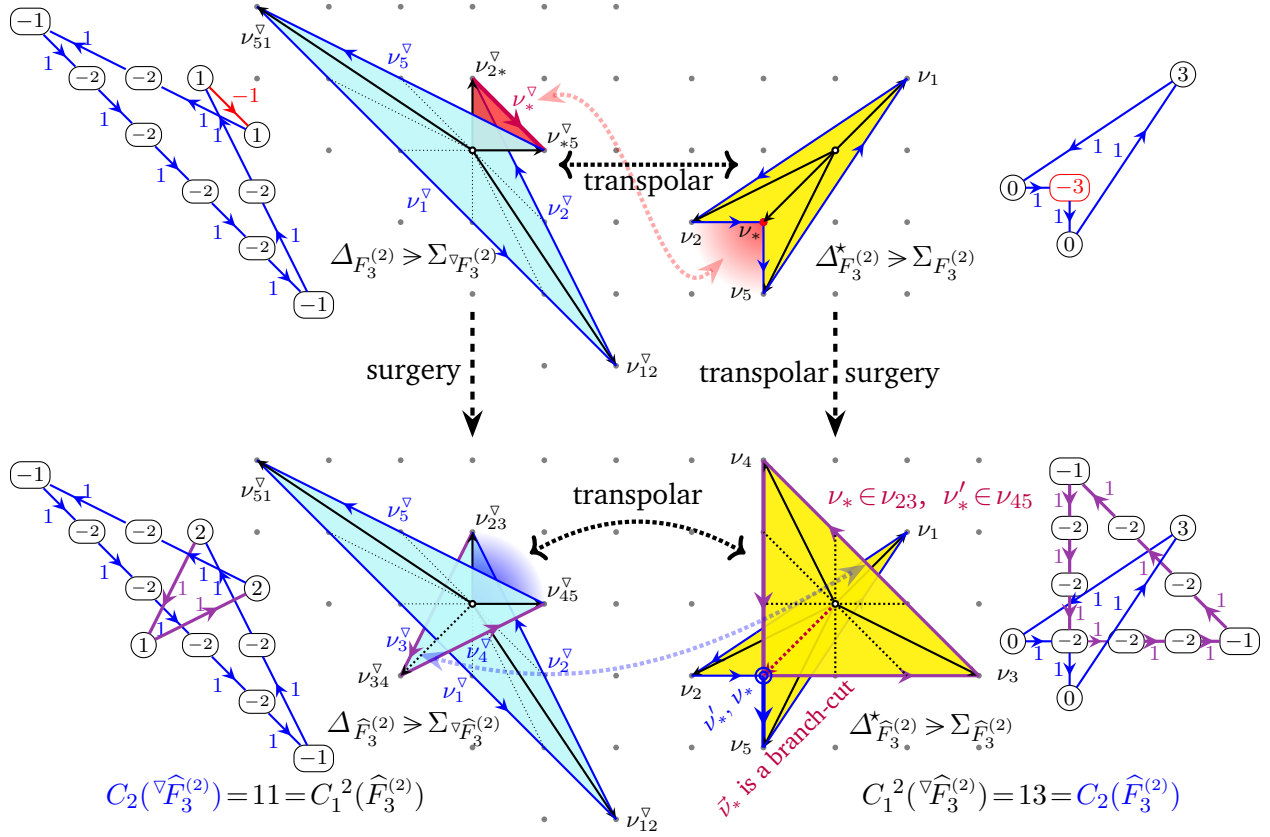


**Figure 4:** Surgical replacement of the negative (CW)  $\nu_*^\nabla \in \Delta_{F_3^{(2)}}$  edge (top, mid-left, red) with a positive (CCW) link  $\nu_3^\nabla \#_{\nu_{34}^\nabla} \nu_4^\nabla$  (bottom, mid-left). This effectively subdivides the (reflex, 270°, CCW) complement of the CW 2-cone over  $\nu_*^\nabla$  by inserting  $\nu_{34}^\nabla$ , and so encodes a blowdown/contraction of sort,  $\widehat{F}_3^{(2)} \rightarrow \nabla F_3^{(2)}$ ; the 1-cone  $\nu_{34}^\nabla$  is a branch-cut. The transpolar of this surgery is shown at right.

**The Encoded Surgery:** Consider decomposing  $\Sigma_{\widehat{F}_3^{(2)}} = \nu_{12} \uplus \nu_{23} \uplus \nu_{34} \uplus \nu_{45} \uplus \nu_{51}$  along the “branch-cut,”  $\nu_*$ , indicating the cross-over of the two layers of this depiction of the multifan:

$$\begin{array}{c} \nu_4 \\ \cdot \\ \cdot \\ \cdot \\ \cdot \\ \nu_1 \\ \cdot \\ \cdot \\ \cdot \\ \nu_2 \\ \cdot \\ \cdot \\ \nu_3 \\ \cdot \\ \cdot \\ \nu_5 \end{array} \begin{array}{c} \nu_* \in \nu_{23}, \nu'_* \in \nu_{45} \\ \Delta_{\widehat{F}_3^{(2)}} \geq \Sigma_{\widehat{F}_3^{(2)}} \end{array} = \begin{array}{c} \nu_4 \\ \cdot \\ \cdot \\ \cdot \\ \cdot \\ \nu_1 \\ \cdot \\ \cdot \\ \cdot \\ \nu_2 \\ \cdot \\ \cdot \\ \nu_3 \\ \cdot \\ \cdot \\ \nu_5 \end{array} \begin{array}{c} \Sigma_{F_3^{(2)}} \setminus \mathbb{P}_*^1 \\ \Delta_{\widehat{F}_3^{(2)}} \geq \Sigma_{\widehat{F}_3^{(2)}} \end{array} \uplus_{2\mathbb{P}_*^1} \begin{array}{c} \nu_4 \\ \cdot \\ \cdot \\ \cdot \\ \cdot \\ \nu_1 \\ \cdot \\ \cdot \\ \cdot \\ \nu_2 \\ \cdot \\ \cdot \\ \nu_3 \\ \cdot \\ \cdot \\ \nu_5 \end{array} \begin{array}{c} \Sigma_{\nabla \mathbb{P}^2} \setminus \mathbb{P}_*^1 \\ \Delta_{\widehat{F}_3^{(2)}} \geq \Sigma_{\widehat{F}_3^{(2)}} \end{array} \quad (5.1)$$

Both sub-fans, in the middle and on the right, are incomplete as  $\nu_* \subset \nu_{23}$  and  $\nu'_* \subset \nu_{45}$  lie in different layers of the original multifan on the left in (5.1). Their glueing (along  $\nu_*$  and  $\nu'_*$ , in each respective layer) then (re-)introduces two  $\mathbb{P}^1$ s, as indicated by the subscript of the adjoining:  $\widehat{F}_3^{(2)} = (F_3^{(2)}) \#_{2\mathbb{P}_*^1} (\nabla \mathbb{P}^2)$  is a *connected sum* of the two components along the two different-layer images of  $\mathbb{P}_*^1 \leftrightarrow \nu_*$ . This agrees with the simple Euler number computation,

$$13 \stackrel{\text{Fig. 4}}{=} \chi(\widehat{F}_3^{(2)}) \stackrel{(5.1)}{=} (\chi(F_3^{(2)}) - \chi(\mathbb{P}_*^1)) + \chi(2\mathbb{P}_*^1) + (\chi(\nabla \mathbb{P}^2) - \chi(\mathbb{P}_*^1)) = (4-2) + (9-2) + 2(2). \quad (5.2)$$

dim	$\Sigma_{\widehat{F}_3^{(2)}} \triangleleft \Delta_{\widehat{F}_3^{(2)}}^*$	$\xleftrightarrow{\nabla}$	$\Delta_{\widehat{F}_3^{(2)}} \triangleright \Sigma_{\widehat{F}_3^{(2)^\nabla}$	dim	$\sum d(\nu_*)d(\nu_*^\nabla)$
0	$d(0) = 1$		$d(0^\nabla) = 11$	3	$\rightarrow 11$
1	$d(\nu_1) = 1$ $d(\nu_2) = d(\nu_5) = 1$ $d(\nu_3) = d(\nu_4) = 1$		$d(\nu_1^\nabla) = 5$ $d(\nu_2^\nabla) = d(\nu_4^\nabla) = 2$ $d(\nu_3^\nabla) = d(\nu_4^\nabla) = 1$	2	$\rightarrow 5$ $\rightarrow 2 \times 2$ $\rightarrow 2 \times 1$ } $11 = C_1^2(\widehat{F}_3^{(2)})$
2	$d(\nu_{12}) = d(\nu_{51}) = 1$ $d(\nu_{23}) = d(\nu_{45}) = 4$ $d(\nu_{34}) = 3$		$d(\nu_{12}^\nabla) = d(\nu_{51}^\nabla) = 1$ $d(\nu_{23}^\nabla) = d(\nu_{45}^\nabla) = 1$ $d(\nu_{34}^\nabla) = 1$	1	$\rightarrow 2 \times 1$ $\rightarrow 2 \times 4$ $\rightarrow 3$ } $13 = C_2(\widehat{F}_3^{(2)})$
3	$d(\nu_{1\dots 5}) = 13$		$d(\nu_{1^\nabla\dots 5}^\nabla) = 1$	0	$\rightarrow 13$

**Table 6:** The cones and their degrees, spanned by the transpolar pair  $(\Delta_{\widehat{F}_3^{(2)}}^*, \Delta_{\widehat{F}_3^{(2)}})$

While the uniform CCW-orientation of multifans such as (5.1) may well imply an almost complex structure, its winding number,  $(w=2) = \text{Td}(\widehat{F}_3^{(2)})$ , obstructs a global complex structure<sup>27</sup>, and a more precise identification of corresponding torus manifolds such as  $\widehat{F}_3^{(2)}$  requires further systematic study.

Correspondingly, the transpolar multitope  $\Delta_{\widehat{F}_3^{(2)^\nabla}$ , at bottom left in Figure 4, may be similarly decomposed  $\nabla\widehat{F}_3^{(2)} = (\nabla F_3^{(2)}) \#_{\mathbb{P}_{23}^1, \mathbb{P}_{45}^1}(\mathbb{P}^2)$ , as shown in Figure 5, which agrees with the corresponding simple Euler

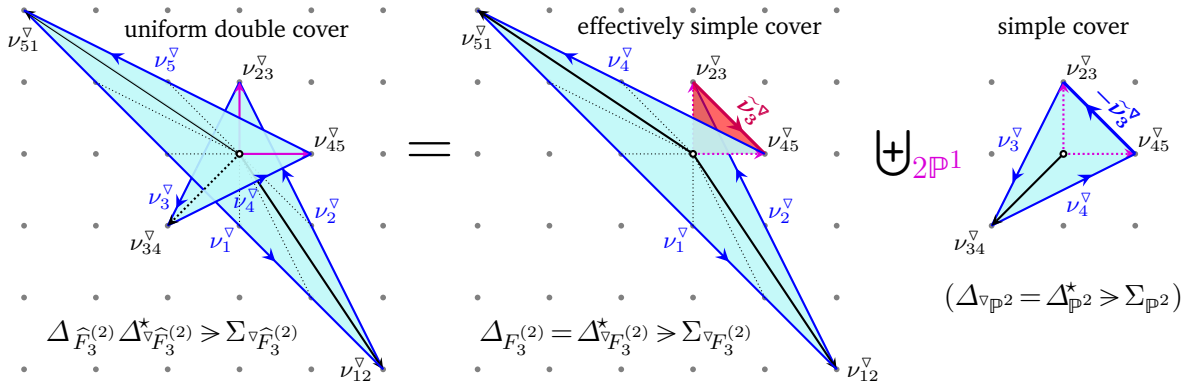


**Figure 5:** Disjoining of the surgery depicted in Figure 4

number calculation

$$11 \stackrel{\text{Fig. 4}}{=} \chi(\nabla\widehat{F}_3^{(2)}) \stackrel{\text{Fig. 5}}{=} (\chi(\nabla F_3^{(2)}) - \chi(\mathbb{P}_*^1)) + (\chi(\mathbb{P}^2) - \chi(\mathbb{P}_*^1)) + \chi(2\mathbb{P}^1) = (8-2) + (3-2) + 2(2). \quad (5.3)$$

In this surgery, the CW 2-cone over  $\widetilde{\nu}_3^\nabla \in \Delta_{F_3^{(2)^\nabla}$  effectively cancels the CCW 2-cone over  $-\widetilde{\nu}_3^\nabla \in \Delta_{\nabla\mathbb{P}^3}$ , and is replaced by the composite  $\nu_3^\nabla \uplus \nu_4^\nabla$ . This suggests interpreting  $\nabla\widehat{F}_3^{(2)}$  (Figure 5, far left) as something akin to a blowup of  $\nabla F_3^{(2)}$  at a point in the chart  $U_{\widetilde{\nu}_3^\nabla}$  (Figure 5, middle).

Indeed, the above examples showcase the utility of multifans and the multitopes that span them in encoding not only toric spaces and a host of their diffeomorphism invariants, but also toric surgeries well beyond the standard blowups and MPCP desingularizations [19–23] and [27]. In particular, the surgery indicated in Figure 5 allows *reverse-engineering*  $\nabla F_m^{(2)}$  from the torus manifold  $\widehat{F}_m^{(2)}$ , specified by the indicated uniformly CCW-oriented (but double-winding) multifan at far left in Figure 5 and the (complex algebraic)

<sup>27</sup>Assuming simple-connectedness ( $h^{0,0}=1, h^{1,0}=0=h^{0,1}$ ) and Poincaré duality ( $h^{2,2}=1, h^{2,1}=0=h^{1,2}$ ) would then imply  $h^{2,0}=1=h^{0,2}$  — which is a K3-like Hodge diamond, however with  $h^{1,1}=9$ .

toric variety  $\mathbb{P}^1$ , its familiar spanning polytope at the far right in Figure 5. In a similar vein,

$$F_2^{(2)} \xleftarrow{3} E_1^{(2)} \xleftarrow{4} \widehat{E}_2^{(2)} \xrightarrow{5} E_2^{(2)} \xrightarrow{4} \mathbb{P}^2 \quad (5.4)$$

somewhat akin to a sequence of blowdown contractions. Both of these suggest, much more generally:

**Claim 5.1 (unflip-folding)** Every **flip-folded** multitope (multifan), wherein some faces (cones) have opposite orientation, may be surgically reverse-engineered in terms of only **uniformly** oriented multitopes (multifans), all of which correspond to torus manifolds [45, 47], algebraic varieties included.

## 5.2 Complex vs. Pre-Complex Structure

Consider the sequence  $E_m^{(2)}$  with  $m=2, \dots, -2$  depicted in Figure 6. The right-hand side of the sequence

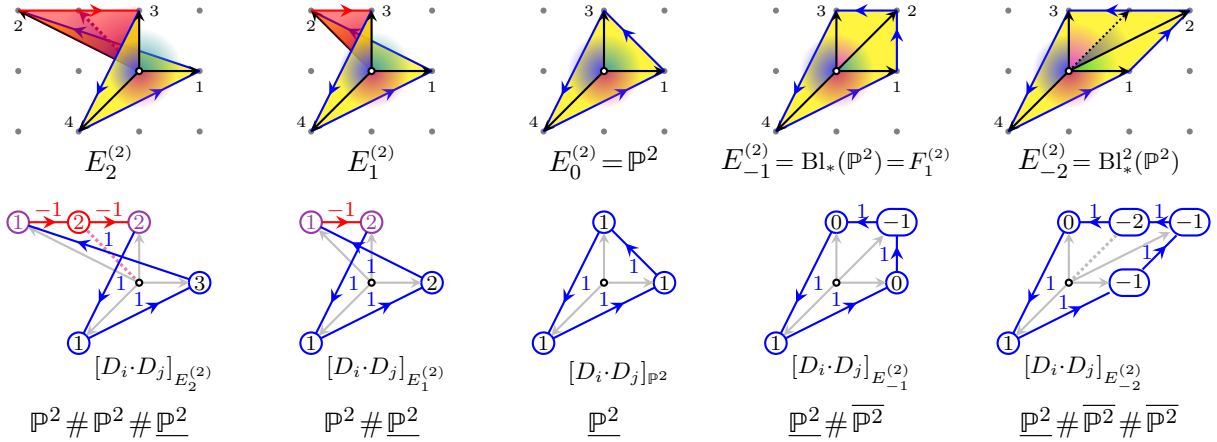


**Figure 6:** The sequence of multigons,  $E_m^{(2)}$  for  $m=2, \dots, -2$ , their respective multifans, and the corresponding Cox divisor intersection numbers, identified with iterative blowups of an “initial” (underlined)  $\mathbb{P}^2$

depicts  $\mathbb{P}^2$  in the middle, its standard blowup at a smooth point (center-right) and the (iterated) double blowup at far right. It is standard [110, Prop. 2.5.8, p. 102] that  $E_{-1}^{(2)} = \text{Bl}_*(\mathbb{P}^2) = F_1^{(2)}$  is diffeomorphic (as an oriented differentiable manifold) to the connected sum,  $\mathbb{P}^2 \# \overline{\mathbb{P}^2}$ , where  $\overline{\mathbb{P}^2}$  denotes the complex projective space with the orientation opposite to the one naturally induced by the complex structure.<sup>28</sup> This corresponds to the fact that the 1-cone  $(1, 1) \in \Sigma_{E_{-1}^{(2)}}$  encodes the exceptional set of self-intersection  $[\mathcal{E}_{(1,1)}]^2 = -1$ , and the base  $\mathbb{P}^1$  of a *local* neighborhood biholomorphic to the total space of  $\mathcal{O}_{\mathbb{P}^1}(-1)$  [110]. This  $\mathcal{E}_{(1,1)} \approx \mathbb{P}^1$  may be identified with the hyperplane<sup>29</sup> in the 2nd (orientation-reversed) summand in the connected sum,  $\mathbb{P}^2 \# \overline{\mathbb{P}^2}$ , with “the rest” of the fan  $\Sigma_{E_{-1}^{(2)}}$  corresponding to the 1st summand. The iterates,  $E_{-2}^{(2)} = \text{Bl}_*^2(\mathbb{P}^2)$  in Figure 6 (far right) and  $E_{-m}^{(2)}$  for  $m \geq 1$  in general, are blowups of  $\mathbb{P}^2$  at “infinitely near points,” and are easily identified as a daisy-chain connected sum of  $\mathbb{P}^2$ ’s, with orientations opposite to the “initial” (underlined) one.

In turn, the 1-cone  $(-1, 1) \in \Sigma_{E_1^{(2)}}$  encodes the exceptional set of self-intersection  $[\mathcal{E}_{(-1,1)}]^2 = +1$ , and so is the base  $\mathbb{P}^1$  with the local neighborhood biholomorphic to the total space of  $\mathcal{O}_{\mathbb{P}^1}(+1)$ . This implies  $E_1^{(2)}$  to be akin to the blowup,  $E_{-1}^{(2)}$ , with however an *opposite* normal space of the exceptional  $\mathcal{E}_{(-1,1)} \approx \mathbb{P}^1$ . It can

<sup>28</sup>The orientation reversal is necessary for the complex structure of one component to extend through the other component compatibly with the orientation of the underlying real space: At the crossover/gluing region, the “radially” inward directions in one component must match the “radially” outward directions in the other component.

<sup>29</sup>It is also convenient to identify the hyperplane  $\mathbb{P}^1 \subset \mathbb{P}^2$  with the “ $\mathbb{P}^1$  at infinity” in the cell-decomposition,  $\mathbb{P}^2 \simeq \mathbb{C}^2 \cup \mathbb{P}^1$ .

thus also be identified with  $E_1^{(2)} \simeq_{\mathbb{R}} \mathbb{P}^2 \# \mathbb{P}^2$  (diffeomorphic as oriented differentiable manifolds), however without orientation-reversal in either summand<sup>30</sup>, which obstructs a global complex structure: Extending the complex structure of (the underlined)  $\mathbb{P}^2 \setminus \{\text{pt.} \in U_{\nu_{13}}\}$  to the region  $(U_{\nu_{12}} \uplus U_{\nu_{23}}) \supset \mathcal{E}_{(-1,1)}$  (replacing  $U_{\nu_{13}}$  as encoded by  $\nu_{13} \rightarrow \nu_{12} \uplus \nu_{23}$ ) is obstructed by the exceptional set  $\mathcal{E}_{(-1,1)}$  and its  $\mathcal{O}_{\mathbb{P}^1}(+1)$ -like local neighborhood. Thus, the non-compact space  $E_1^{(2)} \setminus \mathcal{E}_{(-1,1)}$  is complex, while  $E_1^{(2)}$  is “only” precomplex; this is akin to  $(S^4 \setminus \{\text{pt.}\}) \approx \mathbb{C}^2$  being complex, while  $S^4$  is not.<sup>31</sup> For  $m > 0$ ,  $E_m^{(2)}$  are then daisy-chain connected sums of  $(m+1)$   $\mathbb{P}^{2s}$ s without any orientation reversal, and so are precomplex torus manifolds.

**Conjecture 5.1** (precomplex) *Flip-folded multitopes, such as  $\Delta_{F_m}^*$  for  $m \geq 3$  and  $\Delta_{E_m}^*$  for  $m \geq 1$ , correspond to **precomplex** torus manifolds, where the flip-folded “extension” encodes the obstruction to extending a precomplex structure to a global complex structure, such as in  $\nabla F_m^{(n)}$  and  $E_m^{(n)}$ .*

*Since flip-folded portions of a multitope,  $\Delta_X^*$ , are transpolar to non-convex regions of the transpolar multitope,  $\Delta_X = \Delta_{\nabla X}^*$ , non-convexity in  $\Delta_{\nabla X}^*$  encodes (by mirror symmetry) obstructions to extending a **presymplectic** structure of  $\nabla X$  to a global symplectic structure, such as in  $F_m^{(n)}$  and  $\nabla E_m^{(n)}$ .*

**Remark 5.1** The “optimal model” of Remark 1.8 and Conjecture 4.1 is thereby seen as a torus manifold wherein the obstructions from Remark 1.7 and Conjecture 5.1 are minimized in a suitable ( $\mathbb{T}^n$ -equivariant) (co)homology. By mirror symmetry, analogous considerations apply also to the (pre-)symplectic as well as (pre-)Kähler structures, all of which are typically needed in string applications.  $\blacksquare$

### 5.3 Being Star-Triangulable

The definition of VEX multitopes as being star-triangulable (and with signed multiplicity) relates the numbers of their faces (i.e., cones in the multifans they span) by Euler’s relation. Even/odd-dimensional multitopes  $\Delta$  have their boundary,  $\partial\Delta$ , homotopic to an odd/even-dimensional sphere with  $\chi(\partial\Delta) = 0$ , i.e.,  $\chi(\Delta) = 2$ , respectively, while  $\chi(\Delta) = 1$  in both cases. Using the (signed) face-counting function,  $\sharp(\nu)$ , shows this to hold regardless of the winding number,  $w$ :

$$\begin{array}{ccc}
 \begin{array}{c} \Delta_1 \\ \text{Diagram 1: Star-shaped multitope with 8 vertices and 8 faces} \end{array} & \frac{\sharp(\nu_{i,i+1}), \sharp(\nu_i) = 1}{w=3 \quad \begin{array}{l} \sum_i \sharp(\nu_{i,i+1}) = 8 \\ \sum_i \sharp(\nu_i) = 8 \end{array}}{\sum_i \sharp(\nu_{i,i+1}) - \sum_i \sharp(\nu_i) = 0} & \begin{array}{c} \Delta_2 \\ \text{Diagram 2: Star-shaped multitope with 6 vertices and 6 faces} \end{array} & \frac{\sharp(\nu_{i,i+1}), \sharp(\nu_i) = 1}{w=2 \quad \begin{array}{l} \sum_i \sharp(\nu_{i,i+1}) = 6 \\ \sum_i \sharp(\nu_i) = 6 \end{array}}{\sum_i \sharp(\nu_{i,i+1}) - \sum_i \sharp(\nu_i) = 0} & (5.5)
 \end{array}$$

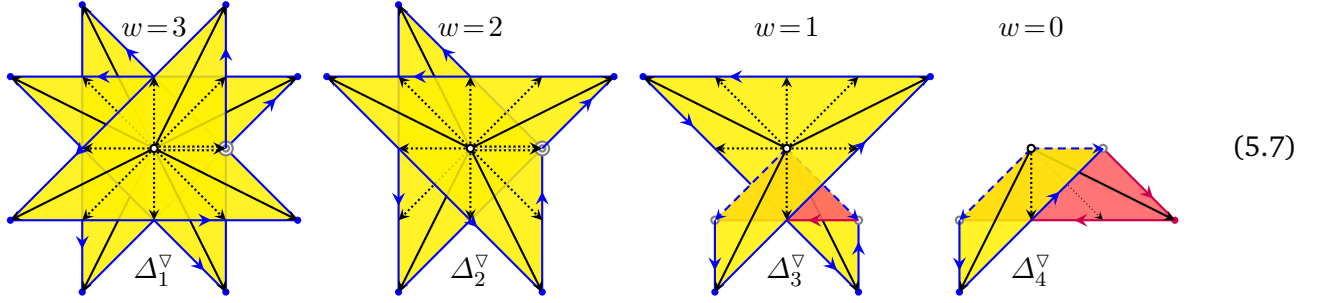
$$\begin{array}{ccc}
 \begin{array}{c} \Delta_3 \\ \text{Diagram 3: Star-shaped multitope with 6 vertices and 6 faces, some shaded red} \end{array} & \frac{\sharp(\nu_{i,i+1}) = \pm 1, \sharp(\nu_i) = \pm 1, 0}{w=1 \quad \begin{array}{l} \sum_i \sharp(\nu_{i,i+1}) = (4-2) \\ \sum_i \sharp(\nu_i) = (3-1) \end{array}}{\sum_i \sharp(\nu_{i,i+1}) - \sum_i \sharp(\nu_i) = 0} & \begin{array}{c} \Delta_4 \\ \text{Diagram 4: Star-shaped multitope with 5 vertices and 5 faces, some shaded red} \end{array} & \frac{\sharp(\nu_{i,i+1}) = \pm 1, \sharp(\nu_i) = \pm 1, 0}{w=0 \quad \begin{array}{l} \sum_i \sharp(\nu_{i,i+1}) = (2-2) \\ \sum_i \sharp(\nu_i) = (1-1) \end{array}}{\sum_i \sharp(\nu_{i,i+1}) - \sum_i \sharp(\nu_i) = 0} & (5.6)
 \end{array}$$

In the left-most example of (5.6),  $\sharp(\nu_{12}), \sharp(\nu_{23}), \sharp(\nu_{34}), \sharp(\nu_{45}) = +1$  and  $\sharp(\nu_{56}), \sharp(\nu_{61}) = -1$ , which implies that  $\sharp(\nu_2), \sharp(\nu_3), \sharp(\nu_4) = +1$ , while  $\sharp(\nu_6) = -1$  so  $\sharp(\nu_1), \sharp(\nu_5) = 0$ . In the right-most example of (5.6), which has no relative interior but does have lattice-primitive vertices and is centered at the origin, we have that  $\sharp(\nu_{12}), \sharp(\nu_{23}), \sharp(\nu_{34}) = +1$  and  $\sharp(\nu_{45}), \sharp(\nu_{51}) = -1$ , which implies that  $\sharp(\nu_2), \sharp(\nu_3) = +1$ , while  $\sharp(\nu_5) = -1$  so  $\sharp(\nu_1), \sharp(\nu_4) = 0$ . This face-counting function is related to (4.4) and (4.5) by  $e_i = \sum_{\nu \in \Sigma(i)} \sharp(\nu)$ .

<sup>30</sup>We thank M. Masuda for suggesting this interpretation; for a not too different but additionally specified example, see [54, § 5].

<sup>31</sup>The precomplex structure on  $S^4$  nevertheless suffices to define a Dolbeault (anti)holomorphic exterior derivative and cohomology [111], which may well suffice for most string theory applications.

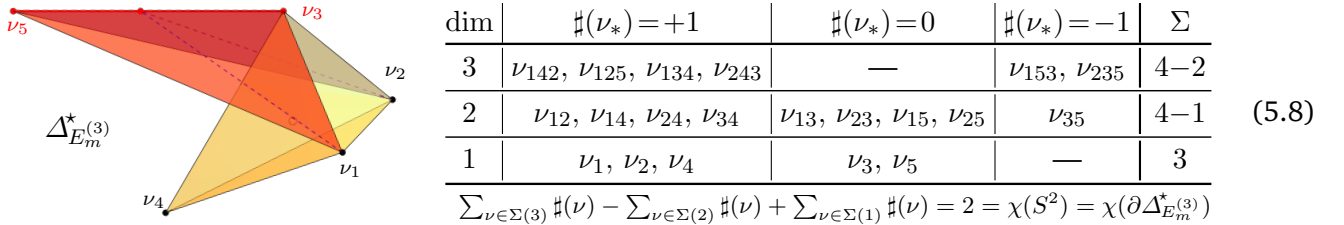
For completeness, we include the VEX multitopes transpolar to those in (5.5) and (5.6):



and invite the Reader to verify that  $\chi(\partial\Delta_i^\nabla)=0$ . The double-drawn lattice-vectors and double-circled lattice points in  $\Delta_1^\nabla$  and  $\Delta_2^\nabla$  indicate a choice of layer-crossing branch cuts/points; dashed lattice vectors indicate (CCW/CW) orientation-changing folds and dotted lattice vectors are MPCP-subdivisions.

Note that  $\sharp(\nu) \neq d(\nu)$  in general: For example, in the right-most example (5.6),  $\sharp(\nu_{24})=1$  even for the un-subdivided cone  $\nu_{24} \in \Delta_4$  (where  $\nu_3$  is omitted from the multifan), while  $d(\nu_{24})=2$ . For lower-dimensional cones in turn,  $d(\nu_i)=1$  for all vertices in all examples, while  $\sharp(\nu_i)$  varies, depending on the orientation of adjacent higher-dimensional cones. For example, the 1-cone  $\nu_1 \in \Delta_3, \Delta_4$  (depicted by a dashed arrow) counts  $\sharp(\nu_1)=0$ , as it forms the interfacing boundary ( $\nu_1 = \nu_{61} \cap \nu_{12}$ )  $\in \Delta_3$  and ( $\nu_1 = \nu_{51} \cap \nu_{12}$ )  $\in \Delta_4$  between a positively and a negatively-oriented 2-cone [38].

Suffice it here to also showcase the more intricate 3-dimensional case:



The facets  $\theta_{ijk}$  and the central cones over them,  $\nu_{ijk} = \triangleleft \theta_{ijk}$ , are oriented away (or toward) the center by their multi-index order, see footnote 16, p. 13. Each edge (and the 2-cone over it) is then oriented by continuity, as the interface between its two adjacent 2-faces. For example:

- $\sharp(\nu_{12}) = +1$  since  $\nu_{12} = \nu_{142} \cap \nu_{125}$ , and  $\sharp(\nu_{142}) = \sharp(\nu_{125}) = +1$ .
- $\sharp(\nu_{13}) = 0$  since  $\nu_{13} = \nu_{134} \cap \nu_{153}$  is folding over between  $\sharp(\nu_{134}) = +1$  and  $\sharp(\nu_{153}) = -1$ .
- $\sharp(\nu_{35}) = -1$  since  $\nu_{35} = \nu_{153} \cap \nu_{235}$ , and  $\sharp(\nu_{153}) = \sharp(\nu_{235}) = -1$ .

Finally, vertices (and 1-cones over them) are also oriented by continuity:

1.  $\sharp(\nu_4 = \nu_{142} \cap \nu_{134} \cap \nu_{243}) = +1$ , since  $\sharp(\nu_{142}) = \sharp(\nu_{134}) = \sharp(\nu_{243}) = +1$ .
2.  $\sharp(\nu_3 = \nu_{13} \cap \nu_{32}) = 0$ , since  $\sharp(\nu_{13}) = \sharp(\nu_{32}) = 0$ , being folds between positive and negative facets. The same holds for  $\nu_5 = \nu_{15} \cap \nu_{52}$  and implies  $\sharp(\nu_5) = 0$ .
3. Approached from any direction outside the  $\nu_{153}$  cone,  $\nu_1$  inherits the outward (+1) orientation of the adjacent facets. Approached from *within* the  $\nu_{153}$  cone, the orientation is inherited from the overlaying cones:  $\sharp(\nu_1 = \nu_{134}^+ \cap \nu_{125}^+ \cap \nu_{153}^-) = +1 + 1 - 1 = +1$ , verifying that  $\sharp(\nu_1) = +1$  is constant, i.e., independent of the (limit) approach. The same holds for  $\nu_2$  and implies  $\sharp(\nu_2) = +1$ .

As indicated in the bottom row in (5.8), the Euler number of  $\partial\Delta_{E_m}^*(3)$  is that of a 2-sphere, supporting the description of VEX multitopes at the start of this section and required for Hibi's Lemma 4.1.

This combinatorial function,  $\sharp(\nu)$ , defined here for VEX multitopes and the multifans they span, seems to be very closely related to the function  $\varepsilon(p)$  originally defined [45] over the tangent bundles of general torus manifolds corresponding to multifans. While the fact that  $n$ -dimensional VEX multitopes are star-shaped domains (albeit multi-layered, with signed multiplicity) and homotopic to  $n$ -dimensional balls seems to provide a key restriction, we are not aware of a general, complete algorithm for the function  $\sharp(\nu)$ , not its relation to the torus manifolds'  $\varepsilon(p)$ . It is clear however that  $d(\nu)$  and  $\sharp(\nu)$  should play distinct roles in (presumably  $T^n$ -equivariant) (co)homological, topological and other related computations, esp. within the context of various string theory and related applications.

## 6 Conclusions and Outlook

Throughout this article, we have examined and tested various computational characteristics associated with candidate pairs of embedding spaces, where the transposition mirror construction [26, 29, 30, 33–37] of Calabi–Yau models is generalized in pairs of simple anticanonical hypersurfaces. The overall framework presented in Claim 1.1 relies on the triple  $(Z_f, X, \mathcal{K}_X^*)$ , where  $Z_f$  is the desired Calabi–Yau hypersurface,  $\{f(x)=0\} \subset X$ ,  $\mathcal{K}_X^*$  is the anticanonical bundle over  $X$ , and  $f(x) \in \Gamma(\mathcal{K}_X^*)$  a suitable section. The mirror model is then part of the analogous triple  $(\tilde{Z}_{\tau_f}, \nabla X, \mathcal{K}_{\nabla X}^*)$ . When  $X$  is a (weak/semi) Fano (complex algebraic) toric variety encoded by a (MPCP-subdivided) reflexive polytope,  $\Delta$ , then  $\nabla X$  is the (complex algebraic) toric variety analogously encoded by the (MPCP-subdivided) polar polytope  $\Delta^\circ$  [27].

Following the work of [38, 39], we find that this framework extends to the much more general VEX multitopes, which are regular, star-triangulable but perhaps flip-folded or otherwise multilayered multi-hedral objects that span multifans [45–51]. They correspond to  $2n$ -dimensional manifolds with an  $n$ -dimensional torus-action,  $T^n = (S^1)^n$  — identified with the  $U(1)^n$  gauge group of the associated gauged linear sigma model [12, 13] and so germane to string theory. Generalizing the standard polar duality (1.4) and acting as an involution among VEX multitopes, the transpolar Construction 1.1 relates the corresponding toric embedding spaces,  $X \xleftrightarrow{\nabla} \nabla X$  as needed in the mirror-symmetric framework (1.1). That is, the mirror symmetry between the anticanonical hypersurfaces  $Z_f \subset X$  and  $\tilde{Z}_{\tau_f} \subset \nabla X$  lifts to the transpolar relation  $X \xleftrightarrow{\nabla} \nabla X$  and  $\mathcal{K}_X^* \xleftrightarrow{\nabla} \mathcal{K}_{\nabla X}^*$ .

By explicit computation in several infinite sequences and many other (2 and 3-dimensional) examples of VEX multitopes, we find that full agreement with the framework (1.1). In particular, § 2 verifies all Chern characteristics — and even detailed Chern classes, computed from the VEX multitopes, including various Todd–Hirzebruch identities and a few other applications of the HRR theorem. § 3 verifies all divisor class intersection numbers and their relation with Chern characteristics. § 4 finds agreement with Hibi’s Lemma 4.1, which extends the standard results about the Poincaré polynomial, including the Dehn–Sommerville relations, typically related to Poincaré duality. However, the so-called unimodality relations (typically related to the Hard Lefschetz theorem) are satisfied by some, but not all VEX multitopes. Finally, § 5 finds that the various multitope features lend themselves to further understanding of the corresponding toric spaces. In particular, we find that the a flip-folded region in a multitope,  $\Delta_X^*$ , corresponds to an obstruction to a global complex structure over  $X$ , rendering it precomplex; see § 5.2 in particular. (At least some toric spaces may do admit a  $(\mathbb{C}^*)^n$ - or just  $(S^1)^n$ -equivariant, and almost, weakly, or stably complex structure; see e.g., [45, 52].) Since flip-folded regions in  $\Delta_X^*$  are transpolar to concave regions in  $\Delta_X = \Delta_{\nabla X}^*$  and mirror symmetry relates (pre)symplectic to (pre)complex structure, it would follow that concave regions in a multitope,  $\Delta_X^*$ , are obstructions for a global symplectic structure over  $X$ .

The Claims, Conjectures and multiple Remarks are herein supported mostly by numerous concrete computations — and the fact that no counter-example has been found, except for the explicitly stated lack

of unimodality of the “ $h$ -vector” for the  $E_m^{(n)}$ -sequence of examples, so its relation to Betti numbers fails. We should like to hope that this provides ample motivation for a more rigorous examination of these claims and conjectures, their possible (dis)proof — or correction, and thereby a more rigorous foundation for the vast breadth of application of the mirror-symmetric framework (1.1) among VEX multitopes.

**VEXing:** Let us conclude with one more motivation for including flip-folded and otherwise multi-layered oriented multitopes (and the toric spaces to which they correspond) by considering the three (trans)polar pairs of multitopes depicted in Figure 7.

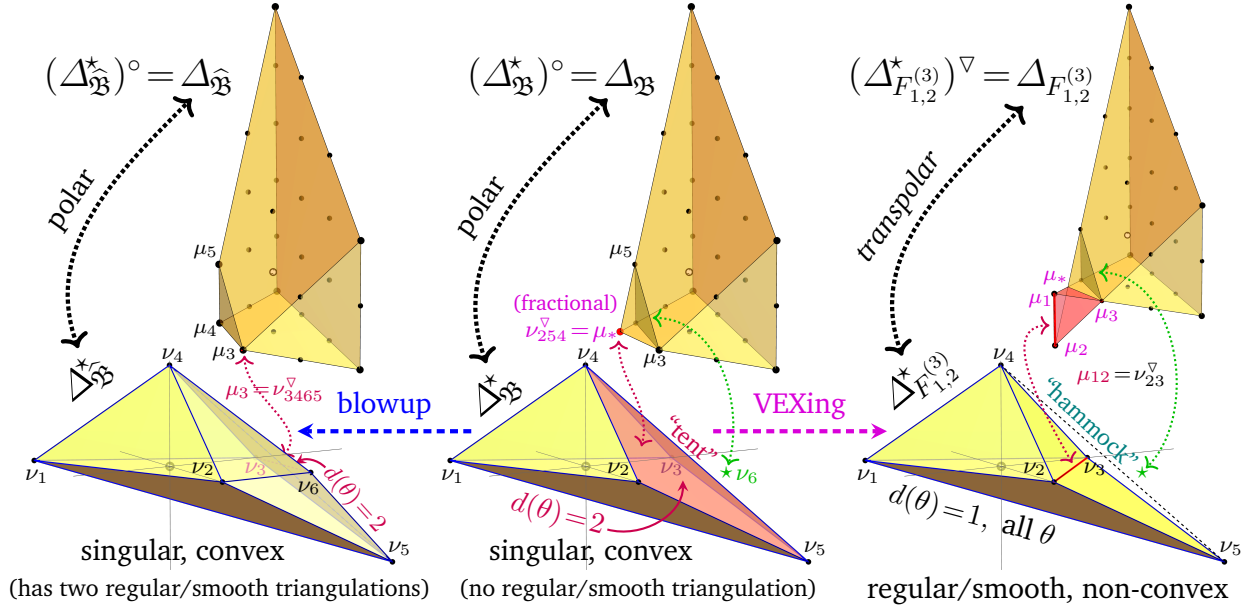


**Figure 7:** Middle: the polar of the (red-shaded)  $d(\theta)=2$  singular facet is fractional. Left: its blowup results in a polar pair of reflexive lattice polytopes. Right: the VEX (reduced) re-triangulation  $\Delta_{\mathfrak{B}}^* \rightarrow \Delta_{F_{1,2}}^{*(3)}$  is non-convex and its transpolar, the Newton multitope, has a flip-folded (red-shaded) extension

► *Middle:* Start with the toric variety encoded by the star-triangulable convex spanning polytope  $\Delta_{\mathfrak{B}}^*$ , middle-bottom in Figure 7, with vertices

$$\Delta_{\mathfrak{B}}^* = \text{Conv}(\nu_1 = (-1, -1, 0), \nu_2 = (1, 0, 0), \nu_3 = (0, 1, 0), \nu_4 = (0, 0, 1), \nu_5 = (1, 2, -1)). \quad (6.1)$$

It spans the (outward, positively oriented) fan

$$\Sigma_{\mathfrak{B}} = \{\nu_{124}, \nu_{143}, \nu_{135}, \nu_{152}, \nu_{345}, \nu_{254}\}, \quad (6.2)$$

of central 3-cones over the facets,  $\nu_{ijk} = \langle \theta_{ijk} \rangle$ , so we use them interchangeably. Since  $d(\nu_{254})=2$ , this cone encodes a  $\mathbb{C}^3/\mathbb{Z}_2$ -like singular chart  $U_{254} \subset \mathfrak{B}$ , and its polar image in the Newton polytope  $\Delta_{\mathfrak{B}} = (\Delta_{\mathfrak{B}}^*)^\circ$  is the fractional (non-lattice) point,  $\theta_{254}^\vee = \mu_* = (-1, -\frac{1}{2}, -1)$ , which cannot encode a regular anticanonical monomial on  $\mathfrak{B}$ ;  $\mu_* \mapsto \sqrt{x_1^5 x_3}$  in terms of the standard Cox variables,  $x_i \leftarrow \nu_i$ .

► *Left:* By removing the (magenta-colored, lower-left) fractional vertex  $\mu_*$  from  $\Delta_{\mathfrak{B}}$ , we reduce  $\Delta_{\mathfrak{B}} \rightarrow \Delta_{\widehat{\mathfrak{B}}}$ , shown at left in Figure 7. The polar of this is the convex spanning polytope  $\Delta_{\widehat{\mathfrak{B}}}^*$ , depicted at bottom-left, where the degree-2 facet  $\theta_{254} \in \partial \Delta_{\mathfrak{B}}^*$  has been subdivided by introducing the new vertex,  $\nu_6 = (1, 1, 0)$ . As  $\nu_6$  lies outside  $\Delta_{\mathfrak{B}}^*$  but within the cone being subdivided,  $\nu_{254}$ , this encodes the standard blowup,  $\widehat{\mathfrak{B}} = \text{Bl}[\mathfrak{B}]$ . The convex polytope  $\Delta_{\widehat{\mathfrak{B}}}^*$  now has a *quadrangular* degree-2 facet,  $\theta_{3465}$  (behind, top-back), which however

has two distinct regular triangulating star-subdivisions, and the corresponding two distinct fans:

$$\Sigma_{\widehat{\mathfrak{B}}'} = \{ \nu_{124}, \nu_{143}, \nu_{135}, \nu_{152}, \underline{\nu_{345}}, \nu_{264}, \nu_{256}, \underline{\nu_{465}} \} \supset \begin{array}{c} \text{3} \\ \swarrow \quad \searrow \\ 4 \quad \text{6} \quad 5 \\ \downarrow \quad \uparrow \\ \quad \quad 2 \end{array} \quad (6.3)$$

$$\Sigma_{\widehat{\mathfrak{B}}''} = \{ \nu_{124}, \nu_{143}, \nu_{135}, \nu_{152}, \underline{\nu_{346}}, \nu_{264}, \nu_{256}, \underline{\nu_{365}} \} \supset \begin{array}{c} \text{3} \\ \swarrow \quad \searrow \\ 4 \quad \text{6} \quad 5 \\ \downarrow \quad \uparrow \\ \quad \quad 2 \end{array} \quad (6.4)$$

The underlined cones distinguish the triangulations; the transformation  $\widehat{\mathfrak{B}}' \leftrightarrow \widehat{\mathfrak{B}}''$  is known as a flop.

► *Right:* Instead, we may re-triangulate the convex polytope  $\Delta_{\mathfrak{B}}^*$  by re-subdividing

$$\underbrace{\triangleleft_{0254} \uplus \triangleleft_{0345}}_{\subset \Delta_{\mathfrak{B}}^*, \begin{array}{c} \text{3} \\ \swarrow \quad \searrow \\ 4 \quad \text{6} \quad 5 \\ \downarrow \quad \uparrow \\ \quad \quad 2 \end{array}} \rightarrow \underbrace{\triangleleft_{0234} \uplus \triangleleft_{0325}}_{\subset \Delta_{F_{1,2}}^{(3)}, \begin{array}{c} \text{3} \\ \swarrow \quad \searrow \\ 4 \quad \text{6} \quad 5 \\ \downarrow \quad \uparrow \\ \quad \quad 2 \end{array}} \uplus \underbrace{\triangleleft_{2345}}_{\text{outer simplex}}, \quad (6.5)$$

where the last, “outer” 3-simplex,  $\triangleleft_{2345}$ , does not contain the origin and so does not define a central cone. Its removal results in the corresponding star-triangulating regular fan:

$$\Sigma_{F_{1,2}}^{(3)} = \{ \nu_{124}, \nu_{143}, \nu_{135}, \nu_{152}, \nu_{234}, \nu_{325} \}. \quad (6.6)$$

Removing this “outer” 3-simplex, replaces the “tent-like” (convex!) region in  $\Delta_{\mathfrak{B}}^*$  by a “hammock-like” (non-convex!) region in  $\Delta_{F_{1,2}}^{(3)}$ . This VEX re-triangulation  $\Delta_{\mathfrak{B}}^* \supset \Sigma_{\mathfrak{B}} \rightarrow \Sigma_{F_{1,2}}^{(3)} \subset \Delta_{F_{1,2}}^{(3)}$  (with “outer” simplices removed) may be called **VEXing**. The resulting polytope,  $\Delta_{F_{1,2}}^{(3)}$  depicted at bottom-right in Figure 7, is regular/smooth, VEX, but not convex: its edge  $\nu_{23}$  is concave, and its image in the transpolar (Newton) multitope is the downward pointed “extension”  $\mu_{12} \in \Delta_{F_{1,2}}^{(3)}$ ; see Figure 7, upper-right.

► *To summarize:* On one hand, the standard blowup (Figure 7, left) extends the spanning polytope, refines the star-triangulating fan, and reduces the transpolar Newton polytope

$$\text{blowup: } \Delta_{\mathfrak{B}}^* < (\Delta_{\mathfrak{B}}^* \uplus \triangleleft_{2546}) = \Delta_{\widehat{\mathfrak{B}}}^* \quad \overset{\circ}{\leftrightarrow} \quad \Delta_{\widehat{\mathfrak{B}}} = (\Delta_{\mathfrak{B}} \setminus \triangleleft_{*345}) < \Delta_{\mathfrak{B}}. \quad (6.7)$$

In turn, VEXing (Figure 7, right) reduces the spanning polytope, re-triangulates the star-triangulating fan, and extends the transpolar Newton polytope

$$\text{VEXing: } \Delta_{\mathfrak{B}}^* > (\Delta_{\mathfrak{B}}^* \setminus \triangleleft_{2345}) = \Delta_{F_{1,2}}^{(3)} \quad \overset{\nabla}{\leftrightarrow} \quad \Delta_{F_{1,2}}^{(3)} = (\Delta_{\mathfrak{B}} \uplus \triangleleft_{123*}) > \Delta_{\mathfrak{B}}. \quad (6.8)$$

The blowup depicted on the left in Figure 7 results in a polar pair of reflexive polytopes,  $(\Delta_{\mathfrak{B}}^*, \Delta_{\widehat{\mathfrak{B}}})$ , which encode the transpolar pairs of (smooth, complex algebraic) toric varieties,  $(\widehat{\mathfrak{B}}', \nabla \widehat{\mathfrak{B}})$  and  $(\widehat{\mathfrak{B}}'', \nabla \widehat{\mathfrak{B}})$ , and can be used to construct multiple mirror pairs of K3 surfaces, constructed as anticanonical hypersurfaces as specified in the diagram (1.1) and Remark 1.1. Analogously, the VEXing depicted on the right in Figure 7 results in a transpolar pair of VEX multitopes,  $(\Delta_{F_{1,2}}^{(3)}, \Delta_{F_{1,2}}^{(3)})$ , which correspond to the pair,  $(F_{1,2}^{(3)}, \nabla F_{1,2}^{(3)})$ , of a (smooth, complex algebraic, albeit non-Fano) toric variety,  $F_{1,2}^{(3)}$ , and its transpolar (smooth, precomplex) torus manifold,  $\nabla F_{1,2}^{(3)}$ ; these encode a combinatorial network of multiple mirror pairs of K3 surfaces, constructed as anticanonical hypersurfaces as specified in the diagram (1.1) and Remark 1.1.

The comparison of (6.3) or (6.4) with (6.5) exhibits that VEXing amounts to *re-triangulating the fan* spanned by the convex  $\Delta_{\mathfrak{B}}^*$  into the fan spanned by the non-convex  $\Delta_{F_{1,2}}^{(3)}$ .

The constructions depicted in Figure 7 have a noteworthy variation: Moving the vertex  $\nu_5 \rightarrow (2, 2, -1)$  causes  $d(\nu_{254}) = 2 = d(\nu_{345})$  but also places the subdividing vertex  $\nu_6$  within the edge  $\theta_{45}$ . This allows subdividing both (now  $\text{deg} = 2$ ) facets,  $\theta_{254}$  and  $\theta_{345}$ , without introducing new vertices, and so provides this stretched version of the convex polytope  $\Delta_{\mathfrak{B}}^*$  with a regular triangulating subdivision that encodes a smooth, Fano toric variety. VEXing as above now produces the non-convex  $\Delta_{F_{2,2}}^{(3)}$ .

**Acknowledgments:** We should like to thank Y. Cui, C.F. Doran, A. Gholampour, K. Iga, H. Schenck and J. Rosenberg for helpful discussions on these topics, and especially M. Masuda for generous help with torus manifolds and the rich and diverse literature on this topic. PB would like to thank the CERN Theory Group for their hospitality over the past several years. His work is supported in part by the Department of Energy grant DE-SC0020220. TH is grateful to the Department of Mathematics, University of Maryland, College Park MD, and the Physics Department of the Faculty of Natural Sciences of the University of Novi Sad, Serbia, for the recurring hospitality and resources.

## A Additional Transpose-Mirror Examples

We further illustrate the combinatorially growing abundance in constructions afforded by the mirror framework Claim 1.1 and Remark 1.1; it is tempting to expect this framework to incorporate many if not all the “multiple mirrors,” as well as the “coincidences” reported in the literature, such as in [112, 113].

### A.1 A Network of Transpose-Mirrors

Supporting Claim 1.1 and extending the analysis in [39], consider two pairwise sub-simplex reductions of the transpolar pair of VEX multitopes  $(\Delta_{F_3}^*, \Delta_{F_3}^{(3)})$ : The spanning multitope (top far left) admits a single

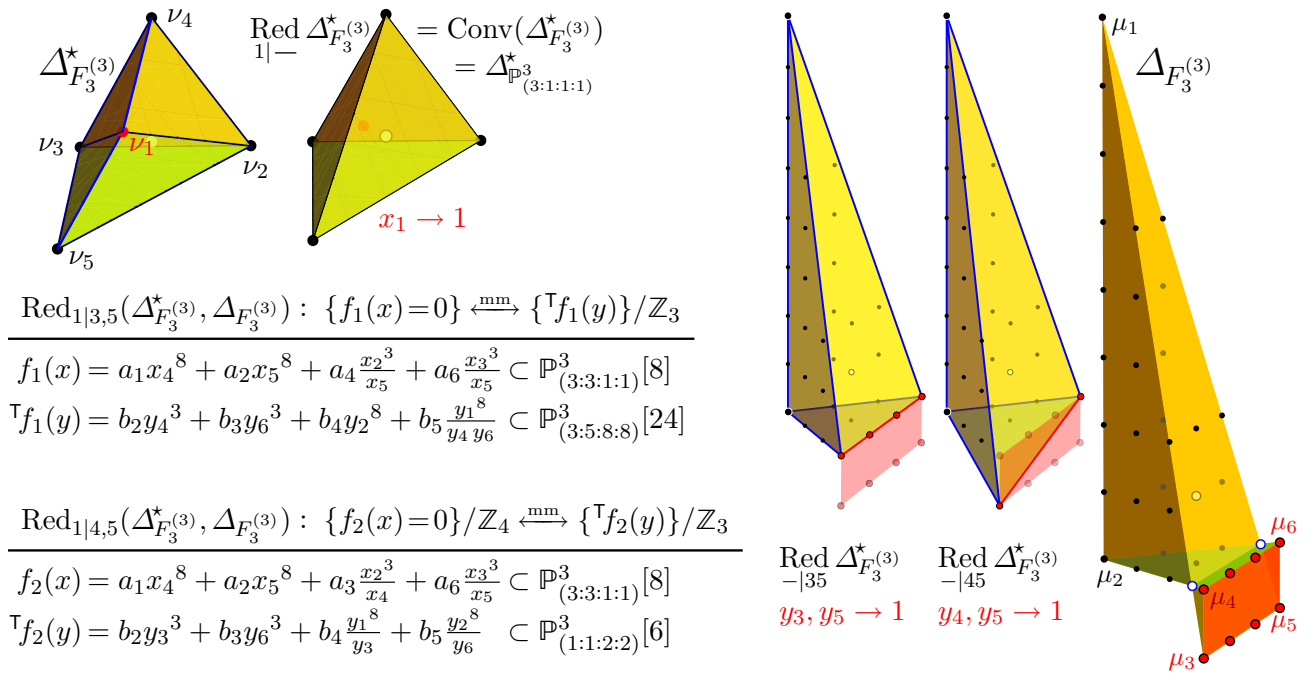


**Figure 8:** The spanning polytope,  $\Delta_{F_m}^*$  (far left), and the (extended) Newton multitope,  $\Delta_{F_m}^{(3)}$  (far right); their sub-simplex reductions and corresponding pairs of transpose polynomials

origin-enclosing sub-simplex reduction,  $\Delta_{F_3}^* \rightarrow \Delta_{\mathbb{P}^3}^*_{(3:3:1:1)}$ , while the (extended) Newton multitope (far right) admits many such reductions. Two of these are indicated in Figure 8, mid-right; their combination with the unique origin-enclosing sub-simplex reduction of  $\Delta^*$  then leads to the two transposition pairs in Figure 8. The symmetry groups are easily found from the rows (vs. columns) of the inverse of the

exponents' matrix [33, 34] and are as follows:

$$\text{Red}_{1|3,5} : \begin{bmatrix} \frac{1}{3} & \frac{2}{3} & 0 & 0 \\ \frac{1}{24} & \frac{1}{24} & \frac{1}{8} & 0 \\ \frac{3}{8} & \frac{3}{8} & \frac{1}{8} & \frac{1}{8} \end{bmatrix} \left\{ \begin{array}{l} G = \mathbb{Z}_3 \times \mathbb{Z}_{24}, \\ Q = \mathbb{Z}_8, \end{array} \right. \text{ vs. } \begin{bmatrix} 0 & 0 & \frac{1}{3} & \frac{2}{3} \\ \frac{1}{8} & 0 & 0 & 0 \\ \frac{5}{24} & \frac{3}{24} & \frac{1}{3} & \frac{1}{3} \end{bmatrix} \left\{ \begin{array}{l} G^\nabla = \mathbb{Z}_3 \times \mathbb{Z}_8, \\ Q^\nabla = \mathbb{Z}_{24}. \end{array} \right. \quad (\text{A.1})$$

Quotienting the transpose (on the right-hand side) by the indicated  $\mathbb{Z}_3$  action then produces  $\tilde{G}^\nabla = \mathbb{Z}_8 = Q$  and  $\tilde{Q}^\nabla = \mathbb{Z}_{24} \times \mathbb{Z}_3 = G$ . One could also quotient the “original” (on the left-hand side) by the indicated  $\mathbb{Z}_3$ -action, leading to  $\tilde{G}^\nabla = \mathbb{Z}_3 \times \mathbb{Z}_8 = Q$  and  $\tilde{Q}^\nabla = \mathbb{Z}_{24} = G$  instead. In turn, the other sub-simplex reduction has the following symmetries:

$$\text{Red}_{1|4,5} : \begin{bmatrix} \frac{1}{3} & \frac{1}{3} & 0 & 0 \\ \frac{1}{24} & \frac{23}{24} & \frac{1}{8} & \frac{7}{8} \\ \frac{3}{8} & \frac{3}{8} & \frac{1}{8} & \frac{1}{8} \end{bmatrix} \left\{ \begin{array}{l} G = \mathbb{Z}_3 \times \mathbb{Z}_{24}, \\ Q = \mathbb{Z}_8, \end{array} \right. \text{ vs. } \begin{bmatrix} \frac{1}{24} & 0 & \frac{1}{3} & 0 \\ 0 & \frac{1}{24} & 0 & \frac{1}{3} \\ \frac{1}{6} & \frac{1}{6} & \frac{1}{3} & \frac{1}{3} \end{bmatrix} \left\{ \begin{array}{l} G^\nabla = (\mathbb{Z}_{24})^2 / \mathbb{Z}_6, \\ Q^\nabla = \mathbb{Z}_6. \end{array} \right. \quad (\text{A.2})$$

Here we quotient the “original” (on the left-hand side) by  $\mathbb{Z}_4 \subset \mathbb{Z}_{24}$ , leading to  $\tilde{G} = \mathbb{Z}_3 \times \mathbb{Z}_6$  and  $\tilde{Q} = \mathbb{Z}_8 \times \mathbb{Z}_4$ . The geometric symmetry of the transpose (on the right-hand side) is

$$(\mathbb{Z}_{24})^2 \supset (g_1^\nabla \times g_2^\nabla) / Q^\nabla = \exp\{2\pi i [ (\frac{1}{24}, 0, \frac{1}{3}, 0) \oplus (0, \frac{1}{24}, 0, \frac{1}{3}) \pmod{(\frac{1}{6}, \frac{1}{6}, \frac{1}{3}, \frac{1}{3})} ]\}, \quad (\text{A.3})$$

$$(\frac{1}{6}, \frac{1}{6}, \frac{1}{3}, \frac{1}{3}) = 4(\frac{1}{24}, 0, \frac{1}{3}, 0) + 4(0, \frac{1}{24}, 0, \frac{1}{3}). \quad (\text{A.4})$$

This has an effective  $\mathbb{Z}_3$  subgroup action generated by the equivalence classes

$$[4(\frac{1}{24}, 0, \frac{1}{3}, 0) - 4(0, \frac{1}{24}, 0, \frac{1}{3}) \pmod{2(\frac{1}{6}, \frac{1}{6}, \frac{1}{3}, \frac{1}{3})}] = [(\frac{1}{6}, \frac{5}{6}, \frac{1}{3}, \frac{2}{3}) \pmod{(\frac{1}{2}, \frac{1}{2}, 0, 0)}]. \quad (\text{A.5})$$

Quotienting by this  $\mathbb{Z}_3$  produces  $\tilde{Q}^\nabla = \mathbb{Z}_6 \times \mathbb{Z}_3 = \tilde{G}$ , and leaves  $\tilde{G}^\nabla = (\mathbb{Z}_{24})^2 / (\mathbb{Z}_6 \times \mathbb{Z}_3) \approx \mathbb{Z}_8 \times \mathbb{Z}_4 = \tilde{Q}$ .

However, notice that  $\{f_1(x)=0\}$  and  $\{f_2(x)=0\}$  are simple (complex-structure) deformations of each other, whereby we obtain the following *evidently incomplete* network of related pairs of mirror models:

$$\begin{array}{ccccc} \{^\top f_1(y)=0\} / \mathbb{Z}_3 & \xleftarrow{\text{mm}} & \{f_1(x)=0\} & \xleftarrow{\text{defo.}} & \{f_2(x)=0\} & \xleftarrow{\text{mm}^?} & \{^\top f_2(y)=0\} / ? \\ \uparrow / \mathbb{Z}_3 & & \downarrow / \mathbb{Z}_3 & & \downarrow / \mathbb{Z}_4 & & \uparrow / ? \\ \{^\top f_1(y)=0\} & \xleftarrow{\text{mm}} & \{f_1(x)=0\} / \mathbb{Z}_3 & & \{f_2(x)=0\} / \mathbb{Z}_4 & \xleftarrow{\text{mm}} & \{^\top f_2(y)=0\} / \mathbb{Z}_3 \end{array} \quad (\text{A.6})$$

Given the identification of finite group actions on the right-hand side of (A.5), finding the “missing mirror” in the top far-right corner of the diagram (A.6) would require enhancing  $Q^\nabla = \mathbb{Z}_6 \rightarrow \mathbb{Z}_{24} \times \mathbb{Z}_3$ . Since the  $\mathbb{Z}_6$  from the  $\mathbb{P}_{(2:2:1:1)}^2$ -projectivization is generated by the sum (A.4), such a  $\mathbb{Z}_{24}$ -enhancement can only be generated by the sum of the two  $\mathbb{Z}_{24}$  generators in (A.3):

$$(\mathbb{Z}_{24}: (\frac{1}{24}, 0, \frac{1}{3}, 0) + (0, \frac{1}{24}, 0, \frac{1}{3})) = (\mathbb{Z}_{24}: \frac{1}{24}, \frac{1}{24}, \frac{1}{3}, \frac{1}{3}), \quad (\text{A.7})$$

which however is not traceless:  $\frac{1}{24} + \frac{1}{24} + \frac{1}{3} + \frac{1}{3} = \frac{3}{4} \notin \mathbb{Z}$ , i.e., does not satisfy the so-called Calabi–Yau condition and so could not be used as a quantum symmetry.

In remedy, we observe that the specification (A.2) may be replaced with

$$\text{Red}_{1|4,5} : \begin{bmatrix} \frac{1}{3} & \frac{1}{3} & 0 & 0 \\ \frac{1}{24} & \frac{23}{24} & \frac{1}{8} & \frac{7}{8} \\ \frac{3}{8} & \frac{3}{8} & \frac{1}{8} & \frac{1}{8} \end{bmatrix} \left\{ \begin{array}{l} G = \mathbb{Z}_3 \times \mathbb{Z}_{24}, \\ Q = \mathbb{Z}_8, \end{array} \right. \text{ vs. } \begin{bmatrix} \frac{1}{24} & 0 & \frac{1}{3} & 0 \\ 0 & \frac{1}{24} & 0 & \frac{1}{3} \\ \frac{1}{6} & \frac{5}{6} & \frac{1}{3} & \frac{2}{3} \end{bmatrix} \left\{ \begin{array}{l} G^\nabla = (\mathbb{Z}'_{24} \times \mathbb{Z}_{24}) / \mathbb{Z}'_6, \\ Q^\nabla = \mathbb{Z}'_6, \end{array} \right. \quad (\text{A.8})$$

where we define the twisted projectivization/quantum (sub)group

$$(\mathbb{Z}'_6: \frac{1}{6}, \frac{5}{6}, \frac{1}{3}, \frac{2}{3}) = (\mathbb{Z}'_6: 4(\frac{1}{24}, 0, \frac{1}{3}, 0) - 4(0, \frac{1}{24}, 0, \frac{1}{3})) \subset (\mathbb{Z}'_{24}: (\frac{1}{24}, 0, \frac{1}{3}, 0) - (0, \frac{1}{24}, 0, \frac{1}{3})). \quad (\text{A.9})$$

The complementary  $\mathbb{Z}_{24}$  needs to be generated by any linear combination in  $(\frac{1}{24}, 0, \frac{1}{3}, 0) \oplus (0, \frac{1}{24}, 0, \frac{1}{3})$  such that all its integral powers differ from those of the generators of  $\mathbb{Z}'_{24}$ , i.e., that all elements of the so-generated  $\mathbb{Z}_{24}$  differ from those of  $\mathbb{Z}'_{24}$ ; this excludes  $(\mathbb{Z}''_{24} : \frac{1}{24}, \frac{1}{24}, \frac{1}{3}, \frac{1}{3}) = (\mathbb{Z}''_{24} : (\frac{1}{24}, 0, \frac{1}{3}, 0) + (0, \frac{1}{24}, 0, \frac{1}{3}))$ , since  $(\mathbb{Z}''_2 : \frac{12}{24}, \frac{12}{24}, \frac{12}{3}, \frac{12}{3}) \subset \mathbb{Z}'_{24}$ . We thus choose  $(\mathbb{Z}^{(1)}_{24} : \frac{1}{24}, 0, \frac{1}{3}, 0)$  and note that it has the traceless subgroup,  $(\mathbb{Z}^{(1)}_3 : \frac{8}{24}, 0, \frac{8}{3}, 0) = (\mathbb{Z}^{(1)}_3 : \frac{1}{3}, 0, \frac{2}{3}, 0)$ , which is also independent of  $Q^\nabla = \mathbb{Z}'_6$  in (A.8). This allows identifying the geometric group on the right-hand (transposed) side of (A.8) as

$$G^\nabla = (\mathbb{Z}'_{24} \times \mathbb{Z}_{24}) / \mathbb{Z}'_6 = (\mathbb{Z}'_{24} / \mathbb{Z}'_6 \approx \mathbb{Z}'_4) \times \mathbb{Z}^{(1)}_{24}. \quad (\text{A.10})$$

These definitions then permit completing a (A.6)-like multiple mirror network:

$$\begin{array}{ccccc} \{\text{T}f_1(y)=0\}/\mathbb{Z}_3 & \xleftarrow{\text{mm}} & \{f_1(x)=0\} & \xleftarrow{\text{defo.}_{\text{cpx. str.}}} & \{f_2(x)=0\} & \xleftarrow{\text{mm}} & \{\text{T}f_2(y)=0\}'/[(\mathbb{Z}'_{24}/\mathbb{Z}'_6) \times \mathbb{Z}^{(1)}_3] \\ \uparrow / \mathbb{Z}_3 & & \downarrow / \mathbb{Z}_3 & & \downarrow / \mathbb{Z}_4 & & \uparrow / (\mathbb{Z}'_{24}/\mathbb{Z}'_6) \approx \mathbb{Z}'_4 \\ \{\text{T}f_1(y)=0\} & \xleftarrow{\text{mm}} & \{f_1(x)=0\}/\mathbb{Z}_3 & & \{f_2(x)=0\}/\mathbb{Z}_4 & \xleftarrow{\text{mm}} & \{\text{T}f_2(y)=0\}'/\mathbb{Z}^{(1)}_3 \end{array} \quad (\text{A.11})$$

where appropriate desingularizing blowups are understood for each quotient, where the primes indicate the use of the twisted quantum group, twisting the Ref. [33, 34] specifications (A.2)–(A.6), but in agreement with the less prescriptive original algorithm [26].

The twisted specifications (A.8)–(A.11) are possible precisely because

$$\text{T}f_2(y) = \left( b_2 y_3^3 + b_4 \frac{y_1^8}{y_3} \right) + \left( b_3 y_6^3 + b_5 \frac{y_2^8}{y_6} \right) \quad (\text{A.12})$$

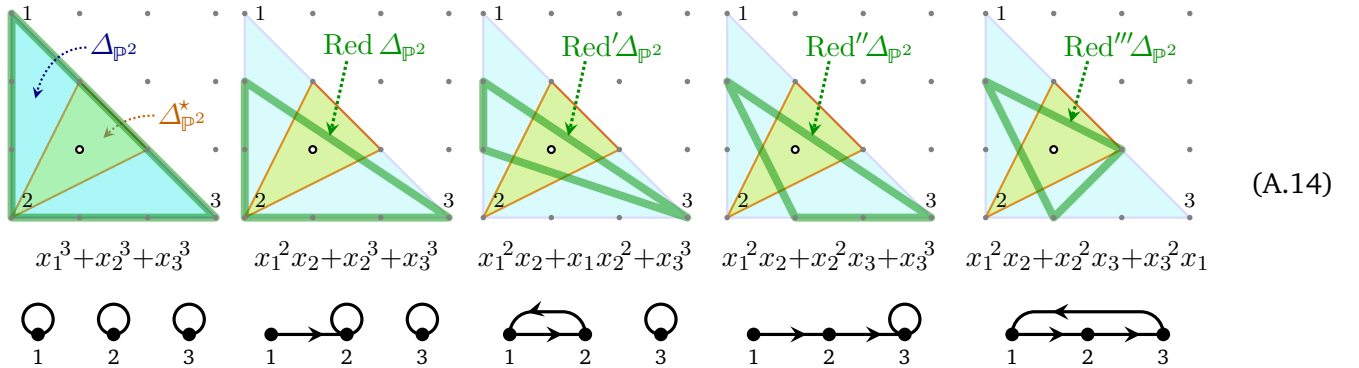
decomposes as a sum of two separate summands, coupled only by the overall  $\mathbb{P}^3_{(1:1:2:2)}$ -projectivization. The fact that the “original,”

$$f_2(x) = \left( a_1 x_4^8 + a_3 \frac{x_2^3}{x_4} \right) + \left( a_2 x_5^8 + a_6 \frac{x_3^3}{x_5} \right), \quad (\text{A.13})$$

correspondingly also decomposes as a sum of two separate parts permits similarly twisting also the  $(G, Q)$ -specifications, which allows additional quotienting options that we however do not explore herein.

## A.2 Origin-Enclosing Simplicial Reductions

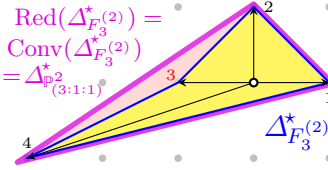
The “origin-enclosing” simplices,  $\text{Red } \Delta_X$ , of Remark 1.1 and footnote 4 on p. 2, formed by appropriate subsets of the lattice points  $\Delta_X \cap M$  are not conceptually new, merely adapted for VEX multitopes: Such reductions in fact appeared in the original proposal of transpose mirror construction [26], adopting the language and diagrams from Arnold’s original classification [114] and Kreuzer and Skarke’s analysis [115]. The simple case of  $\mathbb{P}^2[3]$  has five types of suitable (“invertible” [33, 34]) transverse polynomials:



The Newton triangle,  $\Delta_{\mathbb{P}^2}^*$  (bigger, pale blue), is depicted over the spanning triangle,  $\Delta_{\mathbb{P}^2}$  (smaller, yellow); the thicker (green) triangle outlines  $\text{Red } \Delta_{\mathbb{P}^2}$ , the so-encoded defining polynomial underneath it, and its graphical depiction à la [26, 114] underneath that. Arnold’s original classification [114] guarantees that every other sub-simplex reduction is either equivalent to one of these or not transverse.

### A.3 Origin Non-Enclosing Simplicial Reductions

Supporting Remark 1.1 and footnote 4, p. 2, consider the pair of examples obtained by fixing a sub-simplex reduction of  $\Delta_{F_3}^*$ , and reducing  $\Delta_{F_3}^{(2)}$  to two simplicial subsets,  $\text{Red}'(\Delta_{F_3}^{(2)})$  and  $\text{Red}''(\Delta_{F_3}^{(2)})$ , each of which containing  $0 \in M$  in one of its facets:

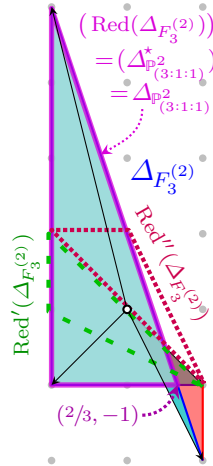


$\text{Red}'(\Delta_{F_3}^*, \Delta_{F_3}^{(2)})$

$$\mathbb{E}_1 = \begin{bmatrix} 0 & 2 & 3 \\ 0 & 1 & 4 \\ 2 & 0 & -1 \end{bmatrix}, \text{ so } \mathbb{E}_1^{-1} \equiv \begin{bmatrix} 9/10 & 4/5 & 4/5 \\ 1/5 & 2/5 & 2/5 \\ 1/2 & 0 & 0 \end{bmatrix}$$


---

 $f_1(x) = x_2^2 x_4^3 + x_2 x_4^4 + \frac{x_1^2}{x_4} \in \mathbb{P}_{(3:1:1)}^2$ 
 $\text{T}f_1(y) = y_3^2 + y_1^2 y_2 + \frac{y_1^3 y_2^4}{y_3} \in \mathbb{P}_{(1:0:1)}^2$



$\text{Red}''(\Delta_{F_3}^*, \Delta_{F_3}^{(2)})$

$$\mathbb{E}_2 = \begin{bmatrix} 0 & 2 & 3 \\ 1 & 2 & 0 \\ 2 & 0 & -1 \end{bmatrix}, \text{ so } \mathbb{E}_2^{-1} \equiv \begin{bmatrix} 1/5 & 9/10 & 2/5 \\ 4/5 & 3/5 & 3/5 \\ 3/5 & 7/10 & 1/5 \end{bmatrix} \quad (\text{A.15})$$


---

 $f_2(x) = x_2^2 x_4^3 + x_1 x_2^2 + \frac{x_1^2}{x_4} \in \mathbb{P}_{(3:1:1)}^2$ 
 $\text{T}f_2(y) = y_2 y_3^2 + y_1^2 y_2^2 + \frac{y_1^3}{y_3} \in \mathbb{P}_{(1:0:1)}^2$

The thicker (magenta) outline highlights: the convex hull,  $\text{Red}(\Delta_{F_3}^*) = \text{Conv}(\Delta_{F_3}^{(2)}) = \Delta_{\mathbb{P}^2(3:1:1)}^*$  (left), and its non-lattice polar (right),  $(\text{Red}(\Delta_{F_3}^{(2)}))^{\circ} = \Delta_{\mathbb{P}^2(3:1:1)} = \text{Conv}((-1, 4), (-1, -1), (2/3, -1))$ . The latter polygon has no lattice point in the right-hand half-space and cannot span the lattice (multi)fan of any compact toric space, which prompts the extension to VEX multitopes [38].

Whereas both  $f_1(x)$  and  $\text{T}f_1(y)$  are transverse, the degrees in the latter are consistent only with  $q(y_2) = 0$ , as indicated by  $(y_1, y_2, y_3) \in \mathbb{P}_{(1:0:1)}^2$ :  $y_2$  is an uncharged “spectator” (super)field in the GLSM with the superpotential  $W = P_0 \text{T}f_1(y)$ , parametrizing a non-compact direction. The same holds for the other reduction, except now also  $f_2(x)$  fails to be transverse. Finally, neither  $\mathbb{E}_1^{-1}$  nor  $\mathbb{E}_2^{-1}$  defines a collection of finite group actions fit for the hallmark exchange of “geometric” and “quantum” symmetries. Thus, neither  $(f_1(x), \text{T}f_1(y))$  nor  $(f_2(x), \text{T}f_2(y))$  can be used to construct transpose mirrors à la [26, 29, 33, 34].

While we are not aware of a rigorous proof that the sub-simplex reductions of both the spanning and the (extended) Newton multitope must enclose the lattice origin for the transpose mirror construction [26, 29, 33, 34], we have not found any counter-example to this, whence statement (1) of Conjecture 1.1.

## References

- [1] P. Candelas, G.T. Horowitz, A. Strominger, and E. Witten, “Vacuum configurations for superstrings,” *Nucl. Phys.* **B258** (1985) 46–74.
- [2] L.J. Dixon, J.A. Harvey, C. Vafa, and E. Witten, “Strings on orbifolds,” *Nucl. Phys.* **B261** (1985) 678–686.
- [3] M.A. Reid, “The moduli space of 3-folds with  $K = 0$  may nevertheless be irreducible,” *Math. Ann.* **278** no. 1-4, (1987) 329–334.
- [4] P. Candelas, A.M. Dale, C.A. Lutken, and R. Schimmrigk, “Complete intersection Calabi–Yau manifolds,” *Nucl. Phys.* **B298** (1988) 493.
- [5] P.S. Green and T. Hübsch, “Connecting moduli spaces of Calabi–Yau threefolds,” *Comm. Math. Phys.* **119** (1988) 431–441.
- [6] P.S. Green and T. Hübsch, “Possible phase transitions among Calabi–Yau compactifications,” *Phys. Rev. Lett.* **61** (1988) 1163–1166.
- [7] P. Candelas, P.S. Green, and T. Hübsch, “Finite distances between distinct Calabi–Yau manifolds,” *Phys. Rev. Lett.* **62** (1989) 1956–1959.
- [8] P. Candelas, P.S. Green, and T. Hübsch, “Rolling among Calabi–Yau vacua,” *Nucl. Phys.* **B330** (1990) 49–102.

- [9] T. Hübsch, *Calabi–Yau Manifolds: a Bestiary for Physicists*. World Scientific Publishing Co., River Edge, NJ, 1992.
- [10] T. Hübsch, “How singular a space can superstrings thread?” *Mod. Phys. Lett.* **A6** (1991) 207–216.
- [11] J. McNamara and C. Vafa, “Cobordism classes and the swampland,” [arXiv:1909.10355 \[hep-th\]](#).
- [12] E. Witten, “Phases of  $N = 2$  theories in two-dimensions,” *Nucl. Phys.* **B403** (1993) 159–222, [hep-th/9301042](#).
- [13] D.R. Morrison and M.R. Plesser, “Summing the instantons: Quantum cohomology and mirror symmetry in toric varieties,” *Nucl. Phys.* **B440** (1995) 279–354, [arXiv:hep-th/9412236 \[hep-th\]](#).
- [14] J. Distler and S. Kachru, “(0, 2) Landau–Ginzburg theory,” *Nucl. Phys. B* **413** (1994) 213–243, [arXiv:hep-th/9309110](#).
- [15] S. Schäfer-Nameki and T. Weigand, “F-theory and 2d (0, 2) theories,” *JHEP* **05** (2016) 059, [arXiv:1601.02015 \[hep-th\]](#).
- [16] L. Freidel, R.G. Leigh, and D. Minic, “Metastring theory and modular space-time,” *JHEP* **06** (2015) 006, [arXiv:1502.08005 \[hep-th\]](#).
- [17] P. Berglund, T. Hübsch, and D. Minic, “Mirror symmetry, Born geometry and string theory,” in *Nankai Symposium on Mathematical Dialogues: Celebrating the 110th Anniversary of the Birth of Prof. S.-S. Chern*, Y.-H. He, M.-L. Ge, C.-M. Bai, J. Bao, and E. Hirst, eds. Springer Verlag, Singapore, Sept., 2022.
- [18] G. Kempf, F. Knudsen, D. Mumford, and B. Saint-Donat, *Toroidal Embeddings I*. No. 339 in Lecture Notes in Mathematics. Springer, 1973.
- [19] V.I. Danilov, “The geometry of toric varieties,” *Russian Math. Surveys* **33** no. 2, (1978) 97–154.
- [20] T. Oda, *Convex Bodies and Algebraic Geometry: An Introduction to the Theory of Toric Varieties*. A Series of Modern Surveys in Mathematics. Springer, 1988.
- [21] W. Fulton, *Introduction to Toric Varieties*. Annals of Mathematics Studies. Princeton University Press, 1993.
- [22] G. Ewald, *Combinatorial Convexity and Algebraic Geometry*. Springer Verlag, 1996.
- [23] D.A. Cox, J.B. Little, and H.K. Schenck, *Toric Varieties*, vol. 124 of *Graduate Studies in Mathematics*. American Mathematical Society, 2011.
- [24] M. Kreuzer and H. Skarke, “Complete classification of reflexive polyhedra in four dimensions,” *Adv. Theor. Math. Phys.* **4** no. 6, (2000) 1209–1230, [arXiv:hep-th/0002240](#).
- [25] B.R. Greene and M.R. Plesser, “Duality in Calabi–Yau moduli space,” *Nucl. Phys.* **B338** (1990) 15–37.
- [26] P. Berglund and T. Hübsch, “A generalized construction of mirror manifolds,” *Nucl. Phys.* **B393** no. 1-2, (1993) 377–391, [arXiv:hep-th/9201014 \[hep-th\]](#).
- [27] V.V. Batyrev, “Dual polyhedra and mirror symmetry for Calabi–Yau hypersurfaces in toric varieties,” *J. Alg. Geom.* **3** no. 3, (1994) 493–535, [arXiv:alg-geom/9310003](#).
- [28] V.V. Batyrev and L.A. Borisov, “On Calabi–Yau complete intersections in toric varieties,” in *Higher-dimensional complex varieties (Trento, 1994)*, pp. 39–65. de Gruyter, Berlin, 1996.
- [29] P. Berglund and M. Henningson, “Landau–Ginzburg orbifolds, mirror symmetry and the elliptic genus,” *Nucl. Phys.* **B433** (1995) 311–332, [arXiv:hep-th/9401029 \[hep-th\]](#).
- [30] P. Candelas, X. de la Ossa, and S.H. Katz, “Mirror symmetry for Calabi–Yau hypersurfaces in weighted  $\mathbf{P}^4$  and extensions of Landau–Ginzburg theory,” *Nucl. Phys.* **B450** (1995) 267–292, [arXiv:hep-th/9412117](#).
- [31] V.V. Batyrev and L.A. Borisov, “Mirror duality and string-theoretic Hodge numbers,” *Invent. Math.* **126** no. 1, (1996) 183–203, [arXiv:math/9909009 \[math.AG\]](#).
- [32] V.V. Batyrev and L.A. Borisov, “Dual cones and mirror symmetry for generalized Calabi–Yau manifolds,” in *Mirror symmetry, II*, vol. 1 of *AMS/IP Stud. Adv. Math.*, pp. 71–86. Amer. Math. Soc., Providence, RI, 1997.
- [33] M. Krawitz, N. Priddis, P. Acosta, N. Bergin, and H. Rathnakumara, “FJRW-rings and mirror symmetry,” *Communications in Mathematical Physics* **296** no. 1, (Oct., 2009) 145–174, [arXiv:0903.3220 \[math.AG\]](#).
- [34] M. Krawitz, *FJRW rings and Landau–Ginzburg Mirror Symmetry*. PhD thesis, University of Michigan, Ann Arbor, MI, 2010. [arXiv:0906.0796 \[math.AG\]](#).
- [35] L.A. Borisov, “Berglund–Hübsch mirror symmetry via vertex algebras,” *Comm. Math. Phys.* **320** no. 1, (2013) 73–99, [arXiv:1007.2633 \[math.AG\]](#).
- [36] M. Artebani, P. Comparin, and R. Guilbot, “Families of Calabi–Yau hypersurfaces in  $\mathbf{Q}$ -Fano toric varieties,” *J. Math. Pure & Appl.* **106** no. 2, (2016) 319–341, [arXiv:1501.05681 \[math.AG\]](#).

- [37] D. Favero and T.L. Kelly, “Derived categories of BHK mirrors,” *Adv. Math.* **352** (2019) 943–980, [arXiv:1602.05876 \[math.AG\]](#).
- [38] P. Berglund and T. Hübsch, “A generalized construction of Calabi–Yau models and mirror symmetry,” *SciPost* **4** no. 2, (2018) 009 (1–30), [arXiv:1611.10300 \[hep-th\]](#).
- [39] P. Berglund and T. Hübsch, “Hirzebruch surfaces, Tyurin degenerations and toric mirrors: Bridging generalized Calabi–Yau constructions,” *Adv. in Th. Math. Phys.* **26** no. 8, (2022) 2541–2598, [arXiv:2205.12827 \[hep-th\]](#).
- [40] L.B. Anderson, F. Apruzzi, X. Gao, J. Gray, and S.-J. Lee, “A new construction of Calabi–Yau manifolds: Generalized CICYs,” *Nucl. Phys.* **B906** (2016) 441–496, [arXiv:1507.03235 \[hep-th\]](#).
- [41] P. Berglund and T. Hübsch, “On Calabi–Yau generalized complete intersections from Hirzebruch varieties and novel K3-fibrations,” *ATMP* **22** no. 2, (2018) 261 – 303, [arXiv:1606.07420 \[hep-th\]](#).
- [42] A. Garbagnati and B. van Geemen, “A remark on generalized complete intersections,” *Nucl. Phys.* **B925** (2017) 135–143, [arXiv:1708.00517 \[math.AG\]](#).
- [43] A.C. Avram, P. Candelas, D. Jancic, and M. Mandelberg, “On the connectedness of moduli spaces of Calabi–Yau manifolds,” *Nucl. Phys.* **B465** (1996) 458–472, [arXiv:hep-th/9511230 \[hep-th\]](#).
- [44] A.C. Avram, M. Kreuzer, M. Mandelberg, and H. Skarke, “The Web of Calabi–Yau hypersurfaces in toric varieties,” *Nucl. Phys.* **B505** (1997) 625–640, [arXiv:hep-th/9703003 \[hep-th\]](#).
- [45] M. Masuda, “Unitary toric manifolds, multi-fans and equivariant index,” *Tohoku Math. J. (2)* **51** no. 2, (1999) 237–265.
- [46] M. Masuda, “From convex polytopes to multi-polytopes,” *Notes Res. Inst. Math. Analysis* **1175** (2000) 1–15.
- [47] A. Hattori and M. Masuda, “Theory of multi-fans,” *Osaka J. Math.* **40** (2003) 1–68, [arXiv:math/0106229 \[math.SG\]](#).
- [48] M. Masuda and T. Panov, “On the cohomology of torus manifolds,” *Osaka Journal of Mathematics* **43** no. 3, (2006) 711 – 746, [arXiv:math/0306100 \[math.AT\]](#).
- [49] A. Hattori and M. Masuda, “Elliptic genera, torus manifolds and multi-fans,” *Int. J. of Math.* **16** no. 9, (July, 2006) 957–998, [arXiv:math/0107014 \[math.SG\]](#).
- [50] A. Hattori, “Elliptic genera, torus orbifolds and multi-fans; II,” *Int. J. Math* **17** no. 06, (2006) 707–735, [arXiv:math/0501392 \[math.AT\]](#).
- [51] Y. Nishimura, “Multipolytopes and convex chains,” *Proc. Steklov Inst. Math.* **252** (2006) 212–224.
- [52] H. Ishida, “Invariant stably complex structures on topological toric manifolds,” *Osaka J. Math.* **50** (2013) 795–806.
- [53] M.W. Davis and T. Januszkiewicz, “Convex polytopes, Coxeter orbifolds and torus actions,” *Duke Math. J.* **62** no. 2, (1991) 417–451.
- [54] H. Ishida, Y. Fukukawa, and M. Masuda, “Topological toric manifolds,” *Moscow Math. J.* **13** no. 1, (2013) 57–98, [arXiv:1012.1786 \[math.AT\]](#).
- [55] V. Buchstaber and T. Panov, *Toric Topology*. No. 204 in Mathematical Surveys and Monographs. American Mathematical Society, Providence, RI, 2015.
- [56] D. Jang, “Four dimensional almost complex torus manifolds,” [arXiv:2310.11024 \[math.DG\]](#).
- [57] B. Poonen and F. Rodriguez–Villegas, “Lattice polygons and the number 12,” *Am. Math. Monthly* **107** no. 3, (March, 2000) 238–250.
- [58] A. Higashitani and M. Masuda, “Lattice multipolygons,” *Kyoto Journal of Mathematics* **57** no. 4, (Dec, 2017) 807–828, [arXiv:1204.0088 \[math.CO\]](#).
- [59] A. Khovanskii and A. Pukhlikov, “A Riemann–Roch theorem for integrals and sums of quasipolynomials over virtual polytopes,” *St. Petersburg Math. J.* **4** no. 4, (1993) 789–812.
- [60] Y. Karshon and S. Tolman, “The moment map and line bundles over presymplectic toric manifolds,” *J. Diff. Geom.* **38** no. 3, (1993) 465–484.
- [61] A.C. da Silva, V. Guillemin, and A.R. Pires, “Symplectic origami,” *Int. Math. Res. Not.* **2011** no. 18, (Dec, 2010) 4252–4293, [arXiv:0909.4065 \[math.SG\]](#).
- [62] M. Masuda and S. Park, “Toric origami manifolds and multi-fans,” *Proc. Steklov Inst. Math.* **286** (May, 2014) 308–323, [arXiv:1305.6347 \[math.SG\]](#).
- [63] L. Godinho, F. von Heymann, and S. Sabatini, “12, 24 and beyond,” *Adv. Math* **319** (2017) 472–521, [arXiv:1604.00277 \[math.CO\]](#).

- [64] P.S. Aspinwall, B.R. Greene, and D.R. Morrison, “Calabi–Yau moduli space, mirror manifolds and space-time topology change in string theory,” *Nucl. Phys.* **B416** (1994) 414–480, [arXiv:hep-th/9309097](#).
- [65] T. Hübsch and A. Rahman, “On the geometry and homology of certain simple stratified varieties,” *J. Geom. Phys.* **53** (2005) 31–48, [arXiv:math/0210394](#).
- [66] A. Rahman, “A perverse sheaf approach toward a cohomology theory for string theory,” *Adv. Theor. Math. Phys.* **13** no. 3, (2009) 667–693, [arXiv:0704.3298](#).
- [67] M. Banagl, *Intersection Spaces, Spatial Homology Truncation, and String Theory*. No. 1997 in Lecture Notes in Mathematics. Springer, 2010.
- [68] M. Kontsevich, “Homological algebra of mirror symmetry,” in *Proceedings of the International Congress of Mathematicians*, S.D. Chatterji, ed., pp. 120–139. Birkhäuser Basel, Basel, 1995. [arXiv:alg-geom/9411018](#) [[alg-geom](#)].
- [69] D.A. Cox and S. Katz, *Mirror Symmetry and Algebraic Geometry*, vol. 68 of *Mathematical Surveys and Monographs*. American Mathematical Society, Providence, RI, 1999.
- [70] A. Strominger, S.-T. Yau, and E. Zaslow, “Mirror symmetry is T-duality,” *Nucl. Phys.* **B479** (1996) 243–259, [arXiv:hep-th/9606040](#).
- [71] P. Berglund and M. Lathwood, “Tropical Periods for Calabi–Yau Hypersurfaces in non-Fano Toric Varieties,” [arXiv:2212.11906](#) [[hep-th](#)].
- [72] J.E. Reeve, “On the volume of lattice polyhedra,” *Proc. London Math. Soc.* **s3-7** no. 2, (1957) 378–395.
- [73] A. Belyaev and P.-A. Fayolle, “Counting parallel segments: New variants of Pick’s area theorem,” *The Mathematical Intelligencer* **41** no. 4, (2019) 1–7.
- [74] V. Buchstaber and N. Ray, “Tangential structures on toric manifolds and connected sums of polytopes,” *Internat. Math. Res. Notices* **4** (2001) 193–219, [arXiv:math/0010025](#) [[math.AT](#)].
- [75] F. Berchtold, “Lifting of morphisms to quotient presentations,” *Man. Math.* **110** (2003) 33–44, [arXiv:math/0209406](#) [[math.AG](#)].
- [76] A. Ayzenberg and M. Masuda, “Volume polynomials and duality algebras of multi-fans,” *Arnold Math. J.* **2** no. 3, (Sept., 2016) 329–381, [arXiv:1509.03008](#) [[math.CO](#)].
- [77] B. Friedman, S. Picard, and C. Suan, “Gromov–Hausdorff continuity of non-Kähler Calabi–Yau conifold transitions,” [arXiv:2404.11840](#) [[math.DG](#)].
- [78] B.R. Greene and M.R. Plesser, “Mirror manifolds: A Brief review and progress report,” in *2nd International Symposium on Particles, Strings and Cosmology*. 9, 1991.
- [79] F. Hirzebruch, “Über eine Klasse von einfach-zusammenhängenden komplexen Mannigfaltigkeiten,” *Math. Ann.* **124** (1951) 77–86.
- [80] P. Griffiths and J. Harris, *Principles of algebraic geometry*. Wiley Classics Library. John Wiley & Sons Inc., New York, 1978.
- [81] F. Hirzebruch, *Topological Methods in Algebraic Geometry*. Springer-Verlag, New York, 1978.
- [82] A.N. Tyurin, “Fano versus Calabi–Yau,” in *The Fano Conference*, pp. 701–734. Univ. Torino, Turin, 2004.
- [83] N.-H. Lee, *Constructive Calabi–Yau Manifolds*. PhD thesis, University of Michigan, 2006.
- [84] C.F. Doran, A. Harder, and A. Thompson, “Mirror symmetry, Tyurin degenerations and fibrations on Calabi–Yau manifolds,” *Proc. Symp. Pure Math.* **96** (2017) 93–131, [arXiv:1601.08110](#) [[math.AG](#)].
- [85] A. Kanazawa, “Doran–Harder–Thompson conjecture via SYZ mirror symmetry: Elliptic curves,” *Symmetry, Integrability and Geometry: Methods and Applications* **13** (Apr, 2017) 024, [arXiv:1612.04623v4](#) [[math.AG](#)].
- [86] C.F. Doran, J. Kostiuk, and F. You, “The Doran–Harder–Thompson conjecture for toric complete intersections,” *Adv. Math.* **415** (2023) 108893, [arXiv:1910.11955](#) [[math.AG](#)].
- [87] C.F. Doran and A. Thompson, “Mirror symmetry for lattice polarized del Pezzo surfaces,” *Communications in Number Theory and Physics* **12** no. 3, (2018) 543–580, [arXiv:1709.00856](#) [[math.AG](#)].
- [88] L.J. Barrott and C.F. Doran, “Towards the Doran–Harder–Thompson conjecture via the Gross–Siebert program,” [arXiv:2105.02617](#) [[math.AG](#)].
- [89] C.F. Doran and A. Thompson, “The mirror Clemens–Schmid sequence,” [arXiv:2109.04849](#) [[math.AG](#)].
- [90] C.F. Doran, J. Kostiuk, and F. You, “Degenerations, fibrations and higher rank Landau–Ginzburg models,” [arXiv:2112.12891](#) [[math.AG](#)].

- [91] D.A. Cox, “The homogeneous coordinate ring of a toric variety,” *J. Algebraic Geometry* **4** (1995) 17–50, [arXiv:alg-geom/9210008 \[alg-geom\]](#).
- [92] M. Atiyah and F. Hirzebruch, “Riemann–Roch theorems for differentiable manifolds,” *Bull. Am. Math. Soc.* **65** (1959) 276–281.
- [93] J.A. Todd, “The arithmetical invariants of algebraic loci,” *Proc. London Math. Soc.* **43** (1937) 190–225.
- [94] V.V. Batyrev and D.I. Dais, “Strong McKay correspondence, string-theoretic Hodge numbers and mirror symmetry,” *Topology* **35** no. 4, (1996) 901–929, [arXiv:alg-geom/9410001](#).
- [95] C.T.C. Wall, “Classifications problems in differential topology V: On certain 6-manifolds,” *Invent. Math.* **1** (1966) 355–374.
- [96] P. Berglund, B. Campbell, and V. Jejjala, “Machine learning Kreuzer–Skarke Calabi–Yau threefolds,” [arXiv:2112.09117 \[hep-th\]](#).
- [97] A.S. Libgober and J.W. Wood, “Uniqueness of the complex structure on Kähler manifolds of certain homotopy types,” *J. Diff. Geom.* **32** (1990) 139–154.
- [98] P. Berglund, S.H. Katz, and A. Klemm, “Mirror symmetry and the moduli space for generic hypersurfaces in toric varieties,” *Nucl. Phys.* **B456** (1995) 153–204, [arXiv:hep-th/9506091 \[hep-th\]](#).
- [99] G. Barthel, J.-P. Brasselet, K.-H. Fieseler, and L. Kaup, “Combinatorial intersection cohomology for fans,” *Tohoku Mathematical Journal* **54** no. 1, (2002) 1 – 41, [arXiv:math/0002181 \[math.AG\]](#).
- [100] T. Hibi, “Star-shaped complexes and Ehrhart polynomials,” *Proc. Am. Math. Soc.* **123** no. 3, (1995) 723–726.
- [101] M. Masuda, “Equivariant cohomology distinguishes toric manifolds,” *Adv. Math.* **218** (2008) 2005–2012, [arXiv:math/0703330 \[math.AT\]](#).
- [102] M. Atiyah and G.B. Segal, “On equivariant Euler characteristics,” *J. Geom. Phys.* **6** no. 4, (1989) 671–677.
- [103] T. Hübsch, “On a stringy singular cohomology,” *Mod. Phys. Lett.* **A12** (1997) 521–533, [arXiv:hep-th/9612075](#).
- [104] M. Mustață and S. Payne, “Ehrhart polynomials and stringy Betti numbers,” *Mathematische Annalen* **333** (2005) 787–795.
- [105] S. Franco, D. Ghim, S. Lee, R.-K. Seong, and D. Yokoyama, “2d (0, 2) quiver gauge theories and D-branes,” *JHEP* **09** (2015) 072, [arXiv:1506.03818 \[hep-th\]](#).
- [106] S. Franco and R.-K. Seong, “Twin theories, polytope mutations and quivers for GTPs,” [arXiv:2302.10951 \[hep-th\]](#).
- [107] M. Kho and R.-K. Seong, “On the master space for brane brick models,” [arXiv:2306.16616 \[hep-th\]](#).
- [108] H. Ohsugi and T. Hibi, “Special simplices and gorenstein toric rings,” *J. Comb. Theory, Ser. A* **113** no. 4, (2006) 787–795.
- [109] K.A. Adiprasito, S.A. Papadakis, V. Petrotou, and J.K. Steinmeyer, “Beyond positivity in Ehrhart theory,” [arXiv:2210.10734 \[math.CO\]](#).
- [110] D. Huybrechts, *Complex Geometry*. Springer, 2005.
- [111] A.V. Smilga, “Dolbeault complex on  $S^4 \setminus \{.\}$  and  $S^6 \setminus \{.\}$  through supersymmetric glasses,” *Sigma* **7** (2011) 105, [arXiv:1105.3935 \[math-ph\]](#).
- [112] M. Belakovskiy and A. Belavin, “Coincidences between Calabi–Yau manifolds of Berglund–Hubsch type and Batyrev polytopes,” [arXiv:2005.06008 \[hep-th\]](#).
- [113] A. Belavin and D. Gepner, “Relationship between two Calabi–Yau orbifolds arising as hyper-surfaces in a quotient of the same weighted projective space,” *Nucl. Phys. B* **994** (2023) 116313, [arXiv:2306.06667 \[hep-th\]](#).
- [114] V. Arnold, S. Gusein-Zade, and A. Varchenko, *Singularities of Differentiable Maps*, vol. 1. Birkhäuser, Boston, MA, 1985.
- [115] M. Kreuzer and H. Skarke, “On the classification of quasihomogeneous functions,” *Commun. Math. Phys.* **150** (1992) 137, [arXiv:hep-th/9202039](#).

**Results:** Claim 1.1, 1.2, 2.1, 5.1; Conj. 1.1, 1.2, 4.1, 5.1; Constr. 1.1; Cor. 2.1; Def. 1.1, 1.2; Lemma 4.1; Proc. 3.1; Remk. 1.1, 1.2, 1.3, 1.4, 1.5, 1.6, 1.7, 1.8, 1.9, 1.10, 1.11, 2.1, 2.2, 3.1, 3.2, 3.3, 4.1, 4.2, 4.3, 5.1; Thrm. 2.1, 4.1;